

TECHNISCHE UNIVERSITÄT MÜNCHEN

Lehrstuhl für Entwicklungsgenetik

Validation of *P2RX7* and *TMEM132D* as
susceptibility genes for depression
using genetic mouse models

Sandra Maria Walser

Vollständiger Abdruck der von der Fakultät Wissenschaftszentrum Weihenstephan für Ernährung, Landnutzung und Umwelt der Technischen Universität München zur Erlangung des akademischen Grades eines

Doktors der Naturwissenschaften

genehmigten Dissertation.

Vorsitzender: Univ.-Prof. Dr. K. Schneitz
Prüfer der Dissertation: 1. Univ.-Prof. Dr. W. Wurst
2. Univ.-Prof. Dr. A. Gierl

Die Dissertation wurde am 12.12.2011 bei der Technischen Universität München eingereicht und durch die Fakultät Wissenschaftszentrum Weihenstephan für Ernährung, Landnutzung und Umwelt am 10.05.2012 angenommen.

Table of contents

Abstract	6
Zusammenfassung	8
1 Introduction	10
1.1 Epidemiology of depression	10
1.2 Animal models of depression	11
1.3 Linkage and association studies as an unbiased approach to identify candidate genes	14
1.4 Identification of <i>P2RX7</i> as susceptibility gene for depression	17
1.5 Identification of <i>TMEM132D</i> as new candidate gene for panic disorder	24
1.6 Aim of the thesis	28
2 Material and methods	30
2.1 Material	30
2.1.1 Buffers and solutions	30
2.1.1.1 Buffers for agarose gel electrophoresis	30
2.1.1.2 Solutions for <i>in situ</i> hybridization (ISH).....	31
2.1.1.3 Solutions for Southern Blot	32
2.1.1.4 Solutions for Western blot.....	33
2.1.1.5 LacZ staining solutions.....	35
2.1.1.6 Other buffers and solutions	35
2.1.2 Media for bacterial cultures.....	37
2.1.3 Media for cell culture.....	37
2.1.3.1 Media for cell lines	38
2.1.3.2 Media for embryonic stem (ES) cell culture	38
2.1.4 Oligonucleotides	39
2.1.4.1 Primers used for cloning procedures	39
2.1.4.2 Primers used for genotyping	40
2.1.4.3 Primers used for expression analysis	41
2.1.5 Probes (DNA and mRNA).....	42
2.1.6 Antibodies	42
2.1.7 <i>E. coli</i> and yeast strains.....	43
2.1.8 Animals	43
2.2 Methods	44
2.2.1 Microbiological methods	44

2.2.1.1	Preparation of chemically competent bacteria	44
2.2.1.2	Transformation	44
2.2.1.3	Glycerol stocks	44
2.2.2	Preparation and analysis of nucleic acids	45
2.2.2.1	Preparation of plasmid DNA	45
2.2.2.2	DNA preparation from mouse tail tissue	45
2.2.2.3	RNA isolation	45
2.2.2.4	Agarose gel electrophoresis	46
2.2.2.5	Photometric determination of DNA/RNA concentrations	46
2.2.2.6	Restriction digestions of DNA samples for analytical purposes	47
2.2.2.7	Sequencing	47
2.2.3	Polymerase chain reaction (PCR)	47
2.2.3.1	Standard PCR	47
2.2.3.2	Reverse transcription (RT) PCR	48
2.2.4	Cloning techniques	49
2.2.4.1	Restriction digestions of DNA samples for preparative purposes	49
2.2.4.2	DNA gel extraction	49
2.2.4.3	Ligation	50
2.2.4.4	TOPO TA cloning	50
2.2.5	Yeast Two-Hybrid (Y2H) membrane system	51
2.2.6	<i>In situ</i> hybridization	53
2.2.7	Southern blot analysis	58
2.2.8	Western blot analysis	60
2.2.9	LacZ staining	61
2.2.10	Immunohistochemistry/-cytochemistry	61
2.2.11	Cell culture experiments	62
2.2.11.1	Maintaining of cell lines	62
2.2.11.2	Plasmid DNA transfection in cell lines	63
2.2.11.3	Embryonic stem (ES) cell culture	64
2.2.11.4	Preparation and stimulation of primary neurons	66
2.2.12	Preparation of peritoneal macrophages for IL-1 β ELISA	66
2.2.13	Preparation of peritoneal macrophages for calcium imaging	67
2.2.14	<i>In vivo</i> experiments	68
2.2.14.1	Behavioral characterization	68
2.2.14.2	Endocrine analyses	72
2.2.14.3	Chronic social defeat stress paradigm	72
2.2.14.4	Acute stress response and sampling during the CSDS	72
2.2.14.5	Sleep phenotyping and analysis of sleep data	73
2.2.15	Statistics	74

3	Results	75
3.1	Validation of <i>P2RX7</i> as a susceptibility gene for mood disorders using genetic mouse models.....	75
3.1.1	Generation and analysis of <i>P2rx7</i> knockout mice	75
3.1.1.1	Generation of <i>P2rx7</i> knockout mice.....	75
3.1.1.2	Molecular characterization of <i>P2rx7</i> knockout mice	77
3.1.1.2.1	Expression analysis	77
3.1.1.2.2	Functional analysis	79
3.1.1.3	Behavioral characterization of <i>P2rx7</i> knockout mice	79
3.1.2	Generation and characterization of humanized <i>P2RX7</i> mouse mutants	83
3.1.2.1	Generation of humanized mouse mutants.....	83
3.1.2.2	Molecular characterization of humanized mouse mutants.....	85
3.1.2.2.1	Expression analysis	85
3.1.2.2.2	Functional analysis	86
3.1.2.3	Behavioral analysis of humanized mouse mutants.....	88
3.1.2.3.1	Basal characterization	88
3.1.2.3.2	Effects of chronic social defeat stress on <i>hP2RX7</i> mice	88
3.1.2.4	Sleep pattern analysis of humanized mouse mutants	92
3.1.3	Comparison of mouse and human <i>P2RX7</i>	94
3.1.3.1	Breeding of littermates for behavioral testing.....	94
3.1.3.2	Behavioral characterization.....	94
3.2	Validation of <i>TMEM132D</i> as a susceptibility gene for panic disorder and depression	97
3.2.1	Expression analysis of the <i>Tmem132</i> family	97
3.2.2	<i>In vitro</i> studies.....	99
3.2.3	Generation and characterization of <i>Tmem132d</i> knockout mice	104
3.2.3.1	Generation of knockout mice	104
3.2.3.2	Molecular characterization of knockout mice	106
3.2.3.2.1	Expression analysis	106
3.2.3.2.2	Co-localization studies using neuronal markers.....	107
3.2.3.3	Behavioral analysis of knockout mice	110
4	Discussion	112
4.1	Validation of <i>P2RX7</i> as a susceptibility gene for mood disorders using genetic mouse models.....	112
4.1.1	Generation and analysis of <i>P2rx7</i> knockout mice	112
4.1.2	Generation and characterization of humanized <i>P2RX7</i> mouse mutants	116
4.1.3	Comparison of mouse and human <i>P2RX7</i>	124

4.2	Validation of <i>TMEM132D</i> as a susceptibility gene for panic disorder and depression	126
5	Conclusion	131
6	Supplementary data	132
7	References	137
8	Acknowledgements	146
9	Curriculum vitae	147

Abstract

Unipolar depression is one of the main contributors to the global disease burden. About 50% of the risk to develop depression is genetically determined. However, the progress of developing novel and more effective antidepressants is still limited and until now, not a single valid susceptibility gene/genetic variant has been identified. Therefore, novel technologies are needed to discover new target genes for antidepressant treatment and to develop more appropriate animal models to study the functional relevance of these genes with regard to depression. One possible approach is via linkage and association studies which allow genetic investigation of a disease in a non-hypothesis-driven manner. The aim of this study was the validation of two new candidate genes – *P2RX7* and *TMEM132D* – for mood disorders identified by linkage and/or association studies as potential new targets for antidepressant treatment.

Several studies identified an association of a non-synonymous coding single nucleotide polymorphism (SNP) (rs2230912, Gln460Arg) in *P2RX7* with major depression and bipolar disorder. A meta-analysis including all genetic studies supported a contribution of the *P2RX7* polymorphism to an increased susceptibility for the development of mood disorders. In a first step, we analyzed the effects of *P2RX7* ablation on depression- and anxiety-related behavior using a previously established *P2rx7* knockout mouse line. To study the functional relevance of the polymorphism in an appropriate *in vivo* model, we generated humanized mouse mutants in which the murine *P2rx7* gene was substituted by the wild-type or the disease-associated isoform of human *P2RX7*. By this means, we were able to demonstrate the different functional properties of wild-type and disease-associated human *P2RX7* variants with regard to the release of pro-inflammatory cytokines as well as activation of intracellular signaling cascades. In addition, we could show that mice with the heterozygous genotype exhibited an altered response to chronic stress and changes in their sleep quality equivalent to those observed in human depression. Thus, using these humanized mouse lines, we were able to significantly contribute to the functional validation of the human association data *in vivo*.

Two other recent studies identified SNPs in *TMEM132D* to be associated with symptoms of depression and anxiety in subjects suffering from panic disorder,

unipolar depression or attention-deficit/hyperactivity disorder. In a mouse model of extremes in trait anxiety, anxiety-related behavior was positively correlated with *Tmem132d* mRNA expression in the anterior cingulate cortex. Even though these data suggest *TMEM132D* as an interesting candidate gene, the function of *TMEM132D* is completely unknown rendering validation rather difficult. Therefore, we used *in vitro* and *in vivo* approaches to investigate the function of *TMEM132D* in the brain. Our results provide evidence that *TMEM132D* may be involved in the regulation of adhesion/migration processes in the context of neurogenesis in the developing as well as in the adult mouse brain due to interaction with the integrin-actin machinery. Furthermore, the behavioral characterization of *Tmem132d* knockout mice, which were generated using a gene trap approach, supports a potential role of *TMEM132D* in endophenotypes related to mood disorders.

Zusammenfassung

Die unipolare Depression leistet einen Hauptbeitrag zur globalen Krankheitslast. Etwa 50% des Risikos eine Depression zu entwickeln ist genetisch bedingt. Allerdings ist der Fortschritt bei der Entwicklung neuer und effektiver Antidepressiva immer noch sehr begrenzt und bis heute konnte keine einzige genetische Variante identifiziert werden, die für die Entstehung einer Depression hauptverantwortlich ist. Daher werden neue Technologien benötigt, um potentielle Kandidatengene zur Entwicklung neuer Antidepressiva zu identifizieren, und geeignetere Tiermodelle, um die funktionelle Relevanz dieser Gene im Hinblick auf die Entstehung der Erkrankung zu untersuchen. Einen möglichen Ansatz dafür bieten sogenannte Kopplungs- und Assoziationsstudien, die eine hypothesenfreie Analyse der genetischen Basis einer Erkrankung zulassen. Ziel dieser Studie war die Validierung neuer Kandidatengene, *P2RX7* und *TMEM132D*, die in verschiedenen Assoziationsstudien für affektive Störungen identifiziert wurden, als mögliche Angriffspunkte für die Entwicklung neuer Antidepressiva.

In mehreren Studien wurde eine Assoziation eines nicht-synonymen, kodierenden Einzelnukleotid-Polymorphismus (SNP) (rs2230912, Gln460Arg) in *P2RX7* mit unipolarer und bipolarer Depression identifiziert. Die Meta-Analyse aller bisher veröffentlichten genetischen Studien deutet darauf hin, dass der *P2RX7* Polymorphismus das Risiko an Depression zu erkranken erhöht. Zunächst wurde die Auswirkung einer *P2rx7* Deletion auf Depressions- und Angstverhalten mithilfe einer bereits bestehenden knockout Mauslinie analysiert. Zur Untersuchung der funktionellen Relevanz dieses Polymorphismus in einem geeigneten Tiermodell wurden humanisierte Mausmutanten generiert, in denen das murine *P2rx7* Gen durch die Wild-typ oder die Krankheits-assoziierte Isoform des humanen *P2RX7* Gens ersetzt wurde. Auf diese Weise konnten wir die unterschiedlichen Eigenschaften der Wild-typ und der Krankheits-assoziierten humanen *P2RX7* Variante in Bezug auf die Freisetzung von pro-inflammatorischen Zytokinen sowie auf die Aktivierung von intrazellulären Signalkaskaden darlegen. Darüber hinaus konnten wir zeigen, dass Mäuse, die heterozygot für den Polymorphismus sind, eine veränderte Reaktion auf chronischen Stress sowie Veränderungen in der Schlafqualität aufweisen, vergleichbar mit Befunden in depressiven Patienten.

Insgesamt konnten wir mithilfe dieses Tiermodells entscheidend zur *in vivo* Validierung der humanen Assoziationsstudien beitragen.

Zwei weitere aktuelle Studien in Patienten mit einer Panikstörung, Depression oder einem Aufmerksamkeitsdefizit-Syndrom identifizierten SNPs im *TMEM132D* Gen, die mit charakteristischen Symptomen von Depressionen und Angststörungen assoziiert sind. In einem Tiermodell, das auf Extreme von Angstverhalten gezüchtet wurde, konnte erhöhte Ängstlichkeit positiv mit erhöhter *Tmem132d* mRNA Expression im anterioren cingulären Kortex korreliert werden. Obwohl diese Daten *TMEM132D* zu einem interessanten Kandidatengen machen, erschwert die Tatsache, dass über die Funktion von *TMEM132D* bisher sehr wenig bekannt ist, eine Validierung der humanen Studien. Deshalb führten wir verschiedene *in vitro* und *in vivo* Experimente durch, um die Funktion von *TMEM132D* im Gehirn näher zu untersuchen. Unsere Ergebnisse lassen vermuten, dass *TMEM132D* an der Regulierung von Adhäsions- und Migrationsprozessen im Kontext der Neurogenese sowohl während der Entwicklung als auch im adulten Maushirn durch Interaktion mit der Integrin-Aktin Maschinerie beteiligt sein könnte. Darüber hinaus deutet die verhaltensphänotypische Charakterisierung von *Tmem132d* knockout Mäusen, die mithilfe der Genfallen-Methode generiert wurden, auf eine mögliche Rolle von *TMEM132D* bei der Ausprägung von Depressions-assoziierten Verhaltensweisen hin.

1 Introduction

1.1 Epidemiology of depression

Depression, officially termed major depressive disorder (MDD), ranks among the most prevalent diseases worldwide. According to the estimations of the World Health Organization, depression will be the second leading cause of disability in 2020 (Murray and Lopez, 1997). Recent epidemiological studies indicate that severe forms of depression affect 2-5% of the population worldwide, and up to 20% are affected by milder forms of the disease (Kessler et al., 2003). Moreover, depressive patients have a 2-4 fold increased risk of developing cardiovascular diseases and 10-15% of individuals with major depression commit suicide (Keck, 2006).

Up to now, depression is diagnosed according to criteria of the Diagnostic Manual of Mental Disorders (DSM-IV), which characterizes a major depressive episode by at least five of the following symptoms: (1) depressed or irritable mood, (2) decreased interest or loss of pleasure, (3) weight gain or loss, (4) insomnia or hypersomnia, (5) psychomotor retardation or agitation, (6) fatigue or loss of energy, (7) feelings of worthlessness or inappropriate guilt, (8) diminished ability to think or concentrate, (9) recurrent thoughts of death and suicide. The symptoms must be evident almost daily for at least two weeks. Additionally, symptoms of anxiety are also often seen in depressed individuals (Berton and Nestler, 2006).

The genetic risk to develop depression is 40-50% (Levinson, 2006), but there are also several environmental risk factors for MDD. These include gender, stressful life events, adverse childhood experiences and certain personality traits (Fava and Kendler, 2000). Many recent studies support the hypothesis that stressful events correlate with an increased vulnerability for depression in a way that stressful situations often precede the onset of illness and are also associated with the severity of depression (Brown et al., 1987; Dunner et al., 1979; Holsboer, 2001; Nemeroff, 1988). Such stressors can lead to a transient hyperactivation of the hypothalamic-pituitary-adrenocortical (HPA) axis, resulting in increased glucocorticoid secretion. In this regard, depression is often associated with a dysregulation of the HPA axis (Holsboer and Barden, 1996).

In contrast to the epidemiological magnitude of the disease, the progress of pharmacological therapy of depression is still limited (Nestler et al., 2002). All

available antidepressants act via monoamine neurotransmitter systems, but only 50-70% of the patients exhibit acceptable responses to treatment (Morilak and Frazer, 2004). Additionally, slow onset of clinical effects as well as severe side effects associated with antidepressant therapy frequently lead to discontinuation of treatment. Although drugs of the latest generation have fewer side effects, they still exhibit similar effectiveness rates and show a substantial delay of 4-6 weeks between onset of treatment and clinical improvement. Besides that, 25-35% of the patients remain resistant to the treatment even after six weeks of therapy (Berton and Nestler, 2006; Holsboer, 2005). Apart from monoamines, many other targets have been analyzed, including glucocorticoid receptor and corticotropin-releasing hormone receptor antagonists (Berton and Nestler, 2006; Grigoriadis, 2005) as well as histone deacetylase inhibitors (Covington, III et al., 2009). However, so far none of these studies has resulted in a new adequate treatment of the disease. Besides these aspects, the molecular mechanisms underlying depression still remain largely unknown.

All these arguments raise the necessity to discover new candidate genes for antidepressant treatment independent of the monoamine system, and to develop more appropriate animal models to study the functional relevance of these genes with regard to mood disorders.

1.2 Animal models of depression

The highly variable composition of symptoms, course of illness and response to treatment renders it very difficult to accurately define and diagnose depression. As a consequence of that, it is nearly impossible to copy the complexity of such a multifactorial disorder. This does not mean that it is impossible to develop useful animal models, but rather emphasizes the unlikelihood of generating a model that will mirror the full extent of a given human neuropsychiatric disorder (Nestler and Hyman, 2010). Therefore, animal models are used to analyze only certain sub-features of a disease, so-called endophenotypes (Hasler et al., 2004). An endophenotype represents a trait that is intermediate between genotype and disease, not necessarily beholden to the diagnostic criteria for single illness, but in many cases useful to simplify our understanding of complex or heterogeneous disorders (Shyn and

Hamilton, 2010). Psychopathological endophenotypes represent many key symptoms of major depression. Still, one has to consider that not every depression-associated endophenotype can be modeled in mice or other animals, for instance depressed mood, feelings of worthlessness or thoughts of suicide. Nevertheless, several symptoms can be reproduced in an animal model such as anhedonia, anxiety-related behavior, alterations in sleep architecture etc. (Deussing, 2006) (Table 1).

Table 1. Depression-associated endophenotypes that can be modeled in mice (Dedic et al., 2011).

DSM-IV symptoms	Endopenotypes in mice	Appropriate test/analysis
Depressed or irritable mood	Cannot be modeled	
Decreased interest or loss of pleasure	Anhedonia	Sucrose preference Intracranial self-stimulation Conditioned place-preference Female urine sniffing test
Weight gain or loss	Can easily be measured	Abnormal loss or gain of weight after stress
Insomnia or hypersomnia	Abnormal sleep architecture	Assessed by electroencephalogram recordings
Psychomotor retardation or agitation	Alterations in locomotion	Open field test Alterations of home-cage activity Treadmill running Gate analysis
Fatigue or loss of energy	Alterations in locomotion	Reduced homecage activity Treadmill running Nest building
Feelings of worthlessness or inappropriate guilt	Cannot be modeled	
Diminished ability to think or concentrate	Deficits in working and spatial memory	Morris water maze Y-maze Fear conditioning Attentional set-shifting
Recurrent thoughts of death and suicide	Cannot be modeled	
	Additional endophenotypes	
	Anxiety-related behavior	Open field test Elevated plus maze test Dark-light box test Novelty-induced hypophagia Novel object exploration Modified hole board Marble burying
	Changes in social behavior	Social interaction/avoidance Sociability
	Behavioral despair	Forced swim test Tail suspension test Learned helplessness
	Neuroendocrine disturbances	Alterations in corticosterone secretion Dexamethasone suppression Combined dexamethasone/CRH challenge
	Changes in neuroanatomy	Analysis of hippocampal volume by resonance imaging (often reduced in depressed patients)

The methods available to identify endophenotypes include neuropsychological, cognitive, neurophysiological, neuroendocrine, neuroanatomical and biochemical measures (Hasler et al., 2004).

So far a variety of different mouse models has been established to improve our understanding of the pathophysiology of a wide spectrum of psychiatric diseases. However, a full consensus regarding the prerequisites of a valid animal model is still lacking in the scientific community. Up to now, the three criteria set up by McKinney and Bunney (McKinney, Jr. and Bunney, Jr., 1969) are still widely accepted; they include construct validity, face validity and predictive validity.

Construct (or etiologic) validity requires that the symptoms produced in the animal model are based on the same underlying neurobiological mechanisms as in humans. Thus, one tries to recreate processes in the animal which would also initiate the disease in humans (Nestler and Hyman, 2010). The ideal way would be to introduce a known human disease-causing gene variant into a mouse and thereby alter intracellular mechanisms, which in the end lead to the disease (Chadman et al., 2009).

Face validity is achieved when the animal exhibits specific symptoms of the disease which are similar to the human condition. These can be of biochemical, anatomical, neuropathological or behavioral nature. Thus, the concept of face validity can also be regarded as the attempt to reproduce certain endophenotypes which can be accurately measured in the animal model.

Finally, *predictive validity* refers to the ability of the animal to correctly respond to pharmacological treatment, which should correlate with results from clinical trials.

Accordingly, the more of the criteria mentioned above an animal model meets, the more persuasive it will be (Malkesman et al., 2010). In summary, researchers are faced with the challenge of 1) constructing a model with similarity in disease progression and symptomatology to humans, 2) detecting these phenotypes with the appropriate tests and 3) reverting them with treatment modalities that are also effective in humans (Fig. 1).

Prior to all of that, new potential candidate genes for subsequent target validation in an animal model have to be identified. Therefore, novel approaches/technologies are needed to identify genes which are independent of the monoamine system. One

possible approach is via linkage and association studies which will be discussed in more detail.

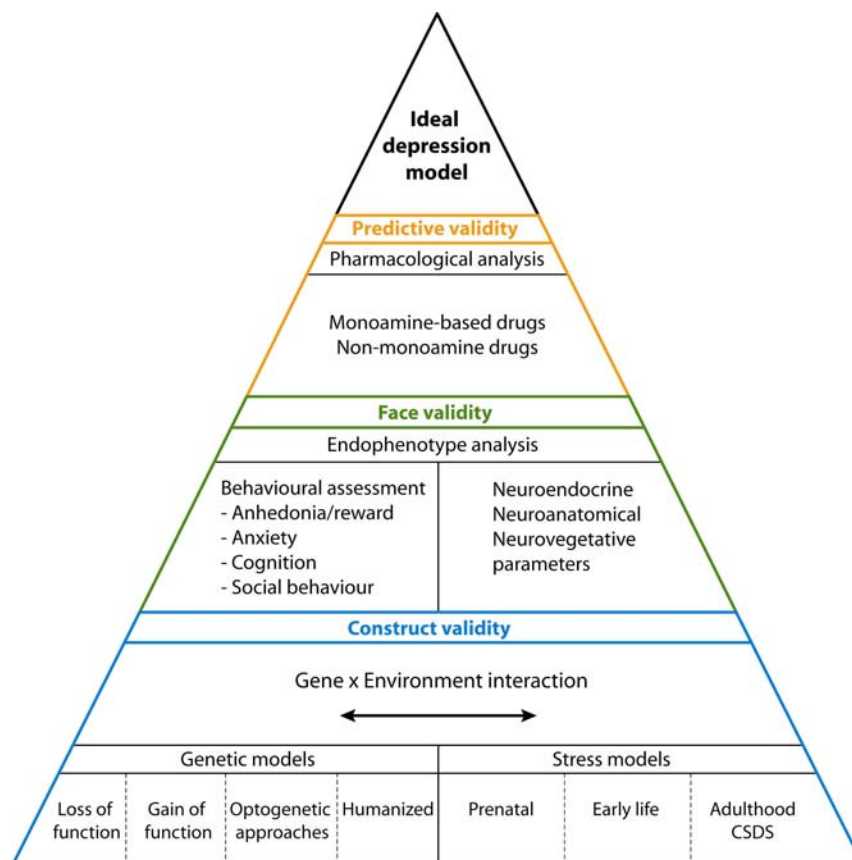


Fig. 1. Towards an ideal mouse model of depression. In order to generate more suitable depression models with strong construct validity, major efforts should be directed towards the combination of genetic modification and environmental challenges in the same subject. This would simulate gene-environment interactions that more plausibly reflect the pathophysiological mechanisms of depression. Such models should show sufficient face validity, as assessed by behavioral and/or physiological parameters and respond to classical and/or novel drugs (predictive validity) (Dedic et al., 2011).

1.3 Linkage and association studies as an unbiased approach to identify candidate genes

In a genome-wide association study (GWAS) a large number of genetic polymorphisms across the whole genome is examined to identify genetic associations with an observable trait or disease. The power of a GWAS is restricted by the sample size and the technical properties of the genotyping platform used with regard to the coverage of genomic locations. GWAS can be used to detect case-

control- or family-based associations (Craddock et al., 2008). The great advantage of this method compared to classical candidate gene studies is that it allows genetic investigation of a disease in a non-hypothesis-driven manner. Using this unbiased approach increases the possibility to find new and even unexpected genes associated with a certain disease. A key factor for this kind of study is a preferably large and well defined sample in order to detect even small effect sizes. There is evidence that for psychiatric disorders most of the heritable risk is due to interactions of combinations of genetic risk variants each with a relatively small effect on the general outcome (Cichon et al., 2009). An obvious challenge concerning the genetic investigation of mood and anxiety disorders in comparison to non-psychiatric diseases is that the phenotype and the clinical picture of mood disorders are more difficult to define. As a consequence, the patient samples used for a GWAS are often rather heterogeneous with regard to sex, age, symptoms, environmental factors and other issues, often leading to inconsistent results obtained by independent association studies analyzing the same polymorphisms. To increase the statistical power of GWAS a so-called meta-analysis can be performed by pooling all GWAS data available for a certain disease and subsequent statistical evaluation in order to increase the sample size.

In a meta-analysis of genetic studies on major depression, associations for several candidate genes have been identified, including apolipoprotein E (*APOE*), dopamine receptor D4 (*DRD4*), guanine nucleotide-binding protein (*GNB3*), methylenetetrahydrofolate reductase (*MTHFR*), dopamine transporter (*SLC6A3*) and serotonin transporter (*SLC6A4*) (Lopez-Leon et al., 2008). *DRD4* and *SLC6A3* are involved in dopaminergic neurotransmission which is known to be affected by antidepressants in the frontal area of the brain and in the nucleus accumbens (Ainsworth et al., 1998; D'Aquila et al., 2000; Tremblay et al., 2002). *SLC6A4* is a drug target of serotonin reuptake inhibitors (SRIs) such as fluoxetine (Routledge and Middlemiss, 1996), and *GNB3* is a target for tricyclic antidepressants and mono-aminoxidase (MAO) inhibitors (Rasnick et al., 1996). The *MTHFR* enzyme metabolizes folate, and lower folate levels were found to be associated with depression (Crellin et al., 1993). The most strongly associated gene, *APOE*, is involved in lipoprotein metabolism, cardiovascular diseases, Alzheimer's disease, cognitive function and immunoregulation (Mahley and Rall, Jr., 2000). Since each of these disorders may be implicated in MDD, *APOE* may represent a feasible

candidate gene which should be further investigated. In another recent meta-analysis of three European ancestry MDD GWAS data sets, no genome-wide significant results were observed. Modest associations for intronic SNPs in *ATP6V1B2*, encoding a subunit for a vacuolar proton pump ATPase, *SP4*, coding for the brain specific Sp4 zinc-finger transcription factor, and *GRM7*, encoding metabotropic glutamate receptor 7, were detected. Of these, *GRM7* may be the most reasonable candidate since previous studies reported changes in *GRM7* expression in response to antidepressant treatment (Shyn et al., 2011). The fact that only five genes were significantly associated with MDD in these meta-analyses does not mean that others may not be related, but rather that the total number of cases and controls studied was not large enough to detect moderate association of genes. Therefore, more studies are still needed.

For bipolar depression (BD), several studies have been published identifying possible susceptibility genes, among these diacylglycerol kinase eta (*DGKH*), an alpha-1 subunit of a voltage-dependent calcium channel (*CACNA1C*), and ankyrin 3 (*ANK3*) which showed robust genome-wide significance and have notably been replicated across samples (Baum et al., 2008; Ferreira et al., 2008; Scott et al., 2009; Sklar et al., 2008; Smith et al., 2009). However, the biological relevance of these genes for BP has to be determined by independent methods.

Additionally, several associations with immune-related genes have been reported (Goltser-Dubner et al., 2010), among these *P2RX7* which will be the main focus of this study. However, all these studies await further replications.

As with other complex phenotypes, GWAS in MDD and BD revealed that the identified variants only account for a small part of genetic variability (Fig. 2). This phenomenon has become known as the “case of the missing heritability” (Maher, 2008). Several explanations for this missing heritability have been suggested, including much larger numbers of variants of smaller effect yet to be found; rare variants, possibly with larger effects, that are poorly detected by available genotyping arrays that focus on variants present in 5% or more of the population; structural variants poorly captured by existing arrays; low power to detect gene-gene interactions; and inadequate accounting for shared environment among relatives. One research strategy to illuminate the genetics of complex diseases is dense genome-wide association genotyping which will be greatly facilitated by whole-genome sequencing (Manolio et al., 2009).

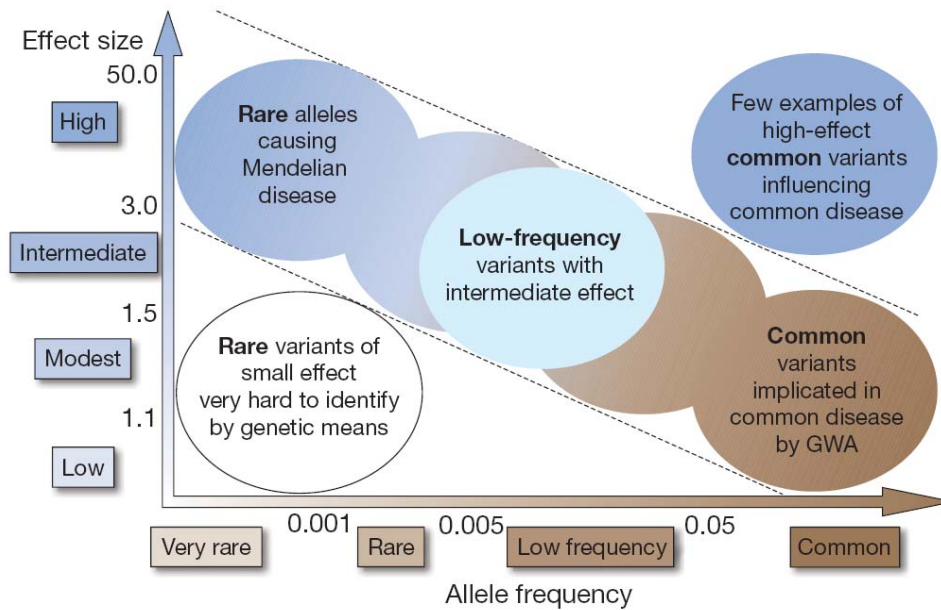


Fig. 2. Feasibility of identifying genetic variants by risk allele frequency and strength of genetic effect (odds ratio). Most interest lies in identifying associations with characteristics shown within diagonal dotted lines (Manolio et al., 2009).

As mentioned earlier, the proper way to validate the biological significance of such implicated risk variations is the generation of appropriate *in vivo* models. Using knockin mouse models, human association data can be validated and pharmacological compounds can be tested *in vivo*.

1.4 Identification of *P2RX7* as susceptibility gene for depression

Since the first report of an association with bipolar disorder in a French Canadian family-based sample (Barden et al., 2006) several studies have investigated associations of single nucleotide polymorphisms (SNPs) in the *P2RX7* gene with BD or MDD, respectively (Table 2). Most studies considered the non-synonymous SNP rs2230912 in exon 13 of the *P2RX7* gene, which leads to a substitution of glutamine (Gln) by arginine (Arg) at codon 460 (Gln460Arg).

Table 2. Overview of linkage and association studies analyzing *P2RX7*. The first five publications identified an association with MDD and/or BP (highlighted in light blue), whereas the last four publications could not detect any association (highlighted in dark blue).

publication	publication date	associated disease	population	controls	cases
Barden et al.	2006	BP	French-Canadian	214	213
Lucae et al.	2006	MDD	German-Caucasian	1029	1000
McQuillin et al.	2008	BP and MDD	London-based	560	613
Soronen et al.	2011	BP and MDD	Finnish	1322	178/272
Heijjas et al.	2008	depression symptoms	Hungarian	178	171
Green et al.	2008	no association	UK-based	690/514	687/1036
Grigoriu-Serbanescu et al.	2009	no association	4 European	2006	1445/2085
Lavebratt et al.	2010	no association	Swedish	2215	435
Viikki et al.	2011	no association	Finnish	391	218

The P2X7 receptor (P2RX7) belongs to the P2X family of ligand-gated ion channels consisting of seven members (Khakh and North, 2006). P2RX7 is a purinergic 595 amino acid cation-selective ion channel with high calcium permeability which opens upon binding of extracellular ATP released with synaptic vesicles of nerve terminals and astrocytes. The receptor is composed of two transmembrane and a large carboxy terminal cytosolic domain (Surprenant et al., 1996). The ATP binding site is suggested to be located between the transmembrane domains nearby a cysteine-rich region of the extracellular domain of the receptor (Gu et al., 2004; Worthington et al., 2002). A lipopolysaccharide (LPS)-binding site has also been identified close to the C-terminus of the receptor (Denlinger et al., 2001; Denlinger et al., 2003), whereby the receptor is able to translate inflammatory signals to signal transduction events. The minimal stoichiometric conformation of the P2RX7 channel is likely to be assembled as a trimer (North and Surprenant, 2000). Unlike other P2X receptor subunits, P2RX7 functions mainly in a homo-oligomeric form (Torres et al., 1999). However, there is evidence for the existence of P2RX7/P2RX4 heteromeric receptors (Antonio et al., 2011; Dubyak, 2007). Furthermore, P2RX7 is activated by relatively high concentrations of ATP compared to the other P2X members. In addition, prolonged activation of the receptor elicits the opening of a transmembrane pore, permeable to large molecular weight molecules up to 800 Da, which finally leads to cell death. Therefore, this receptor was previously also known as the “cell death receptor” (Sperlagh et al., 2006). It has been shown that the C-terminal domain of P2RX7 is responsible for the pore-forming property of the receptor (Adriouch et al., 2002; Surprenant et al., 1996) which is much longer than those of other P2X receptors (Sperlagh et al., 2006).

In addition to the expression in cells of the hemopoietic lineage including monocytes and peripheral macrophages, P2RX7 has been detected in neurons, astrocytes and microglia in various brain regions including the hippocampus and the cortex (Sperlagh et al., 2006).

P2RX7 regulates expression and secretion of inflammatory mediators such as interleukin-1 beta (IL-1 β) in the immune system (Ferrari et al., 1997a; Pelegrin, 2008) and neural functions such as neurotransmitter release, microglial and astroglial activation (Deuchars et al., 2001; Ferrari et al., 1997b; Kataoka et al., 2009) (Fig. 3).

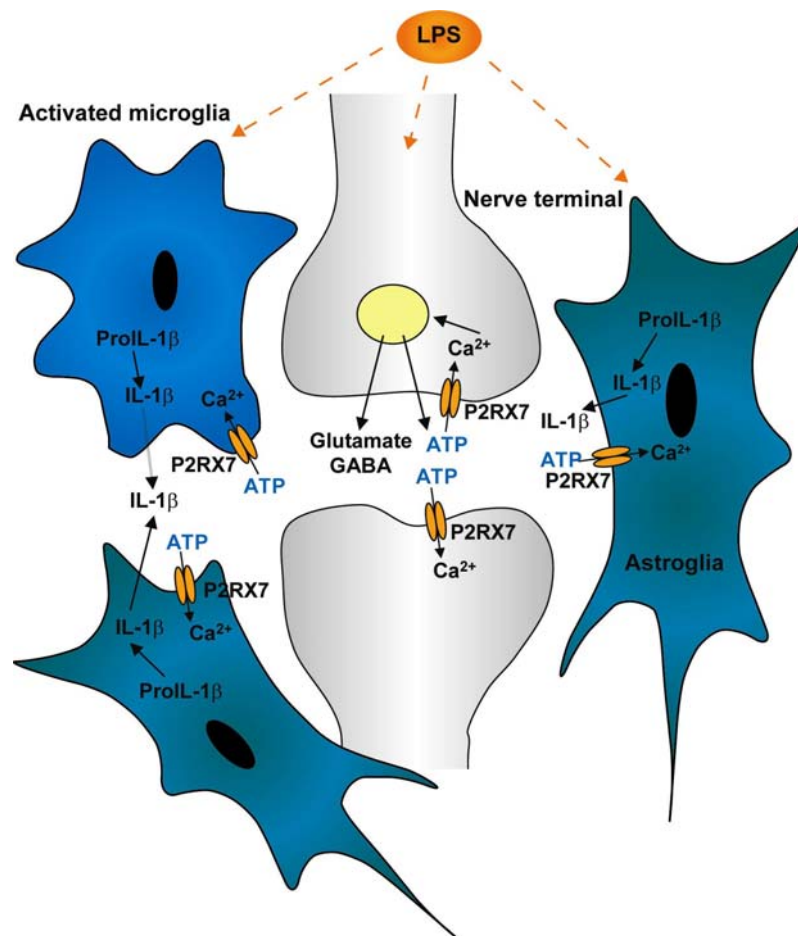


Fig. 3. P2RX7 function in the brain. P2RX7 is expressed in neurons, astrocytes and microglia in the brain. P2RX7 regulates expression and secretion of inflammatory mediators in the immune system and neural functions such as neurotransmitter release, microglial and astroglial activation in response to an inflammatory trigger, such as the bacterial lipopolysaccharide (LPS) (adapted from Sperlagh et al., 2006).

The promotion of the processing of IL-1 β (and the related IL-18) into its biologically active form is one of the best characterized functions of P2RX7. In the presence of high ATP concentrations, the low-affinity receptor is stimulated causing a massive

release of pro-inflammatory mediators, and eventually cell death, if stimulation is protracted. ATP belongs to the damage-associated molecular patterns (DAMPs), endogenous danger signals released following cell damage. ATP can also be released by a variety of injurious agents, for instance the bacterial endotoxin LPS. The innate immune response, in contrast, is stimulated by a small repertoire of conserved determinants, referred to as pathogen-associated molecular patterns (PAMPs), which are associated with potentially harmful foreign organisms and absent from host cells. PAMPs are detected by pattern recognition receptors (PRRs), among them the plasma membrane Toll-like receptors (TLRs) are the best known. To prevent an inappropriate immune reaction, a two-step control system has evolved: during the initial infection phase, mononuclear phagocytes are put in a state of alert by sensing the presence of PAMPs (first step) until detection of DAMPs signal the actual damage (second step). Processing of IL-1 β is mediated by the assembly of the so-called NALP3 inflammasome comprised of the central scaffold proteins NACHT, leucine-rich repeat (LRR), and PYD-containing protein 3 (NALP3). Two main pathways are suggested for NALP3 inflammasome activation (Fig. 4): binding of bacterial products to the NALP3 LRR domain, or depletion of cytosolic K⁺ (Di Virgilio, 2007;Lenertz et al., 2011).

NALP3 activation leads to the release of the inhibitory activity of LRR on NACHT, enabling NALP3 oligomerization. This triggers the recruitment of the accessory protein ASC (in humans also the adaptor protein Cardinal), which in turn binds to and recruits caspase-1 (Casp-1), also known as IL-1 β -converting enzyme (ICE). On the other hand, K⁺ efflux induced by activated P2RX7 can also stimulate the cleavage of pro-caspase-1 to caspase-1. Alternatively, these two pathways might converge via pannexin-1 (Panx-1). The simplest interpretation is that in the sequence leading to inflammasome activation, K⁺ efflux is upstream of Panx-1 and is required for Panx-1 activation. This implies that Panx-1 participates in P2RX7-dependent inflammasome activation not in its property as an ion channel but rather as a transducer of changes in intracellular K⁺ caused by P2RX7. Casp-1 consequently can convert pro-IL-1 β , which accumulates in the cytoplasm, to its bioactive form having a leader sequence for targeting to exocytotic vesicles. Finally, the mature IL-1 β may be released either by exocytosis or, alternatively, by microvesicles that are shed into the pericellular environment (Di Virgilio, 2007;Lenertz et al., 2011).

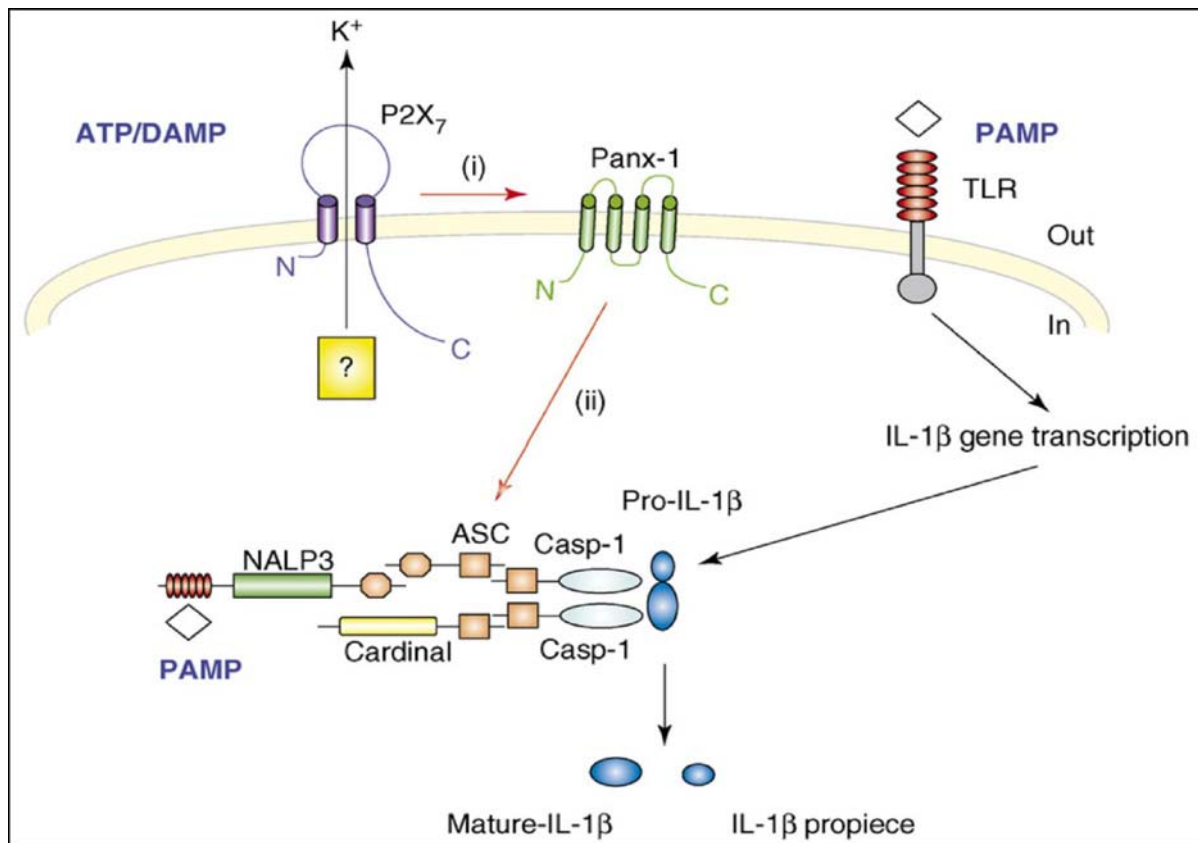


Fig. 4. Hypothetical sequence of events leading to P2RX7 and Panx-1-mediated inflammasome activation. PAMPs bind to TLRs and drive IL-1 β gene expression and accumulation of the pro-cytokine. Extracellular ATP binds to the P2X7 receptor and triggers K⁺ efflux and Panx-1 activation. The functional significance of K⁺ efflux is unknown, although it might facilitate or even initiate inflammasome activation. Likewise, the mechanism of Panx-1 activation by the P2X7 receptor is unknown. Panx-1 in turn activates the inflammasome. The activated inflammasome then cleaves pro-IL-1 β . Thus, stimulation of the inflammasome by extracellular ATP can be split into two steps: (i) recruitment and activation of Panx-1 by the P2X7 receptor, and (ii) activation of the inflammasome by Panx-1 (Di Virgilio, 2007).

It was suggested that P2RX7 may also be involved in the regulation of synaptic transmission at the presynaptic site (Deuchars et al., 2001) and P2RX7-mediated regulation of glutamatergic and GABAergic release from excitatory nerve terminals has been shown in rat hippocampal brain slices (Papp et al., 2004; Sperlagh et al., 2002). Additionally, P2RX7 is involved in the intracellular signaling cascade of ATP-induced extracellular signal-regulated protein kinase (ERK) phosphorylation via protein kinase C (PKC) (Bradford and Soltoff, 2002; Stefano et al., 2007).

The Gln460Arg polymorphism is located in the C-terminal cytosolic domain of the P2RX7 channel protein (Fig. 5) and is therefore likely to affect P2RX7 function.

However, *in vitro* studies analyzing the functional consequences of the Gln460Arg polymorphism could not reveal any significant effects, which is in contrast to the findings when examining other SNPs in *P2RX7*. Currently, about 32 non-synonymous SNPs for the *P2RX7* gene are documented in the dbSNP database (www.ncbi.nlm.nih.gov/SNP). Some of these are depicted in Fig. 5.

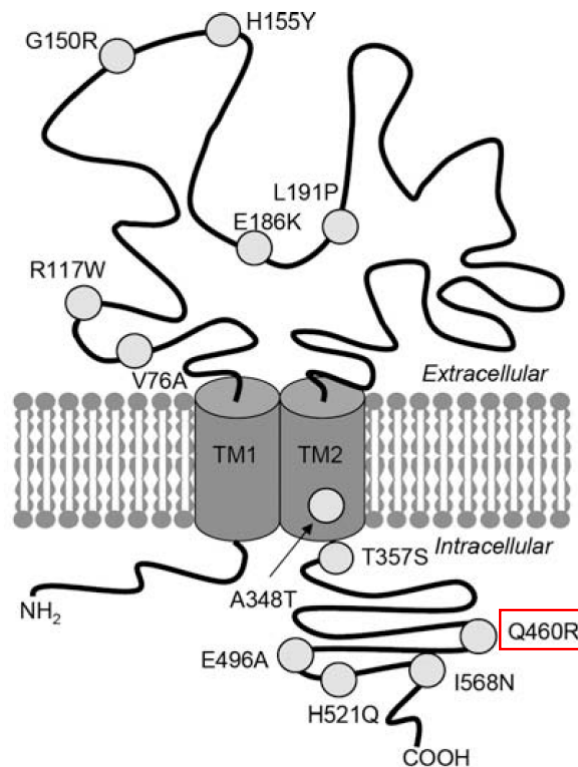


Fig. 5. The Gln460Arg polymorphism. The SNP is located in the C-terminal cytosolic domain of *P2RX7* (Roger et al., 2010).

The first SNP to be functionally described was 1513A>C which changes glutamic acid to alanine at residue 496 (E496A) in the C-terminus of the receptor. The E496A polymorphism leads to the abolition of ATP-induced ethidium⁺ uptake in native or transfected cells, but the immediate ATP-induced opening of the *P2RX7* channel protein is not affected. The second SNP to be analyzed was 1729T>A that changes isoleucine to asparagine at residue 568 (I568N) and which is located in a trafficking motif within the C-terminus of the receptor preventing normal trafficking and cell surface expression of *P2RX7*. A third SNP, 946G>A, changes arginine to glutamine at residue 307 (R307Q) in the ATP-binding pocket of the extracellular domain leading to depleted channel and pore function although the surface expression of the receptor is not altered. A splice site mutation (g>t) at position +1 of the first intron

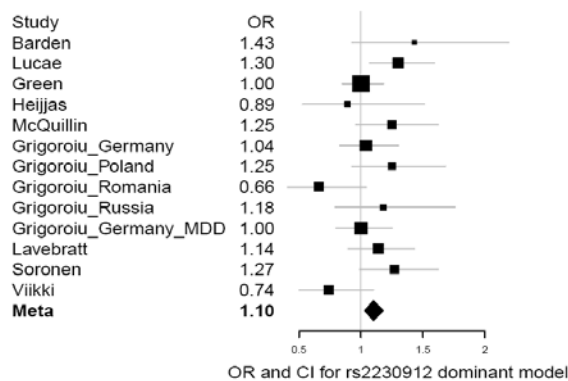
causes a null allele in almost 1% of Caucasian individuals due to nonsense-mediated mRNA decay. A fifth polymorphism (1096C>G) changes threonine to serine at amino acid 357 (T357S) resulting in impaired channel and pore functions of P2RX7. A sixth polymorphism (489C>T) changes amino acid 155 from histidine to tyrosine (H155Y) in the ectodomain producing a gain of function effect on P2RX7 pore function and calcium influx. Finally, a seventh polymorphism has been described at 474G>A leading to a G150R substitution which reduces receptor function in native cells (Fuller et al., 2009). In another recent study, the functional effects of twelve non-synonymous SNPs in the *P2RX7* gene previously identified in individuals with affective mood disorders were investigated. Therefore, site-directed mutagenesis was used to introduce the SNPs into the human *P2RX7* gene, and functional effects were tested by whole cell patch-clamping in order to examine channel activity and measurements of ethidium⁺ uptake to analyze pore formation. They confirmed the functional effects of several previously established SNPs (H155Y, A166G, A348T, T357S, E496A and I568N) which modify receptor function (Gu et al., 2001; Wiley et al., 2003; Cabrini et al., 2005; Shemon et al., 2006; Fuller et al., 2009), and revealed that several other SNPs (V76A, R117W, G150R, E186K, L191P and Q521H) can also alter receptor function. Three mutations led to a complete loss of function (G150R, E186K and I568N), five SNPs significantly impaired receptor function (V76A, R117W, L191P, T357S, E496A), and two resulted in a marked gain of function (H155Y and A348T). In contrast, no functional effect was observed with the Q460R mutant arising from the rs2230912 SNP which was most frequently associated with affective mood disorders (Roger et al., 2010; Sluyter et al., 2010).

However, there is currently no consensus as to whether this SNP confers susceptibility to mood disorders. While some studies reported association of this SNP with BD or MDD (Hejjas et al., 2009; Lucae et al., 2006; McQuillin et al., 2009; Soronen et al., 2011) other studies did not detect significant associations (Green et al., 2009; Grigoriou-Serbanescu et al., 2009; Lavebratt et al., 2010; Viikki et al., 2011) (Table 2).

Therefore, a meta-analysis was performed taking into account the nine published studies. The meta-analysis revealed a significant effect of rs2230912 on MDD/BD case-control status which can be explained by a dominant ($p = 0.0085$, OR = 1.10) or a heterozygous-disadvantage model ($p = 0.005$, OR = 1.11) (Fig. 6). However, the

functional impact of the SNP *in vivo* has not been studied yet and will be one of the main objectives of this study.

(a) Dominant model



(b) Heterozygous disadvantage model

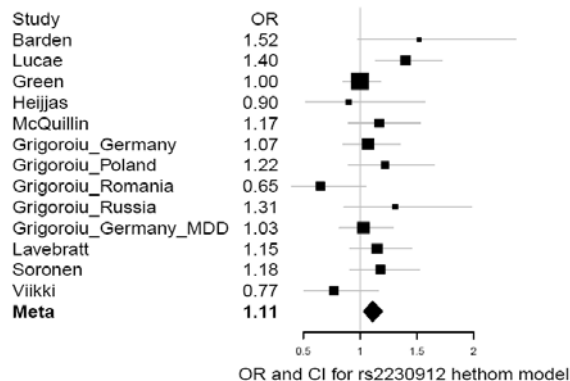


Fig. 6. Forest plot of the meta-analysis. Depicted are the odds ratios (OR) for the associations revealed in the nine different publications and the meta-analysis which can be explained by a dominant model (a) or a heterozygous disadvantage model (b). The study of Grigoriou-Serbanescu was analyzed separately according to the different ethnic groups (Aprile-Garcia et al., submitted).

1.5 Identification of *TMEM132D* as new candidate gene for panic disorder

In a recent whole-genome association study, Erhardt and colleagues found SNPs in the *TMEM132D* gene, located on chromosome 12, to be associated with panic disorder (PD) in three independent Caucasian samples (combined sample consisting of 909 cases and 915 controls). The highest associated SNP (rs7309727) showed a significant case-control association with PD. The T allele was found to be the risk allele for PD. The second best associated SNP in *TMEM132D*, rs11060369, showed a trend for association (Fig. 7).

Additionally, independent SNPs in this gene were also associated with the severity of anxiety symptoms in patients suffering from PD as well as in individuals affected by unipolar depression. The strongest association was found for rs900256, a SNP located in intron 4 of the gene. Two more markers in close proximity, rs879560 and rs10847832, were also associated with severity of anxiety symptoms (Fig. 7).

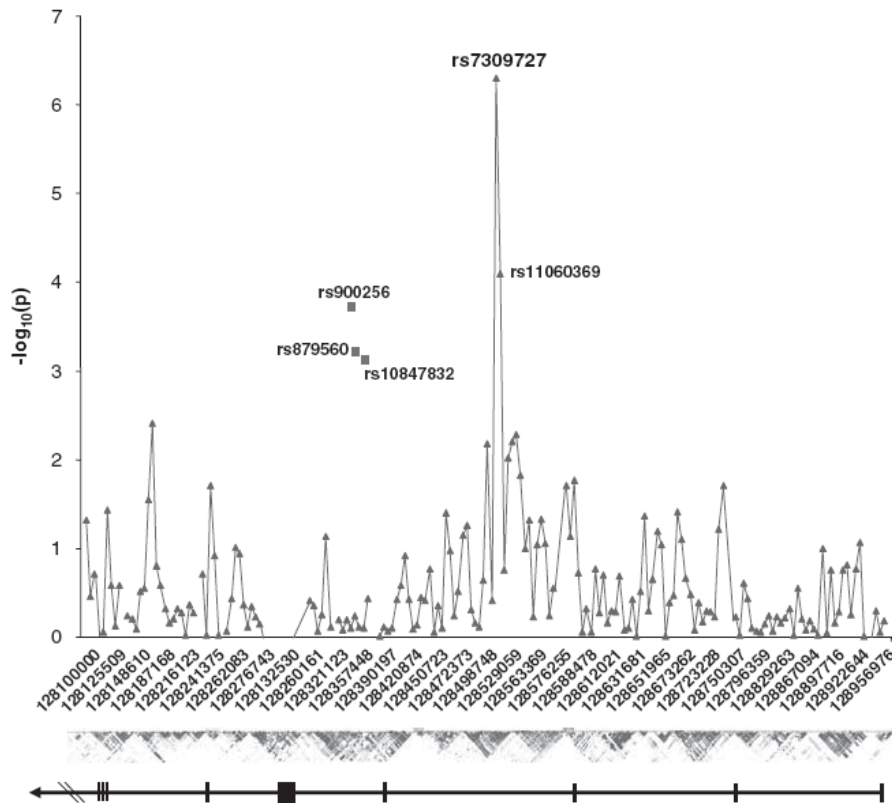


Fig. 7. Illustration of the SNPs found in the *TMEM132D* gene. The x axis represents the position on chromosome 12 with the position of *TMEM132D* (exons as vertical lines) and the linkage disequilibrium (LD) structure of this region. On the y axis, the p values are shown as $-\log_{10}$ (case-control panic: triangles; severity of anxiety: squares) (Erhardt et al., 2011).

Interestingly, the three SNPs associated with severity of anxiety symptoms were separated by two hotspots of recombination from rs7309727 and rs11060369, associated with PD in the case-control design (Erhardt et al., 2011). Furthermore, it was shown that *TMEM132D* mRNA expression is increased in post mortem tissues of healthy controls carrying the SNP (Myers et al., 2007). In parallel, mice bred for high anxiety-related behavior exhibit enhanced *Tmem132d* mRNA expression in the anterior cingulate cortex which is involved in the processing of anxiety- and fear-related stimuli (Erhardt et al., 2011).

In another recent study, an association of the rs11060369 SNP in *TMEM132D*, which was already identified in the GWAS analyzing PD, with attention-deficit/hyperactivity disorder (ADHD) in children was detected (Mick et al., 2011). It has been shown that individuals with ADHD are more prone to develop additional psychiatric morbidity with mood, anxiety, behavioral, or substance abuse disorders (Angold et al., 1999; Biederman et al., 1991). For the GWAS, the Child Behavior Checklist Dysregulation Profile (CBCL-DP) (Althoff et al., 2010a) defined from the

Anxious/Depressed, Attention Problems and Aggression scales was used. Children with elevated CBCL-DP scores are more susceptible for psychopathology, psychiatric hospitalization, and suicidality (Ayer et al., 2009; Biederman et al., 2009; Meyer et al., 2009; Youngstrom et al., 2005), but also impaired CBCL-DP scores have been associated with an increased vulnerability to develop anxiety, mood, disruptive behavior, and drug abuse disorders 14 years later in adulthood (Althoff et al., 2010b).

Thus, *TMEM132D* may be an important new candidate gene with regard to depression and anxiety.

TMEM132D, also termed mature oligodendrocytes transmembrane protein (MOLT), was found to be expressed in mature oligodendrocytes in the brain (Nomoto et al., 2003). TMEM132D belongs to the TMEM132 family which consists of the members TMEM132A, B, C, D and E.

Table 3. Homology of TMEM132D with other family members. Chromosome positions and homology of murine protein sequences of TMEM132 family members is depicted.

	chromosome	consensus positions	identity positions
TMEM132A	19	43,30%	29,20%
TMEM132B	5	55,50%	43,10%
TMEM132C	5	66,50%	55,10%
TMEM132D	5	100%	100%
TMEM132E	11	49,50%	34,90%

The different members are not very homologous (Table 3) but the transmembrane sequence is highly conserved (Fig. 8). The structure of the TMEM132D protein as well as the molecular function is largely unknown.

	(1049)	1049	1060	1070
TMEM132A (842)		LGMYALIGVFCLAILVFLVNGVVFVLF		
TMEM132B(1013)		IGMYALICVFCCLAAILVFLINCVAFVWF		
TMEM132C (926)		IGMYALIGVFCCLAAILVFLINCATFAFF		
TMEM132D (916)		IGMYALIGVFCCLAAILVFLINCVTFALK		
TMEM132E (798)		IGMYALIGVFCCLAAILVFLINCLIVEVLF		
Consensus(1049)		IGMYALLGVFCCLAAILVFLINCV FALK		

Fig. 8. The sequence of the transmembrane domain is highly conserved within family members. A multiple alignment of murine protein sequences representing the transmembrane domain is shown. The full consensus is depicted in yellow.

Bioinformatic analysis of the TMEM132D protein sequence using different protein databases provides evidence for a potential single-pass type I transmembrane protein (see supplementary data). Further screening for sites and motifs in the TMEM132D protein revealed two interesting possible protein sites: (1) the amino acids 235-237 of mouse TMEM132D represent a potential cell attachment sequence called RGD (Arg-Gly-Asp) which was originally discovered in fibronectin and is recognized by integrins (Ruoslahti, 1996), (2) the amino acids 472-486 of mouse TMEM132D are similar to a thrombospondin type 3 repeat which binds to calcium. Thrombospondin is an adhesive glycoprotein which mediates cell to cell or cell to matrix interactions and can bind to fibrinogen, fibronectin, laminin and collagen (Adams, 2001). These findings suggest that TMEM132D may be involved in cell adhesion/migration and cell-cell interaction, respectively.

However, the true cellular and molecular functions of TMEM132D have to be addressed by *in vitro* and *in vivo* experiments.

1.6 Aim of the thesis

Considering the variety of drawbacks of currently used antidepressant drugs, the present study aimed to validate new candidate genes – *P2RX7* and *TMEM132D* – identified by linkage and/or association studies as potential new targets for treatment of mood disorders independent from the monoamine system.

The fact that the *P2RX7*-Gln460Arg polymorphism has been identified in several genetic studies for unipolar and bipolar depression rendered *P2RX7* a reasonable candidate to be analyzed. Although there are certain inconsistencies regarding the GWAS results, a meta-analysis supports a contribution of the *P2RX7*-Gln460Arg polymorphism to increased susceptibility for the development of mood disorders. Moreover, heterozygote carriers of *P2RX7*-wild-type (WT) and *P2RX7*-Gln460Arg are over-represented among patients with major depression (Lucae et al., 2006). However, the precise role of this SNP *in vivo* and in heterozygous individuals carrying both *P2RX7* variants is not known. These considerations led us to study the functional consequences of this SNP in the context of increased risk for depression and the depressive phenotype. Therefore, the following specific aims were addressed:

- a) What are the effects of *P2rx7* ablation on depression- and anxiety-related behavior?
- b) What are the functional consequences of the SNP on *P2X7* receptor function?
- c) What are the effects of the SNP on endophenotypes associated with mood disorders under basal conditions and in response to an environmental challenge?

To **a)** Total *P2rx7* knockout mice previously established in our group were analyzed in terms of depression- and anxiety-related behavior.

To **b)** Transgenic mice expressing human *P2RX7*-WT and *P2RX7*-Gln460Arg, respectively, were generated and analyzed regarding release of pro-inflammatory cytokines and activation of intracellular signaling cascades.

To **c)** Humanized *P2RX7* mice were behaviorally characterized with respect to endophenotypes related to mood disorders under normal housing conditions as well as in response to chronic social defeat stress serving as environmental trigger. In addition, analysis of sleep pattern/architecture was performed.

The association of different SNPs in *TMEM132D* not only with depression-related symptoms but also with aspects of anxiety in patients suffering from major depression, panic disorder or ADHD suggests *TMEM132D* as another interesting candidate gene. However, the function of *TMEM132D* is completely unknown and the SNPs which were found to be associated are all intronic rendering validation of the human findings rather difficult. Therefore, we used *in vitro* and *in vivo* approaches to investigate the general function of *TMEM132D* in the brain as well as its possible contribution to endophenotypes related to mood disorders. Therefore, the following questions were addressed:

- a) Is *Tmem132d* expressed in the brain and if yes, in which spatial and temporal window?
- b) Which is the intracellular localization of *TMEM132D*?
- c) What is the effect of *TMEM132D* overexpression on cell morphology?
- d) Which proteins are possible interaction partners of *TMEM132D*?
- e) Is *TMEM132D* expressed in neurons and if yes, in which types of neurons?
- f) What are the effects of *Tmem132d* disruption on endophenotypes related to mood disorders?

To **a)** The expression pattern of *Tmem132d* and other *Tmem132* family members during several postnatal stages and in the adult mouse brain was analyzed using *in situ* hybridization.

To **b)** The intracellular localization of *TMEM132D* was determined using a GFP-fusion construct expressed in cell culture.

To **c)** The consequences of *TMEM132D* overexpression were assessed *in vitro*.

To **d)** A membrane yeast-two-hybrid screen was carried out to identify interacting membrane/soluble proteins.

To **e)** *Tmem132d* reporter knockout animals were generated using a gene trap strategy. These knockout mice were used to analyze cell-type specific expression of *TMEM132D* in the brain.

To **f)** *Tmem132d* knockout mice were characterized with regard to depression- and anxiety-related behavior.

2 Material and methods

2.1 Material

2.1.1 Buffers and solutions

All buffers and solutions were prepared using Millipore Q-distilled water. Chemicals were purchased from Sigma, Roth and Merck unless indicated otherwise.

2.1.1.1 Buffers for agarose gel electrophoresis

1x TRIS acetate EDTA (TAE) buffer

4.84 g tris(hydroxymethyl)-aminomethan (TRIS)

1.142 ml acetic acid

20 ml 0.5 M ethylenediaminetetraacetic acid (EDTA), pH 8.0

800 ml H₂O_{bidest.}

adjust pH to 8.3 with acetic acid

adjust volume to 1 liter with H₂O_{bidest.}

6x DNA loading buffer (orange)

1 g orange G

10 ml 2 M Tris-HCl, pH 7.5

150 ml glycerol

adjust volume to 1 liter with H₂O_{bidest}

2.1.1.2 Solutions for *in situ* hybridization (ISH)

10x triethanolamine (TEA)

1 M TEA

pH 8.0

adjust H₂O_{bidest.}, add 1 ml DEPC/liter

incubate overnight

2x autoclave

Hybridization-mix (hybmix)

50 ml formamide

1 ml 2 M Tris-HCl, pH 8.0

1.775 g NaCl

1 ml 0.5 M EDTA, pH 8.0

10 g dextransulphate

0.02 g ficoll 400

0.02 g polyvinylpyrrolidone 40 (PVP40)

0.02 g bovine serum albumin (BSA)

5 ml tRNA (10 mg/ml)

1 ml carrier DNA (salmon sperm, 10 mg/ml)

4 ml 5 M dithiothreitol (DTT)

store as 1 to 5 ml aliquots at -80°C

Hybridization chamber fluid

250 ml formamide

50 ml 20x SSC

200 ml H₂O_{bidest.}

5 M DTT/diethyl pyrocarbonate (DEPC)

7.715 g DTT

4 ml DEPC-H₂O

shake the falcon tube until the powder is nearly solved

adjust volume to 10 ml with DEPC-H₂O

10x proteinase K buffer/DEPC

500 ml 1 M Tris-HCl, pH 7.5

100 ml 0.5 M EDTA, pH 8.0

adjust volume to 1 liter with DEPC-H₂O

autoclave

5x NTE

146.1 g NaCl

50 ml 1 M Tris-HCl, pH 8.0

50 ml 0.5 M EDTA, pH 8.0

adjust volume to 1 liter with H₂O_{bidest.}, add 1 ml DEPC

incubate overnight

autoclave

2.1.1.3 Solutions for Southern Blot

Lysis buffer

10 mM Tris-HCl

10 mM EDTA

10 mM NaCl

0.5% sarcosyl

1 mg/ml proteinase K (Sigma Aldrich)

Denaturation buffer

0.5 M NaOH

1.5 M NaCl

Neutralization buffer

1.5 M NaCl

0.5 M Tris-HCl, pH 7.5

1 mM EDTA

Wash buffer I

2% SSC
0.1% sodium dodecyl sulfate (SDS)

Wash buffer II

0.2% SSC
0.1% SDS

2.1.1.4 Solutions for Western blot

RIPA lysis buffer

50 mM Tris, pH 8.0
150 mM NaCl
0.1% SDS
1.0% NP-40
0.5% sodium deoxycholate

Loading buffer (4x)

50% glycerol
125 mM Tris-HCl, pH 6.8
20% SDS
1% bromophenol blue
5% β -mercaptoethanol

12% resolving gel for SDS PAGE (10 ml)

3.3 ml H₂O
4.0 ml 30% acrylamide mix
2.5 ml 1.5 M Tris-HCl, pH 8.8
0.1 ml 10% SDS
0.1 ml 10% ammonium persulfate
0.004 tetramethylethylenediamine (TEMED)

5% stacking gel for SDS PAGE (1 ml)

0.68 ml H₂O
0.17 ml 30% acrylamide mix
0.13 ml 1.0 M Tris-HCl, pH 6.8
0.01 ml 10% SDS
0.01 ml 10% ammonium persulfate
0.001 ml TEMED

Running buffer (10x SDS PAGE)

30.3 g Tris
144 g glycine
50 ml 20% SDS
adjust to 1 liter H₂O

Transfer buffer

400 ml methanol
6.06 g Tris
28.8 g glycine
fill up with 2 liters H₂O
pH 8.3

10x TBS

12.11 g Tris
87.66 g NaCl
pH 7.6

1x TBS-T

900 ml H₂O
100 ml 10x TBS
0.1 ml tween-20
(for 5% milk solution dissolve 5 g milk powder in 100 ml TBS-T)

2.1.1.5 LacZ staining solutions

LacZ-fix

4% paraformaldehyde (PFA)/PBS, pH 7.4
0.005 M ethylene glycol tetraacetic acid (EGTA)
0.001 M MgCl₂
diluted in 0.1 M PBS, pH 7.4

LacZ wash buffer

0.002 M MgCl₂
0.01% deoxycholate
0.02% Nonidet P40 (NP40)
diluted in 0.1 M PBS, pH 7.4

LacZ staining solution

0.1% X-Gal (stock solution in DMF)
0.005 M potassium-ferrocyanide
0.005 M potassium-ferricyanide
diluted in LacZ wash buffer

2.1.1.6 Other buffers and solutions

10x phosphate buffered saline (PBS)

1.37 M NaCl
27 mM KCl
200 mM Na₂HPO₄ x 12 H₂O
20 mM KH₂PO₄
pH 7.4
adjust H₂O_{bidest.}, add 1 ml DEPC/liter
incubate overnight
2x autoclave

20x standard saline citrate (SSC)

3 M NaCl

300 mM sodium citrate

pH 7.4

adjust H₂O_{bidest.}, add 1 ml DEPC/liter

incubate overnight

2x autoclave

Cryoprotection solution

125 ml ethyleneglycol

125 ml glycerol

250 ml PBS (1x)

TBFI solution

30 mM KAc

50 mM MnCl₂

100 mM RbCl

10 mM CaCl₂

15% glycerol

adjust pH 5.0 with acetic acid, filter sterile

TBFII solution

10 mM NaMOPS, pH 7.0

10 mM RbCl₂

15 mM CaCl₂

15% glycerol

filter sterile

2.1.2 Media for bacterial cultures

Lysogeny broth (LB) medium

1% (w/v) bacto-tryptone (BD)
0.5% (w/v) bacto-yeast-extract (BD)
1.5% (w/v) NaCl
pH 7.4 with NaOH
autoclave

LB agar plates

1% (w/v) bacto-tryptone
0.5% (w/v) bacto-yeast-extract
1.5% (w/v) NaCl
1.5% (w/v) bacto-agar (BD)
pH 7.4 with NaOH
autoclave

Super optimal broth (SOC) medium

2.0% (w/v) bacto-tryptone
0.5% (w/v) bacto-yeast-extract
10 mM NaCl
2.5 mM KCl
10 mM MgSO₄
10 mM MgCl₂
autoclave
add 20 mM glucose
filtered sterile

2.1.3 Media for cell culture

All cell culture solutions were obtained from Invitrogen unless indicated otherwise.

2.1.3.1 Media for cell lines

Growth medium

500 ml Dulbecco's modified eagle medium (DMEM)

50 ml fetal calf serum (FCS)

5 ml glutamine

10 ml penicillin/streptomycin (5000 U/ml)

Freezing medium

95% FCS

5% dimethylsulfoxide (DMSO)

2.1.3.2 Media for embryonic stem (ES) cell culture

Medium for TBV2 ES cells

500 ml DMEM (high glucose)

75 ml FCS (PAN Biotech)

5 ml L-glutamine (200 mM)

5 ml MEM nonessential amino acids (100x)

1 ml mercaptoethanol (50 mM)

90 µl LIF (107 U/ml) (Chemicon)

for selection, 200 µg/ml geneticin (G418) was added

Medium for EMFI feeder cells

500 ml DMEM (high glucose)

50 ml FCS (PAA)

5 ml L-glutamine (200 mM)

6 ml MEM nonessential amino acids (100x)

Freezing medium

5 ml FCS (PAN Biotech)

3 ml ES cell medium

2 ml DMSO

2.1.4 Oligonucleotides

2.1.4.1 Primers used for cloning procedures

name	sequence
mP2RX7_ISH_for	5'-TTGACTTGCTCATCAACACATACTCCAG-3'
mP2RX7_ISH_rev	5'-GCGTTGCTCCGGTAGGCGAGA-3'
hP2RX7_ISH_for	5'-TCGACTTCCTCATCGACACTT-3'
hP2RX7_ISH_rev	5'-GTGGCTCTCAGGGAGTTGAG-3'
mTmem132a_Ex11_for	5'-GTCCGAAGCGAGTCGAGTT-3'
mTmem132a_3UTR_rev	5'-GCCCTCCCTCTTGACCATAG-3'
mTmem132b_Ex1_for	5'-CAGCGTGGTGGTCTACCCTA-3'
mTmem132b_Ex3_rev	5'-TCATGGAGTCTTCCACAGGA-3'
mTmem132c_3UTR_for	5'-AACGGAAGGAGCTCTCAGTG-3'
mTmem132c_3UTR_rev	5'-CTTGGGCAGAAGGCTAACAG-3'
mTmem132d_Ex9_for	5'-CAGACGATGGGTGTCCTTCT-3'
mTmem132d_3UTR_rev	5'-CCTTAAACGCGCATCTTTGT-3'
mTmem132e_3UTR_for	5'-TGAGTGTTGGGGAACAGTTG-3'
mTmem132e_3UTR_rev	5'-TGGGTAGAACCCAAGAGGTG-3'
P2RX7_5'SB_for	5'-TAGTCTGGCCCAAGGAACTG-3'
P2RX7_5'SB_rev	5'-AGTCCCTGGAGCAAACACAG-3'
P2RX7_3'SB_for	5'-AGGCTAAGATGCTGGCAATGC-3'
P2RX7_3'SB_rev	5'-CCCATGGACACTCCTCACAC-3'
P2RX7_5'HA_for	5'- <i>PacI</i> -GTCATGTGACAACTGCATGC-3'
P2RX7_5'HA_rev	5'- <i>MfeI</i> -GCTGGATCATCAGACTCTGT-3'
P2RX7_3'HA_for	5'- <i>AscI</i> -AGT-TTG-CAA-AGC-CGA-GAA-AA-3'
P2RX7_3'HA_rev	5'- <i>EcoRI</i> -GTCCTTTTTGCAAGGCTGAGG-3'
mMOLT_EGFP-N1_for	5'-AT- <i>HindIII</i> -ATGTGCCCATCTGAGATG-3'
mMOLT_EGFP-N1_rev	5'-AT- <i>EcoRI</i> -GTACGTGCTCGTGTAAC-3'
TD_pBT3-SUC_for	5'-ATTAACAA- <i>SfiI</i> -CGAGGGATCCTGGAGAGCATTTCAGCGG-3'
TD_pBT3-SUC_rev	5'-AACTGATT- <i>SfiI</i> -CCTACGTGCTCGTGTAACCTCTCCAT-3'

2.1.4.2 Primers used for genotyping

name	sequence	comment
P2rx7-KO_for	5'-GCAGTCTCTCTTTGCCTCGT-3'	484 bp wild-type and a 317 bp mutant PCR product
P2rx7-KO_rev	5'-GACCGAAGGCAAGAACTGAC-3'	
P2rx7-KO_rev2	5'-GGAAAGACCGCGAAGAGTTTG -3'	
hP2RX7-SNP_for	5'-GTGGATGAATCCCACATTAGGATGGTG-3'	557 bp product restricted with <i>PvuII</i> results in a 171 bp, 332 bp and 54 bp fragment for hWT and a 503 bp and 54 bp fragment for hMT
hP2RX7-SNP_rev	5'-TACTGCCCTTCACTCTTCGGAAAC-3'	
P2RX7_mIntron1_for	5'-AGACTGTCACCAGCAGCAGCTC-3'	933 bp for wild-type and a 613 bp mutant PCR product
P2RX7_hEx6-7_rev	5'-CAGGATGTTTCTCGTGGTGTAG-3'	
P2RX7_mIntron2_rev	5'-CATACTTCTCCGTGGTCTAC-3'	
neo_triplePCR_for1new	5'-CCACCAACGTGTCCTTGAC-3'	867 bp neo-pos. and a 1173 bp product for neo-neg.
neo_triplePCR_for2	5'-CTCGTCCTGCAGTTCATTCA-3'	
neo_triplePCR_rev	5'-CGTCGACTGTCTTCTGGTCA-3'	
NEO-GT1	5'-AGCCAACGCTATGTCCTGATAG-3'	503 bp product
NEO-GT2	5'-TGAATGAACTGCAGGACGAGG-3'	
Flipase-for	5'-TTCGAATCATCGGAAGAAGC-3'	413 bp product
Flipase-rev	5'-TTGCCGGTCCTATTTACTCG-3'	
TD-KO_5'E302C11_for	5'-ACTGGTCACATTGTATCCACAGTC-3'	1172 bp product
TD-KO_5'E302C11_rev	5'-CCTATAGTGAGTCGTATTCTCCCG-3'	
TD-KO_3'E302C11_for	5'-CACAGTCAGACAGAGACAACACAG-3'	1361 bp product
TD-KO_3'E302C11_rev	5'-GAGGCTGTAAGACTCCACGTAAAT-3'	
Cre_for	5'-GATCGCTGCCAGGATATACG-3'	574 bp product
Cre_rev	5'-AATCGCCATCTTCCAGCAG-3'	
CTSQ_for	5'-ACAAGGTCTGTGAATCATGC-3'	1098 bp product
CTSQ_rev	5'-TTACAATGTGGATTTTGTGGG-3'	
i-Cre 1_for	5'-GGTTCTCCGTTTGCCTCAGGA-3'	290 bp for wild-type and a 375 bp mutant PCR product
i-Cre 2_rev	5'-CTGCATGCACGGGACAGCTCT-3'	
i-Cre 3_rev	5'-GCTTGCAGGTACAGGAGGTAGT-3'	
LACZ-1for	5'-CGCCATTTGACCACTACC-3'	631 bp product
LACZ-2rev	5'-GGTGGCGCTGGATGGTAA-3'	

2.1.4.3 Primers used for expression analysis

name	sequence	comment
mP2rx7_E1-8_for	5'-TGCACATGATCGTCTTTTCC-3'	nts 261-959 of accession no. NM_011027
mP2rx7_E1-8_rev	5'-ACCAGCTGTCTAGGTTGC-3'	
mP2rx7_E6-8_for	5'-GCCGAAAACCTTCACCGTACT-3'	nts 716-959 of accession no. NM_011027
mP2rx7_E6-8_rev	5'-ACCAGCTGTCTAGGTTGC-3'	
mP2rx7_E1-tau-lacZ_for	5'-TGCACATGATCGTCTTTTCC-3'	nts 261-tau-lacZ of accession no. NM_011027
mP2rx7_E1-tau-lacZ_rev	5'-GTTTTCCAGTCACGACGTT-3'	
mP2rx7_E3-4_for	5'-CTATGTCAAGTCAGAAGGCCAAG-3'	(Taylor et al., 2009); nts 484-585 of accession no. NM_011027
mP2rx7_E3-4_rev	5'-TCCATCCACCCCTTTTACAAC-3'	
mP2rx7_E1-4_for	5'-CACATGATCGTCTTTTCCTAC-3'	(Nicke et al., 2009); nts 263-560 of accession no. NM_011027 of <i>P2rx7(a)</i> or respective nts of (k)
mP2rx7_E1'-4_for	5'-GCCCGTGAGCCACTTATGC-3'	
mP2rx7_E1-4_rev	5'-GGTCAGAAGAGCACTGTGC-3'	
β -actin_for	5'-ATCGTGCGTGACATCAAAGA-3'	nts 702-1146 of accession no. NM_007393
β -actin_rev	5'-ACATCTGCTGGAAGGTGGAC-3'	
mTmem132a_Ex6_for	5'-AACTGTCCGAGTTCCTGTGG-3'	nts 1166-1670 of accession no. ENSMUST00000025645
mTmem132a_Ex8_rev	5'-CGGATTTGTTCCAGAGTGGT-3'	
mTmem132b_Ex_for	5'-CAGCGTGGTGGTCTACCCTA-3'	nts 701-1131 of accession no. ENSMUST00000031446
mTmem132b_Ex_rev	5'-TCATGGAGTCTTCCACAGGA-3'	
mTmem132c_Ex6_for	5'-GCAAGATGGACTCTGTGGTG-3'	nts 1625-2204 of accession no. ENSMUST00000051260
mTmem132c_Ex8_rev	5'-GAGGTGGCCTTGTTGTTCTC-3'	
mTmem132d_Ex6_for	5'-GGCAAGGTGAACGTGGTAGT-3'	nts 2202-2789 of accession no. ENSMUST00000044441
mTmem132d_Ex8_rev	5'-AGTGGCAAAGATGGCTCTGT-3'	
mTmem132e_Ex6_for	5'-ATGAACGCCAGAGTCACCTT-3'	nts 1414-1923 of accession no. ENSMUST00000092852
mTmem132e_Ex8_rev	5'-ACTGACCTTCTCCTCCGTCA-3'	

2.1.5 Probes (DNA and mRNA)

Probes for ISH

probe	antisense transcript	vector	accession nr.	bp
mouse <i>P2rx7</i>	Sp6	pCRII TOPO	NM_011027	1215-1636
human <i>P2RX7</i>	T7	pCRII TOPO	NM_002562	1195-1616
<i>Tmem132a</i>	T7	pCRII TOPO	ENSMUST00000025645	3014-3416
<i>Tmem132b</i>	Sp6	pCRII TOPO	ENSMUST00000031446	701-1131
<i>Tmem132c</i>	Sp6	pCRII TOPO	ENSMUST00000051260	3499-3954
<i>Tmem132d</i>	Sp6	pCRII TOPO	ENSMUST00000044441	3871-4276
<i>Tmem132e</i>	T7	pCRII TOPO	ENSMUST00000092852	3610-4027

Probes for Southern blot

probe	vector	length
5'probe	pCRII TOPO	633 bp
3'probe	pCRII TOPO	(499 bp); plasmid was digested with <i>Bam</i> HI and <i>Bst</i> EII resulting in a fragment of 250 bp

2.1.6 Antibodies

Antibodies for Western blot analysis

antibody	dilution	company
anti-phospho-p44/42 MAPK (ERK 1/2) (rabbit)	1:1000	Cell Signaling
anti-tyr-tubulin YL1/2 (rat)	1:10000	Cell Signaling
Anti-rabbit (HRP-linked)	1:1000	Cell Signaling
Anti-rat (HRP-linked)	1:1000	Cell Signaling

Antibodies for Immunohistochemistry/-cytochemistry

antibody	dilution	company
anti-NeuN (mouse)	1:1000	Chemicon
anti-MAP2 (rabbit)	1:1000	Chemicon
anti-Glu (rabbit)	1:1000	Sigma Aldrich
anti-GAD67 (mouse)	1:1000	Chemicon
anti- β Gal (chicken)	1:1000	Abcam
anti-rabbit (Alexa 594)	1:1000	Invitrogen
anti-mouse (Alexa 594)	1:1000	Invitrogen
Anti-chicken (Alexa 488)	1:1000	Invitrogen
Rhodamine Phalloidin	1:140	Cytoskeleton, Inc.

2.1.7 *E. coli* and yeast strains

strain	genotype	company
DH5 α	<i>fhuA2</i> Δ (<i>argF-lacZ</i>)U169 <i>phoA</i> <i>glnV44</i> Φ 80 Δ (<i>lacZ</i>)M15 <i>gyrA96</i> <i>recA1</i> <i>relA1</i> <i>endA1</i> <i>thi-1</i> <i>hsdR17</i>	Invitrogen
XL1-Blue	<i>recA1</i> <i>endA1</i> <i>gyrA96</i> <i>thi-1</i> <i>hsdR17</i> <i>supE44</i> <i>relA1</i> <i>lac</i>	Invitrogen
NMY51	MATa <i>his3</i> Δ 200 <i>trp1-901</i> <i>leu2-3,112</i> <i>ade2</i> LYS2:: <i>(lexAop)</i> 4-HIS3 <i>ura3</i> ::(<i>lexAop</i>)8- <i>lacZ</i> <i>ade2</i> ::(<i>lexAop</i>)8-ADE2 GAL4	Dualsystems Biotech

2.1.8 Animals

All animal experiments were conducted in accordance with the guide for the care and use of laboratory animals of the government of Bavaria, Germany. All animals were housed singly under standard laboratory conditions and were maintained on a 12 h light-dark cycle (lights on between 7:00 a.m. and 7:00 p.m.) with food and water *ad libitum*.

2.2 Methods

2.2.1 Microbiological methods

2.2.1.1 Preparation of chemically competent bacteria

5 ml of DH5 α or XL1-Blue *E. coli* culture was grown overnight in LB medium. On the next day, 100 ml LB medium was inoculated with the overnight culture and grown on a shaker at 37°C until bacteria have grown to an optical density (OD) of OD_{550nm} < 500. Bacteria were then centrifuged for 15 min at 5000 rpm at 4°C. The supernatant was decanted and the pellet was gently resuspended on ice in 30 ml cold TBF1. After incubation on ice for 20 min bacteria were centrifuged for 5 min at 4000 rpm at 4°C. The pellet was gently resuspended in 3.6 ml TBFII and 100 μ l aliquots were prepared. Competent bacteria were frozen at -80°C.

2.2.1.2 Transformation

Chemically competent DH5 α or XL1-Blue *E. coli* bacteria, stored at -80°C, were thawed on ice. DNA was added and mixed with the bacteria by gently tapping the tube. Bacteria were incubated for 30 min on ice. For uptake of plasmid DNA, competent cells were heat-shocked at 42°C for 90 sec and subsequently put on ice. 1 ml SOC medium was added and cells were incubated on a shaker at 37°C for 1 h. Cells were plated on LB plates containing the appropriate antibiotic for selection (100 μ g/ml ampicillin or 50 μ g/ml kanamycin) and incubated overnight at 37°C. Single colonies were picked and inoculated in 5 ml LB medium containing the appropriate selection marker (100 μ g/ml ampicillin or 50 μ g/ml kanamycin) and grown overnight at 37°C on a shaker at 250 rpm for subsequent DNA preparation.

2.2.1.3 Glycerol stocks

For long-term storage, 750 μ l of an overnight bacteria culture was mixed with 250 μ l 80% glycerol and frozen at -80°C.

2.2.2 Preparation and analysis of nucleic acids

2.2.2.1 Preparation of plasmid DNA

E. coli bacteria containing plasmid DNA were usually grown in autoclaved, sterile LB medium with a selective antibiotic, ampicillin (100 µg/ml) or kanamycin (50 µg/ml), overnight at 37°C. Small (5 ml culture) and large (100 ml culture) scale preparations of plasmid DNA were carried out by means of the respectively Plasmid Mini-, Midi- and Plasmid Maxi-Kit from Qiagen, according to the provided protocol.

2.2.2.2 DNA preparation from mouse tail tissue

For genotyping PCRs of transgenic mice, tail tissue was digested in 100 µl 50 mM NaOH for 30 min at 99°C followed by a neutralization step using 30 µl 1 M Tris-HCl (pH 7.0) and stored at 4°C. 1-2 µl of the tail lysates were used as template for PCRs.

2.2.2.3 RNA isolation

RNA was isolated either from mammalian cells or from murine tissues using the TRIzol protocol (Invitrogen). Tissue or harvested cells were homogenized in 1 ml/mg TRIzol reagent using a TURRAX® (IKA Labortechnik, Staufen, Germany) or insulin canulas (BD Biosciences). Solutions were incubated at room temperature for 5 min. After addition of 200 µl chloroform tubes were shaken vigorously for 3 min at room temperature. By centrifugation for 15 min at 13000 rpm at 4°C (5403 centrifuge, Eppendorf) the phenol and water phases were separated. The aqueous upper phase containing the RNA was transferred into a fresh 1.5 ml Eppendorf tube and RNA was precipitated with 500 µl isopropanol/ml TRIzol for 1 h at -20°C. Precipitated RNA was centrifuged for 10 min at 13000 rpm at 4°C. The pellet was washed with 1 ml of cold 70% ethanol by centrifugation at 10000 rpm at 4°C for 10 min. RNA pellet was dried at 37°C and dissolved in 20-50 µl H₂O_{bidest} at 65°C for 10 min.

2.2.2.4 Agarose gel electrophoresis

For separation of DNA by gel electrophoresis, agarose (Invitrogen) was boiled in 1x TAE buffer with agarose concentration depending on the DNA fragment size. For fragments between 100 and 1000 bp 2% agarose gels were chosen. For bigger fragments 0.8-1% agarose gels were applied. 0.1 µg/ml ethidiumbromide was added to boiled and liquid agarose in 1x TAE which was spilt in a gel electrophoresis chamber (PeqLab). DNA or RNA samples mixed with 1/6 of 6x sample loading buffer were loaded. As size marker smart ladder (Eurogentec, Brussels, Belgium) was used. Electrophoresis was carried out with 80-140 V for 1-2 h. The DNA fragments were detected with a UV light camera (Biometra, Göttingen, Germany).

2.2.2.5 Photometric determination of DNA/RNA concentrations

Optical density (OD) values were measured with the Photometer GeneQuant II (Pharmacia Biotech) and DNA concentrations were calculated subsequently using the following equation:

$$\text{DNA concentration } [\mu\text{g/ml}] = \text{OD}_{260} \times f \times n$$

OD₂₆₀ = Optical density of a strongly diluted DNA/RNA solution determined with a spectrophotometer at a wavelength of 260 nm

f = Dilution factor

n = Set by default 50 µg/ml for DNA and 40 µg/ml for RNA for 1 cm quartz cuvettes

The ratio of the absorbance readings at 260 nm was used to estimate the purity of nucleic acid preparations. Expected ratio of a very pure DNA preparation was OD₂₆₀ equals 1.8 or 2.0, respectively.

2.2.2.6 Restriction digestions of DNA samples for analytical purposes

Restriction enzymes from Fermentas or New England Biolabs (NEB) were used. Enzyme units added to a reaction were empirically determined and working buffers were chosen in accordance to the information provided by the suppliers. 1-2 μl of DNA samples were incubated for 1 h at 37°C and fragment sizes subsequently analyzed on an agarose gel.

2.2.2.7 Sequencing

Sequencing reactions were performed at Sequiserve (Vaterstetten, Germany). The sequencing results were analyzed using *Vector NTI* software (Invitrogen).

2.2.3 Polymerase chain reaction (PCR)

2.2.3.1 Standard PCR

To amplify specific cDNA fragments for expression analyses or expression vector clonings polymerase chain reactions were performed using the Thermoprime Plus DNA polymerase (ABgene, Hamburg, Germany) as follows:

PCR reaction:

1 μl	cDNA/genomic DNA
1 μl	primer forward (10 pmol, Sigma Aldrich)
1 μl	primer reverse (10 pmol, Sigma Aldrich)
1 μl	dNTPs (dATP, dTTP, dCTP, and dGTP, 10 mM each, Roche Applied Science)
5 μl	10x reaction buffer IV (ABgene)
3 μl	MgCl ₂ solution (25 mM, ABgene)
0.5 μl	Thermoprime Plus DNA polymerase (5 U/ μl , ABgene)
37.5 μl	H ₂ O (Ampuwa)
50 μl	final volume

PCR was carried out in a PCR machine (GeneAmp PCR System 9700, Applied Biosystems) with the following temperature settings:

PCR program :

94°C	2 min	
94°C	30 sec	
x°C	30 sec	(35 cycles)
72°C	x sec	
72°C	5 min	
8°C	∞	

Annealing temperature and elongation time were chosen in dependence of the melting temperature of the primers and the amplicon size.

2.2.3.2 Reverse transcription (RT) PCR

First strand cDNA synthesis from total RNA was performed using the SuperScript™ II reverse transcriptase kit from Invitrogen according to the provided protocol. To test for genomic DNA contaminations, one control reaction lacking the reverse transcriptase was carried out for each RNA sample.

Reverse transcription

x µl	RNA (1 µg)
1 µl	oligo d(T) primer
y µl	H ₂ O
11 µl	in total

The reaction mix was heated at 65°C for 2 min, then chilled on ice.

RT-mastermix:

4 μ l	5x buffer (Invitrogen)
2 μ l	0.1 M DTT (Invitrogen)
1 μ l	10 mM dNTPs
1 μ l	RNase inhibitor (40 U/ μ l; Roche)

8 μ l of mastermix were added to each sample and the tubes were incubated at 40°C for 2 min.

Subsequently, samples were incubated with 1 μ l Superscript II for 60 min at 42°C followed by 15 min at 70°C and stored at -20°C.

2.2.4 Cloning techniques

2.2.4.1 Restriction digestions of DNA samples for preparative purposes

Restriction enzymes from Fermentas or New England Biolabs (NEB) were used. Enzyme units added to a reaction were empirically determined and working buffers were chosen in accordance to the information provided by the suppliers. 10 μ g of DNA samples were incubated overnight at 37°C and the desired fragment was purified by gel extraction.

2.2.4.2 DNA gel extraction

For purification of DNA fragments out of an agarose gel the QIAquick Gel Extraction Kit (Qiagen) was used according to manufacturer's instructions. DNA was eluted using 30 μ l of H₂O_{bidest.} Extracted DNA concentration was estimated using agarose gel electrophoresis and different amounts of the DNA marker smart ladder.

2.2.4.3 Ligation

For ligations the Rapid DNA Ligation Kit (Fermentas) was used. 50 ng of vector backbone was ligated to 3x molar excess of insert. The appropriate amount of insert was calculated as following:

$$m \text{ insert (ng)} = 3 \times 50 \text{ ng} \times (\text{bp of insert}/\text{bp of backbone vector})$$

Ligation mix:

50 ng	linearized backbone vector
x ng	insert
4 μ l	5x buffer
ad. 19 μ l	H ₂ O _{bidest}
1 μ l	T4 ligase

After incubation for 1 h at room temperature the ligation was further incubated overnight at 16°C. On the next day, a heat shock transformation using 1-2 μ l of the ligation product was performed.

2.2.4.4 TOPO TA cloning

TOPO TA cloning from Invitrogen is based on the biochemical properties of DNA topoisomerase type I. PCR products with A-overhangs, derived from PCR reactions carried out with Taq DNA polymerase (Roche Applied Science) are inserted into a cut vector which carries T-overhangs with covalently bound topoisomerase.

Probes for *in situ* hybridization were cloned into the pCRII-TOPO vector (Invitrogen) according to the manufacturer recommendations. The pCRII-TOPO vector contains Sp6 and T7 promoters which allow *in vitro* transcription.

For blue-white selection of the colonies, 40 μ l of 40 mg/ml X-Gal in dimethylformamide (DMF) solution were previously added to LB-agar plates. After 37°C overnight incubation white colonies were picked for screening.

2.2.5 Yeast Two-Hybrid (Y2H) membrane system

The Y2H membrane (Stagljar et al., 1998;Thaminy et al., 2003) system is based on the split-ubiquitin mechanism and is used to identify the interactions between an integral membrane protein and either other membrane proteins or soluble proteins. Since the interaction is detected *in situ* at the membrane, the assay represents a more physiological situation than a conventional yeast two-hybrid screening, in which only subdomains of integral membrane proteins can be assayed and the interaction takes place in the nucleus.

In a Y2H membrane screening, a membrane protein of interest – the bait protein – is fused to the C-terminal half of ubiquitin (Cub) and the artificial transcription factor LexA-VP16 (Fig. 9A). A second protein of interest – the prey protein – is fused to the mutated N-terminal half of ubiquitin (NubG) (Fig. 9B), in which the isoleucine (I) at position 3 of the protein is exchanged for a glycine (G). Only if bait and prey interact, NubG and Cub are forced into close proximity, resulting in the reconstitution of split-ubiquitin. The reconstituted ubiquitin is immediately recognized by ubiquitin-specific proteases which cleave the polypeptide chain between Cub and LexA-VP16. As a result, the artificial transcription factor is released from the membrane and translocates to the nucleus where it binds to the LexA operators upstream of a reporter gene. This leads to transcriptional activation of reporter genes (Fig. 9C), two auxotrophic growth markers (*HIS3* and *ADE2*), whose activation enables the yeast to grow on defined minimal medium lacking histidine or adenine, and *LacZ*, encoding the enzyme β -galactosidase, whose expression leads to color development in a β -galactosidase assay.

The used NMY51 strain carries the *ADE2* reporter gene under the control of *lexA* operators. When no protein-protein interaction takes place, the *ADE2* gene is not transcribed and the adenine synthesis pathway of the yeast is blocked, leading to accumulation of a color-absorbing intermediate. Thus, in the absence of a protein-protein interaction, NMY51 colonies appear to be pink. The presence of two interacting proteins activates the *ADE2* gene and thereby the adenine synthesis pathway. Consequently, NMY51 colonies expressing an interacting protein pair are faint pink to white, depending on the strength of interaction.

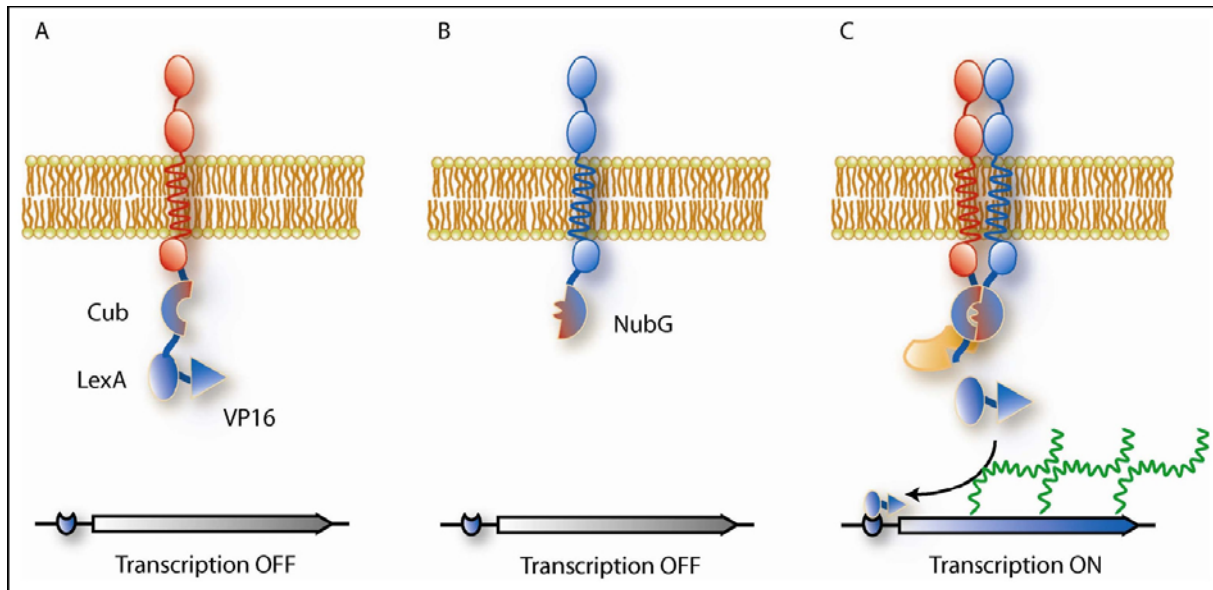


Fig. 9. The Y2H membrane system (Dualsystems Biotech manual). The bait protein (red) – an integral membrane protein – can interact with either other membrane proteins (blue) or soluble proteins (not shown).

The Y2H membrane screening was carried out using the DUALmembrane kit 3 (Dualsystems Biotech, Schlieren, Switzerland) according to the manufacturer's instructions (Fig. 10).

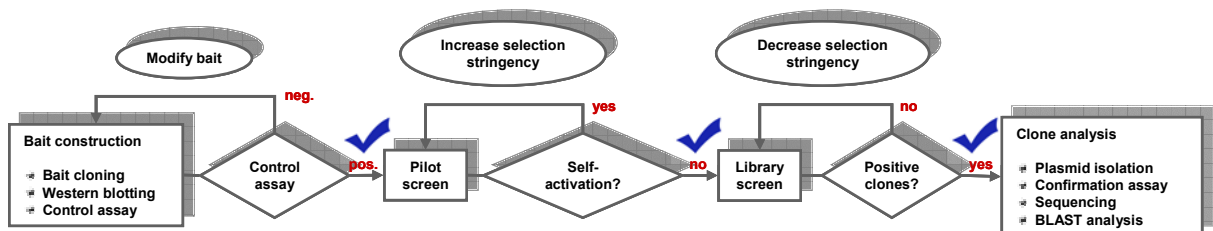


Fig. 10. Work-flow of the Y2H membrane system (adapted from Dualsystems Biotech manual).

The bait was cloned into the pBT3-SUC vector. Expression of the bait was verified by transformation into NMY51 and subsequent Western blot analysis. Self-activation of the bait was tested in a control assay. Screening stringency was optimized in a pilot screen. A mouse adult brain cDNA library (NubG-X) from Dualsystems Biotech was used in the library screen in which the interactors were selected. Using a β -galactosidase assay, the strongest interactors were selected and plasmids were isolated from yeast and retransformed into *E. coli* for amplification. Isolated prey plasmids were sequenced and a BLAST analysis was performed to identify interacting proteins.

2.2.6 *In situ* hybridization

Tissue preparation

For *in situ* hybridization 2-3 months old male animals were sacrificed by decapitation. Brains were carefully removed, immediately shock frozen on dry ice, and stored at -80°C until further processing.

Frozen brains were mounted on polyfreeze tissue freezing medium (Polyscience Inc.) and coronally cut on a cryostat (HM 560 M, Microm) in 20 µm thick consecutive sections. Brain sections were mounted on super frost plus microscope slides (Menzel), dried on a 37°C warming plate, and stored at -20°C. For comparability of the results brains from control mice and mutant mice were always cut in parallel on one slide and cutting order was changed after each pair.

Template amplification

PCR reaction:

1 µl	plasmid template
1 µl	primer forward (10 pmol, Sigma Aldrich)
1 µl	primer reverse (10 pmol, Sigma Aldrich)
1 µl	dNTPs (dATP, dTTP, dCTP, and dGTP, 10 mM each, Roche Applied Science)
5 µl	10x reaction buffer IV (ABgene)
3 µl	MgCl ₂ solution (25 mM, ABgene)
0.5 µl	Thermoprime Plus DNA polymerase (5 U/µl, ABgene)
37.5 µl	H ₂ O (Ampuwa)
50 µl	final volume

PCR program :

94°C	3 min	
94°C	30 sec	
67°C	30 sec	(35 cycles)
72°C	60 sec	
72°C	5 min	
4°C	∞	

To prevent RNA degradation all precautions were taken to avoid RNase activity.

Preparation of riboprobes

In vitro transcription:

x µl (200 ng)	PCR product
x µl	H ₂ O-DEPC (total volume is 30 µl)
3 µl	10x transcriptions buffer (Roche)
3 µl	NTP-mix (rATP/rCTP/rGTP 10 mM each; Roche)
1 µl	0,5 M DTT
1 µl	RNasin (RNase-inhibitor; 40 U/µl; Roche)
6 µl	³⁵ S-thio-rUTP from Amersham (12,5 mCi/mM; 1250 Ci/mmol)
1 µl	T7 or SP6 RNA polymerase (20 U/µl)

The reaction samples were mixed gently by tapping the Eppendorf tube and spinned down quickly. Then the samples were incubated at 37°C for 3 hours in total; after 1 h another 0.5 µl of RNA polymerase was added.

To destroy the DNA template, 2 µl RNase-free DNase I (10 U/µl; Roche Molecular Diagnostics) were added and samples were incubated for 15 min at 37°C.

Purification of riboprobes

For purification of riboprobes the Qiagen RNeasy Kit was used. RNA was diluted in 100 µl RNase-free water and 1 µl of the probe was measured in 2 ml scintillator solution (Zinsser Analytic, Frankfurt, Germany) in a beta-counter (LS 6000 IC,

Beckmann Coulter). For *in situ* hybridization 35000 to 70000 cpM/ μ l and 90 μ l/slide (7 Mio/slide) were needed.

Pretreatment of cryo-slides

Slides were taken out of the -20°C freezer and warmed up for least 1 h while still in the box. Then they were spread out on clean cotton tissue and dried for another 15 min. For pretreatment the following protocol was applied.

1. fix	10 min	4% PFA/PBS	ice-cold (4°C) Add 600 μ l acetic anhydride to TEA while stirring bar is rapidly rotating
2. rinse	3x 5 min	1x PBS/DEPC (0.1 M)	
3.	10 min	0.1 M triethanolamine-HCl 0.2 (pH8.0) (TEA) (200 ml)	
4. rinse	2x 5 min	2x SSC/DEPC	
5. dehy.	1 min	60% ethanol/DEPC	
6.	1 min	75% ethanol/DEPC	
7.	1 min	95% ethanol/DEPC	
8.	1 min	100% ethanol/DEPC	
9.	1 min	CHCl ₃	
10.	1 min	100% Ethanol/DEPC	
11.	1 h	air dry (dust free)	

Hybridization

An appropriate amount of hybridization mix (hybmix) containing the riboprobe was prepared. 90 to 100 μ l hybmix and 3.5 to 7 Million counts per slide were needed, respectively.

The hybridization mix containing the probe was heated to 90°C for 2 min, put shortly on ice, then on RT.

The solution was pipetted onto the slides and coverslips were carefully put on them, avoiding air bubbles in between.

The slides were carefully placed into a hybridization chamber containing hybridization chamber fluid to prevent drying out of the hybridization chamber and the chamber was sealed with adhesive tape.

The slides were incubated in an oven at 55-68°C overnight (up to 20 h).

Washes

After hybridization the coverslips were carefully removed and the following protocol was applied.

1.	4x 5 min	RT	4x SSC	
2.	20 min	37°C	0.5x NTE (20 µg/ml RNaseA)	Add 500 µl RNaseA (10 mg/ml) to 250 ml of NTE
3.	2x 5 min	RT	2x SSC/1 mM DTT	50 µl of 5 M DTT/250 ml
4.	10 min	RT	1x SSC/1 mM DTT	50 µl of 5 M DTT/250 ml
5.	10 min	RT	0.5x SSC/1 mM DTT	50 µl of 5 M DTT/250 ml
6.	2x 30 min	64°C	0.1x SSC/1 mM DTT	50 µl of 5 M DTT/250 ml
7.	2x 10 min	RT	0.1x SSC	
8.	1 min	RT	30% ethanol in 300 mM NH ₄ OAc	
9.	1 min	RT	50% ethanol in 300 mM NH ₄ OAc	
10.	1 min	RT	70% ethanol in 300 mM NH ₄ OAc	
11.	1 min	RT	95% ethanol	
12.	2x 1 min	RT	100% ethanol	
13.	1 h	RT	air dry (dust free)	

Autoradiography

Dried *in situ* sections were exposed to a special high performance X-ray film (BioMax MR from Kodak) for one until three days.

Dipping

The slides were dipped in a pre-warmed photographic emulsion (KODAK NTB2 emulsion, Rochester, NY, USA, diluted one to one with Ampuwa water, stored at 4°C) for about 4 sec and dried overnight at RT. Then they were packed into light-tight black boxes with sufficient desiccant (silica gel capsules), labelled and sealed with tape. The slides were exposed for three to four weeks at 4°C depending on the signal intensity of the X-ray film.

Development

The boxes were equilibrated to room temperature for 2 h while still sealed. The slides were developed in KODAK D 19 developer (Sigma P5670) for 3 min at RT, rinsed 30 sec in tap water and fixed in KODAK fixer (cat# 197 1720) for 5 min. Then they were rinsed in running tap water for 25 min. Using a strong razor blade the emulsion was scratched from the back side of the slides and the slides were air dried.

Nissl staining

After development brain sections were counterstained with the synthetic dye cresyl violet. This basic aniline dye is able to stain the RNA of the rough endoplasmatic reticulum, called Nissl substance, in the cytoplasm of neurons.

1.	20 min	0.5% Cresyl violet acetate
2.	1 min	water
3.	2x 1 min	70% ethanol
4.	1 min	96% ethanol + 1 ml of acetic acid
5.	2x 1 min	96% ethanol
6.	2x 1 min	100% ethanol
7.	2x 5 min	xylol

2.2.7 Southern blot analysis

Preparation of DNA samples

The 96-well gelatine plates containing embryonic stem (ES) cells were incubated with 50 μ l lysis buffer containing Proteinase K overnight at 56°C. On the next day, plates were centrifuged for 2 min at 2500 rpm and DNA was precipitated with 10 ml ice-cold 100% ethanol containing 150 μ l 5 M NaCl followed by 30 min incubation on a shaker. After centrifugation, plates were washed 3x with 70% ethanol and dried at 37°C. The precipitated ES cell DNA was digested overnight at 37°C using 30-60 units of the appropriate restriction enzyme (NEB). On the next day, digested DNA was separated on a 0.8% agarose gel for approximately 4 h at 100 V.

DNA transfer (Southern blot)

The gel was incubated in denaturation buffer 2x for 15 min on a shaker to separate DNA strands. Afterwards, the gel was incubated 2x in neutralization buffer for 15 min, followed by a 10 min equilibration step in 20x SSC.

For DNA transfer onto a Nylon membrane (Hybond N⁺, GE Helthcare) the following scheme was used:

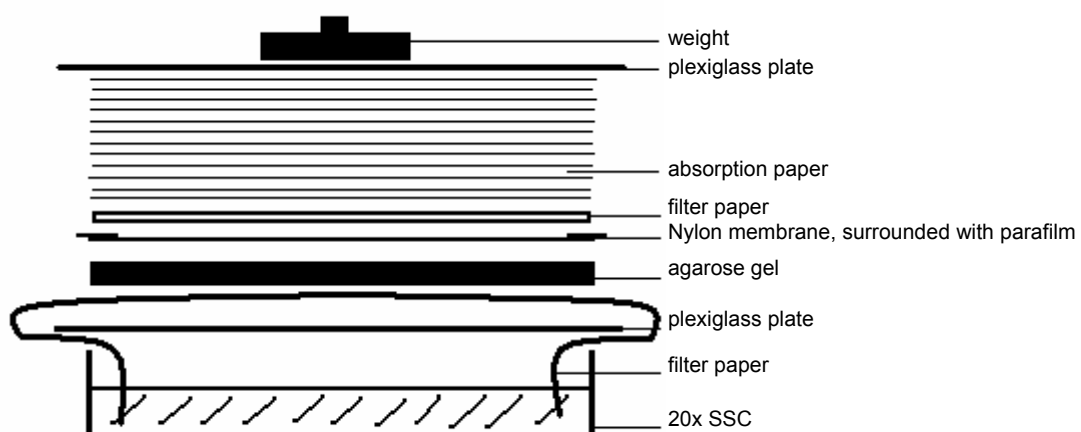


Fig. 11. Southern blot assembling.

After a transfer time of 12-20 h the blot was unbuilt and the DNA on the membrane was immobilized by cross linking under UV-light (UV-Stratalinker® 2400, Statagene).

Probe labeling

For radioactive labeling of the DNA probe the Megaprime DNA labeling system (Amersham) was used.

Mix:

25 ng	DNA probe
ad 30.5 μ l	H ₂ O
5 μ l	primer

Samples were incubate for 5 min at 95°C; then chilled on ice. Afterwards, 10 μ l Megaprime reaction buffer were added and the following compounds in the hot lab:

2.5 μ l	[α - ³² P]-dCTP 50 μ Ci (GE Healthcare)
2 μ l	Klenow fragment
50 μ l	total volume

Samples were incubated for 30 min at 37°C. The labelled probe was pipetted onto Microspin S300 columns (Amersham) and centrifuged for 2 min at 3000 rpm to remove unincorporated nucleotides. 1 μ l of the purified probe in 2 ml scintillator fluid (Zinsser Analytic, Frankfurt, Germany) was measured in the beta-counter (LS 6000 IC, Beckmann Coulter).

Hybridization

For prehybridization, the membrane was placed into a glass tube and 10 ml Rapid-Hyb mix (Amersham) without probe were added and heated at 65°C rotating for 1-2 h. In parallel, the radioactive probe was heated together with 100 μ l salmon sperm DNA for 5 min at 95°C. Subsequently, the probe mix was added to the reaction tube and the membrane was hybridized rotating overnight at 65°C.

Washes

On the next day, the hybmix was removed and the membrane was washed for 20 min with 2x SSC, 0.1% SDS rotating at 65°C. In a second step, the membrane was washed 2x with 0.2x SSC, 0.1% SDS for 20 min rotating at 65°C. The membrane was then dried on absorbent papers and put into a transparent foil.

Development

The membrane was placed in a film cassette and a Kodak film was added. Dependent on the signal strength, the film was exposed for 1-7 days and developed in an automatic developing machine (XP 2000, Kodak).

2.2.8 Western blot analysis

Samples for Western blot analysis were lysed in RIPA buffer and the appropriate amount of loading buffer was added. Samples were boiled at 95°C for 5 min to denature the proteins and subsequently put on ice. 30 µl of the samples and 10 µl of the prestained protein ladder PageRuler™ (Fermentas) were separated on a 12% SDS-PAGE (for Sodium Dodecyl Sulfate PolyAcrylamide Gel Electrophoresis) for 3 h at RT, 100 V and subsequently transferred onto a PVDF membrane (Millipore) overnight at 4°C, 25 V. For both steps, Western blot chambers from Bio-Rad were used. On the next day, membranes were blocked for 1 h with 5% milk in TBS-T at RT. Incubation of the first antibody, diluted in 5% milk in TBS-T, was carried out overnight at 4°C on a rotator. Afterwards, membranes were washed 3x for 10 min with TBS-T followed by the incubation with the secondary antibody (Cell Signaling), diluted in 5%, for 1 h at RT on a rotator. The membranes were washed with TBS-T and immunoreactive bands were detected using an ECL detection kit (Millipore) and a Kodak film which was developed using an automated development machine (XP 2000, Kodak).

2.2.9 LacZ staining

Mice were intracardially perfused using LacZ-Fix solution for 5-7 min, followed by a 1 min washing step with PBS. After preparation, the brain was additionally fixed for 1 h in LacZ-fix and then incubated overnight at 4°C in 20% sucrose/PBS. On the next day, the brain was frozen on dry-ice and cut at a cryostat (HM 560 M, Microm) in 50 µm thick sections and collected in cryoprotection solution. For staining, the sections were immersed for 5 min in LacZ-wash buffer and then incubated in LacZ-staining solution at 37°C for up to 12 h in the dark. After washing with PBS, brain sections were incubated again in LacZ-fix to increase signal strength overnight at 4°C. Finally, sections were mounted on super frost plus slides (Menzel), immersed in xylol and embedded with DPX mounting solution (BDH).

2.2.10 Immunohistochemistry/-cytochemistry

In case of using cell lines, cells were grown on polylysine-coated coverslips (VWR) in 24-well plates. In case of using brain tissue, the brain was cut with a cryostat (HM 560 M, Microm) in 50 µm thick sections and collected in cryoprotection solution.

To fix the cells/brain sections, they were treated with warmed PFA 4% in 4% sucrose/PBS for 10-30 min at RT. After three 5 min washing steps, cells/sections were permeabilized 3x for 5 min using PBS-Triton X-100 0.1%. Cells/slices were washed for 5 min with PBS and subsequently treated with PBS-Triton X-100 0.1%, 5% BSA for 1 h to block the reaction. Afterwards, cells/sections were washed 2x for 5 min. Incubation with the first antibody, diluted in PBS-Triton 0.01%, 5% BSA, was carried out overnight at 4°C. After a three times washing step with PBS, an Alexa Fluor secondary antibody (Invitrogen), diluted in PBS-Triton 0.01%, 5% BSA, was added and incubated for 1 h at RT. Cells/sections were washed three times with PBS and mounted with antifade mounting media (Vector Labs) containing DAPI that was used to stain cellular nuclei. Sections were mounted on super frost plus slides (Menzel) before mounting.

2.2.11 Cell culture experiments

2.2.11.1 Maintaining of cell lines

To avoid contaminations cell culture experiments were carried out under sterile conditions using a sterile hood (Heraeus Instruments, Hanau, Germany). Cells were grown at 37°C with 5% CO₂ in a sterile incubator (Heraeus). Every second day cells were passaged or medium was refreshed.

Thawing of cells

A frozen vial of cells was thawed quickly at 37°C and centrifuged at 1200 rpm for 5 min. The cell pellet was resuspended gently in 5 ml growth medium and cells were split onto 6 cm plates (Nunc) each containing a total of 5 ml growth medium. The cells were incubated at 37°C, 5% CO₂ for 3 days.

Splitting of cells

Medium was removed from the plates and the monolayer was washed with about 5-7 ml DPBS (1x) (Invitrogen). 1 ml 0.5% trypsin/EDTA (1x) (Invitrogen) was added and plates were incubated for about 5 min at 37°C until the cells were detached. To stop the reaction, 10 ml DMEM was added and cell suspension was pipetted up and down for several times to break any cell aggregates. An appropriate amount of the cells was plated immediately on new dishes containing DMEM. The plates were swirled to ensure an even distribution in the medium.

Freezing of cells

For long-term storage of cell lines freshly thawed cells were passaged at least twice until they were refrozen. Therefore a confluent plate was trypsinized and centrifuged. Cells were resuspended in 3 ml of freezing medium and aliquoted in three cryo tubes (Nalgene, Roskilde, Denmark). The tubes were cooled down slowly overnight to -80°C using an isopropanol-filled freezing container (Nalgene). Afterwards cell tubes were stored in liquid nitrogen.

Counting of cells

For determination of the cell number a Neubauer chamber was used. After trypsination cells were resuspended in growth medium and 10 μ l of the suspension were counted. The mean value (m) of two counted quadrants was used to calculate the cell number: cells/ml = m x 10000.

2.2.11.2 Plasmid DNA transfection in cell lines

The following procedure was used to transfect DNA into mammalian cell lines in a 12-well format. All amounts and volumes are given on a per well basis. Complexes were prepared using a DNA (μ g) to lipofectamine 2000 (Invitrogen) (μ l) ratio of 1:2 to 1:3 (in a 12-well format 1.6 μ g DNA and 4.0 μ l lipofectamine 2000 were used). Cells were transfected at high cell density for high efficiency, high expression levels, and to minimize cytotoxicity.

One day before transfection, 2×10^5 cells were plated in 1 ml of growth medium with the usual amount of serum so that the cells were 90-95% confluent at the time of transfection. Before transfection medium was aspirated and medium without antibiotics and serum was added to arrest the cell cycle. For each transfection sample, complexes were prepared as follows: DNA was diluted in 100 μ l of Opti-MEM (Invitrogen) reduced serum medium without serum and mixed gently. Lipofectamine 2000 was mixed gently before use, then the appropriate amount was diluted in 100 μ l of Opti-MEM medium and incubated for 5 min at RT. After the incubation, the diluted DNA was combined with diluted lipofectamine 2000 (total volume = 200 μ l), mixed gently and incubated for 20 min at RT. 200 μ l of complexes was added to each well containing cells and medium and mixed gently by rocking the plate back and forth. Cells were incubated at 37°C in a 5% CO₂ incubator for 24 h.

2.2.11.3 Embryonic stem (ES) cell culture

Preparation of feeder cells

ES cells are cultured on so-called feeder cells which are embryonic mouse fibroblasts (EMFI). Feeder cells prevent differentiation of ES cells and provide growth factors. Feeders were unfrozen and incubated on 3x 15 cm plates each containing a total of 25 ml DMEM at 37°C, 5% CO₂, for 3 or 4 days. After another passage of 1:3, cells were treated for 2 h at 37°C with 150 µl Mitomycin C (1 mg/ml in PBS, Sigma Aldrich) during their exponential growth phase for mitotic inactivation. Feeder cells were trypsinized, counted and an amount of 1x10⁴ cells/cm² was plated on new dishes containing DMEM. EMFI cells were allowed to attach overnight before ES cells were added.

Culturing of ES cells

TBV2 ES cells were unfrozen, plated on 2x 10 cm feeder plates containing ES cell medium and incubated at 37°C, 5% CO₂. On the next day, ES cells were passaged on new feeder plates in a 1:4 dilution and grown for about 3 days.

Electroporation and selection of ES cells

ES cells were trypsinized, counted and a dilution of 1x10⁷ cells/800 µl per electroporation cuvette was prepared. 20 µg DNA in a volume of 20 µl of the linearized vector construct digested with the proper enzyme was added to the cell suspension. The mix was transferred to an electroporation cuvette and electroporated using the Bio Rad gene pulser at 0.24 kV, 500 µF. The cuvette was removed and incubated on ice for 10-20 min. Then, the cell suspension from one cuvette was carefully transferred into 2 ml ES cell medium containing LIF and the suspension from one cuvette was distributed to 2x 10 cm feeder plates containing already 9 ml medium with LIF. Two days after electroporation, the ES cell medium was exchanged for selection medium containing 200 µg/ml of the antibiotic geneticin (G418). In addition the G418-resistant feeder cells, only those ES cells can survive which carry the transgene containing the neomycin selection marker. After about 6-8

days of selection, drug resistant colonies should have appeared and be ready for analysis.

Picking of ES cell colonies

Before picking, medium in the original electroporation plate was removed and 10 ml PBS was added. With the aid of a binocular, single ES cell colonies were carefully scraped off the plate using a pipette, aspirated and transferred to a conical 96-well plate. After trypsination, cells were plated on fresh 96-well feeder plates containing 100 μ l ES medium.

Splitting of ES cell colonies

After 3 days, each ES cell clone was analyzed using a binocular and passaged in a 1:2, 1:3 or 1:4 dilution depending on the respective cell density. This synchronization step is necessary to avoid differential growth of the single clones. Cells were trypsinized and resuspended in an appropriate amount of medium. Then the cells were plated on fresh 96-well feeder plates containing 150 μ l/well ES cell medium. After two days, one plate was splitted again on two feeder plates and the other one on two gelatine-coated plates for Southern blot analysis. Therefore, 96-well plates were previously incubated with 50 μ l of 0.1% autoclaved gelatine for 20 min. Since inactivated EMFI cells are not able to expand on these gelatine plates, the DNA portion of feeder cells in the Southern blot analysis can be neglected.

Freezing of ES cell colonies

For freezing of ES cell clones grown on feeder plates, cells were trypsinized and resuspended in 70 μ l cold ES cell medium. 150 μ l freezing medium was added and mixed with the cell suspension. Plates were covered with parafilm, surrounded with tissue towels, transferred into a paperbox, and frozen at -80°C . Gelatine plates were incubated 1-2 days longer until the cells became very dense. Then, cells were washed 2x with PBS and frozen without medium for Southern blot analysis.

Expand positive ES cell clones for blastocyst injection

TBV2-ES cell plates containing the positive clones were unfrozen using a waterbath. Cells were resuspended in 100 µl selection medium and transferred to a new 96-well feeder plate containing 100 µl selection medium. Cells were expanded consecutively on 24-well plates, 6-well plates, 6 cm plates, 2x 10 cm plates. On the day of blastocyst injection, ES cells plates were trypsinized, resuspended in 1.5 ml ES cell medium and stored on ice. The blastocyst injection was carried out in collaboration with the Institute of Developmental Genetics (IDG), Helmholtz Zentrum München (Neuherberg).

2.2.11.4 Preparation and stimulation of primary neurons

Hippocampi from embryonic day 18 (E18) CD1 fetuses were separated from diencephalic structures and digested with 0.25% trypsin containing 1 mM EDTA (Invitrogen) for 20 min at 37°C with gentle shaking. 30.000 to 70.000 (24-well plates) or 10⁶ (10 cm plates) neurons were plated on coverslips or tissue culture plates, respectively, coated with poly-D-lysine (1 mg/ml) and laminin (5 µg/ml), in neurobasal medium supplemented with B27 containing 0.5 mM glutamine (all reagents from Invitrogen). Neurons were grown for at least 14 days *in vitro* (DIV) before stimulation. Primary neurons were stimulated with 1 mM of the P2RX7 receptor agonist 2',3'-O-(benzoyl-4-benzoyl)-adenosine 5'-triphosphate (BzATP, Sigma Aldrich) for 2 min, 5 min, 10 min and 60 mM KCl as positive control. Afterwards, cells were lysed in 200 µl RIPA buffer for Western blot analysis.

2.2.12 Preparation of peritoneal macrophages for IL-1β ELISA

Mice (2-3 months old) were killed by an overdose of isoflurane and peritoneal macrophages were immediately collected by lavaging the peritoneal cavities of mice with DMEM containing 5% of fetal calf serum and penicillin/streptomycin (100 units/ml and 100 µg/ml, respectively). Lavage fluids from 3-5 animals were pooled and the cells were collected by centrifugation. Cells were re-suspended, counted and 0.5x10⁶ cells per well were plated in 24-well plates in which the cells

were allowed to attach overnight. The next day, 3 µg/ml of lipopolysaccharide (LPS, serotype 0111:B4, Sigma Aldrich) were added, and the cells were allowed to prime for 2 h. The cells were then challenged with 2 mM BzATP for 30 min. Finally, supernatants were collected and analyzed for IL-1β using an ELISA kit following the manufacturer's instructions (Endogen, Pierce Technology, Rockford, IL, USA).

2.2.13 Preparation of peritoneal macrophages for calcium imaging

Peritoneal macrophages were collected as described above. Cells were re-suspended, counted and 0.5×10^6 cells per well were plated on coverslips coated with poly-D-lysine (1 mg/ml) in 24-well plates in which the cells were allowed to attach overnight. Conventional, wide-field fluorescence imaging was performed using a variable scan digital imaging system (TILL Photonics, Martinsried, Germany) attached to an upright microscope (Axioskop, Zeiss, Jena, Germany; 60x water immersion objective, N.A. 0.90, Olympus Europe, Hamburg, Germany) and a CCD camera as a sensor (Retiga 2000RV, QImaging, Surrey, Canada). Cells were dye-loaded with the Ca^{2+} -selective dye Fluo-4 (Fluo-4-AM, 1 µM, Invitrogen; Excitation 485 nm, Emission > 510 nm) by applying to the culture media. Cells were incubated at 37°C for 1 h in a dark incubator. For wide-field imaging of Fluo-4, background-corrected fluorescence signals were collected from defined regions of interest after excitation at 485 nm and images were acquired at 2 Hz. After background subtraction, the fluorescence emission was calculated using TillVision software (TILL Photonics, Martinsried, Germany) and data were analyzed off-line using "IGOR Pro"-Software (WaveMetrics, Inc., Lake Oswego, OR). BzATP or KCl (stock concentration BzATP = 100 mM; KCl = 3mM) were Bolus-applied to the bath containing 2 ml HEPES Ringer (140 mM NaCl, 3 mM KCl, 10 mM glucose, 10 mM HEPES, 1 mM CaCl_2 and 4.5 mM sucrose, pH 7.35).

2.2.14 *In vivo* experiments

2.2.14.1 Behavioral characterization

At an age of seven to eight weeks, the mice were separated and habituated to single housing and test room conditions for a period of minimum two weeks; mice of different genders were kept and investigated in two separate rooms. Following the habituation period all animals underwent a series of tests.

All behavioral tests were performed during the light phase, starting at 9 a.m. Scoring was performed by a trained observer, blind to the treatment/genotype, using pre-defined keyboard buttons and automatic video tracking of the ANY-maze software (Stoelting Co., Wood Dale, IL).

Forced Swim Test (FST)

Each mouse was gently placed into a glass beaker (height 24 cm, diameter 12 cm) filled with water (25-26 °C) to a height of 12 cm and the behavior during the 5 min test session was scored directly. At the end of the individual session, mice were removed and transferred to their individual home cage. Duration and frequency of occurrence of the following behaviors were measured: struggling (vigorous attempts at climbing the walls of the beaker); swimming (active swimming around without any upward directed movements); and floating (absence of movement other than necessary to keep balance).

Dark/Light box (DaLi)

The test box consists of black and white PVC and is divided into two compartments, connected by a tunnel (4x7x10 cm). The white compartment (30x20x25 cm) was brightly illuminated by cold light with an intensity of 680-700 lux; light intensity in the dark compartment (15x20x25 cm) was < 5 lux. At the beginning of a 5 min test period each mouse was placed in the center of the dark compartment, facing the tunnel. Mice were filmed from above with two cameras and the following parameters were scored directly from a monitor:

Time spent in each compartment (dark, tunnel, and lit), latency until the first full entry (with four paws) and the number of full entries into the lit compartment. In addition,

stretched attend postures (the animal stretches to its full length and either retracts to original position without moving forward or cautiously moves forward), rearings and self-grooming were scored. The apparatus was wiped out with water before each trial.

Open Field (OF)

The open field test was used to characterize locomotor activity in a novel environment. The open field was made of grey PVC and consisted of six compartments of the same size (50x50x40 cm), allowing to test 6 animals in parallel. Light intensity was 15-20 lux. At the beginning of a test, each mouse was placed in the corner of a compartment, facing the middle. During the 15-30 min test period, the animal was recorded by means of a video camera mounted above the apparatus. The distance covered by the animal was analyzed automatically using the ANY-maze software. In this process each compartment was virtually subdivided in an inner (10x10 cm) and an outer zone. Measured parameters were total distance covered; number, time and latency of inner zone exploration; and number of boli. The compartments were wiped out with water before each trial.

Acoustic Startle Response (ASR) and Prepulse Inhibition Testing (PPI)

Acoustic startle response and prepulse inhibition testing was carried out using the set-up as described in Golub et al. (Golub et al., 2009). The mice were placed in a tubular enclosure and tested inside a SR-LAB™ (San Diego Instruments) apparatus with background noise set to 50 dB(A). For ASR, after an acclimatisation period of five minutes, the mice were subjected to noise impulses of varying intensities (75 dB(A), 90 dB(A), 105 dB(A) and 115 dB(A)) in random order. The data depicted on the graphs represent the mean peak startle amplitude in mV \pm SEM in response to 30 pulses of each intensity, as well as 12 background noise (BG) measurements. For PPI, ASR was elicited using noise pulses at 115 dB(A). The acclimatisation period of five minutes was followed by 20 habituation pulses at 115 dB(A). Three different prepulse intensities were used (55, 65 and 75 dB(A)) with interpulse intervals (IPI, prepulse onset to pulse onset) of 5, 10, 25, 50 or 100 ms, making a total of 15 different prepulse conditions. Each of the different prepulse conditions was

presented 14 times in random order. ASR was also elicited 22 times at 115 dB(A) without prepulse in order to determine the baseline response. As a control, each of the three prepulse intensities were presented alone six times during the trial sequence. On the graphs, trials with different prepulse intensities (55, 65 and 75 dB(A)) are presented separately. The data depicted represent prepulse inhibition as a percentage change from baseline (without prepulse) for each interpulse interval. For both ASR and PPI, the intertrial interval ranged from 13 to 17 s.

Elevated Plus Maze (EPM)

The elevated plus maze was used to assess anxiety-related behavior. The apparatus was made of grey PVC and consisted of a plus-shaped platform with four intersecting arms, elevated 37 cm above the floor. Two opposing open (30x5 cm) and closed arms (30x5x15 cm) were connected by a central zone (5x5 cm). Animals were placed in the center of the apparatus facing the closed arm and were allowed to freely explore the maze for 5 min.

Sociability Test

The sociability test as previously described (Moy et al., 2004; O'Tuathaigh et al., 2007; Sankoorikal et al., 2006), was slightly modified to mainly assess the social preference between an unfamiliar juvenile Balb/c mouse and an object of choice (in this case a dummy mouse). The apparatus contained a three chamber box (50x25 cm) with one centre and two outer chambers (left and right chamber 19x25x40 cm; centre chamber 12x25x40 cm). Two small openings with trap doors served as access points from one chamber to the other. The apparatus was filled with bedding and evenly illuminated with 3-5 lux. The paradigm consists of two separate stages.

Stage 1: Habituation

The animals were allowed to freely explore the apparatus on two consecutive days for 10 min. During this time, only the empty wire cages were present in the chambers.

Stage 2: Sociability trial

On the third day of testing, an unfamiliar male juvenile BALB/c mouse was introduced into the left chamber, enclosed in the wire cage while a dummy mouse was placed in the opposite chamber (alteration occurred after 3 consecutive trials). The test mouse was placed in the middle chamber for 5 min with both trap doors being shut. These were then opened and the test animal was allowed to explore the rest of the apparatus for an additional 10 min. The time spent interacting with mouse and object was scored by a trained observer and the discrimination index was obtained as follows: $\text{interaction time with mouse (s)} / (\text{interaction time with mouse (s)} + \text{interaction time with object (s)})$.

Social Approach/Avoidance Test

The social approach/avoidance test was carried out as described (Berton et al., 2006). In brief, the test consisted of two trials. In the first trial, each experimental mouse was introduced into the open field arena for 2.5 min containing an empty wire mesh cage, located at one end of the apparatus (marked as the interaction zone). During the second trial an unfamiliar male juvenile BALB/c mouse was introduced into the wire mesh cage, allowing for nose contact between the bars but prevented fighting. The time spent in the interaction zone, as well as the time spent interacting with the empty wire cage and the unfamiliar mouse were analyzed.

Female Urine Sniffing Test (FUST)

The female urine sniffing test, designed to monitor reward-seeking behavior was adopted and performed according to Malkesman and colleagues (Malkesman et al., 2010). Animals were habituated to a sterile cotton-tip in their home cages one hour before testing. The test comprised three stages, all of which were conducted in non-aversive conditions (2-3 lux) in the animals' home cages. First (water trial), the animals were exposed to a cotton tip dipped in sterile water for 3 min. After an interval of 45 min, mice were exposed to a second cotton tip, this time dipped in fresh urine, which had previously been collected from females in estrus (urine trial). The sniffing duration of both, water and urine were analyzed.

2.2.14.2 Endocrine analyses

Retrobulbar blood was taken using glass capillaries under isoflurane anesthesia. A.m. values were measured at 9:00 a.m., p.m. values were measured at 4:00 p.m.; acute restraint stress was applied for 10 min; feedback values were measured 90 min after restraint stress 7 days later. Plasma corticosterone concentrations were measured in duplicate by commercially available RIA kits (MP Biomedicals, Eschwege, Germany).

2.2.14.3 Chronic social defeat stress paradigm

The chronic social defeat was performed as previously described (Berton et al., 2006;Wagner et al., 2011). In brief; experimental mice (9-13 mice per group between 11-13 weeks of age) were submitted to chronic social defeat stress for 21 consecutive days. They were introduced into the home cage of a dominant CD1 resident for no longer than 5 min, and were subsequently defeated. Following defeat, animals spent 24 hours in the same cage, which was separated via a holed steel partition, enabling sensory but not physical contact. Every day experimental mice were exposed to a new unfamiliar resident. Control animals were housed in their home cages throughout the course of the experiment. All animals were handled daily; weight and fur status were assessed every 3-4 days (fur was evaluated as described (Mineur et al., 2003)). Behavioral testing took place during the last week of the paradigm and included the open field, elevated plus maze, sociability, social approach/avoidance, as well as the female urine sniffing test.

2.2.14.4 Acute stress response and sampling during the CSDS

On day 19 of the chronic stress procedure animals were subjected to an acute stress challenge in the form of the FST for 6 min. Blood samples were collected by tail cut 15 min following the start of the FST, and corticosterone plasma concentrations were measured with a radioimmune assay according to the manufacturers manual (MP Biomedicals Inc; sensitivity 6.25 ng/ml). Animal sacrifice was performed by decapitation on day 21 of the experiment. In order to obtain basal corticosterone

levels, trunk blood was collected and processed. Thymus and adrenal glands were removed and stored in Ringer's solution. In order to determine the organ weight, additional surrounding tissue was removed and the thymus and adrenal glands were weighted.

2.2.14.5 Sleep phenotyping and analysis of sleep data

To monitor spontaneous sleep-wake behavior, mice were chronically implanted with electroencephalographic (EEG) and electromyographic (EMG) electrodes as previously described (Kimura et al., 2010;Romanowski et al., 2010). The baseline recording was conducted 2 weeks after recovery from surgery. The polysomnographic setup was as same as previously reported (Kimura et al., 2010;Romanowski et al., 2010).

Polygraphic data were assessed by a LabView-based acquisition program (EGEraVigilanz, SEA, Cologne, Germany), in which a FFT algorithm, adapted from a report by (Louis et al., 2004) serves to carry out semiautomatic classification of vigilance states combined with power spectrum analysis. Vigilance states are defined as wake, non-rapid eye movement (NREM) sleep (NREMS), or rapid eye movement (REM) sleep (REMS), respectively, in 4 s epochs and manually corrected if necessary. Time spent in each vigilance state was expressed in percentage/2 h. Slow-wave activity (SWA) during NREMS was calculated between 0.5-4 Hz in the delta range at a 0.5 Hz-bin and normalized for each animal by the total power averaged from all epochs scored as NREMS throughout the 24 h period across all frequency bins from 0.5 to 29 Hz, as previously described elsewhere (Baracchi and Opp, 2008;Franken et al., 1998). SWS₂ was detected when the power of delta waves was higher than 50% of the sum total power in each epoch scored as NREMS, referring to a report by (Popa et al., 2006). Sleep architecture and spectral distributions of EEG activity were also analyzed as described previously (Jakubcakova et al., 2011).

2.2.15 Statistics

Data and statistical analysis were performed with the computer programs GraphPad Prism 5.0 and SPSS 16.00. All results are shown as means \pm standard error of the mean (SEM). The effects of genotype and stress on behavior and neuroendocrine data were examined by two-way-multivariate analysis of variance with post-hoc t-test (level of significance, $p < 0.05$). To examine body weight, fur state and startle response, analysis of variance with repeated measures design was applied. Calcium Imaging data were analyzed by repeated measures ANOVA. For the meta-analysis, genotypic distributions were derived from the corresponding publications either directly or from given allele frequencies. For each sample odds ratios and standard errors for the allelic, dominant and heterozygous-disadvantage model were calculated using Fisher's exact test. The meta-analysis was performed in R using the inverse variance method.

3 Results

3.1 Validation of *P2RX7* as a susceptibility gene for mood disorders using genetic mouse models

3.1.1 Generation and analysis of *P2rx7* knockout mice

3.1.1.1 Generation of *P2rx7* knockout mice

Total *P2rx7* knockout mice were previously established in our group. For disruption of the *P2rx7* gene in the mouse a targeting vector was constructed, which allows for subsequent recombinase mediated cassette exchange (RMCE) via phiC31 integrase and which contains a *tau-LacZ* reporter gene. The homology arms enframe a 9.5 kb reporter-selection cassette comprising the following components (from 5' to 3'): adenovirus type 2 RNase gene splice acceptor (SA), encephalomyocarditis virus internal ribosome entry site (IRES), *tau-lacZ* reporter gene, bovine growth hormone polyadenylation sequence (bGHpA), PGK-Neo-bGHpA, PGK-Puro Δ TK-bGHpA, 3x pA (PGK pA, 2x SV40 pA). The entire reporter–selection cassette is flanked by RMCE compatible *attP* sites. The vector was designed to substitute 2.3 kb including exon 2 of the *P2rx7* gene that will ultimately result in a frameshift and complete loss of P2RX7 function (Fig. 12a). The SA-IRES-tau-LacZ-bGHpA and the 3x pA were isolated and modified from a previously constructed ROSA26 targeting vector (Lu et al., 2008). The PGK-Puro Δ TK-bGHpA was isolated from pYtC37 (Chen and Bradley, 2000).

The linearized (via *PacI*) targeting vector bearing 10.0 kb homology to the murine *P2rx7* locus was electroporated into TBV2 ES cells. Mutant ES cell clones were identified by Southern blot analysis of genomic ES cell DNA digested with *EcoRI* using the 3' external probe (Fig. 12b). Mutant ES cells were used to generate chimeric mice by blastocyst injection. Germ-line transmission of the modified *P2rx7* allele was confirmed in offspring from male chimeras bred to wild-type C57BL/6J mice (Fig. 12c, d).

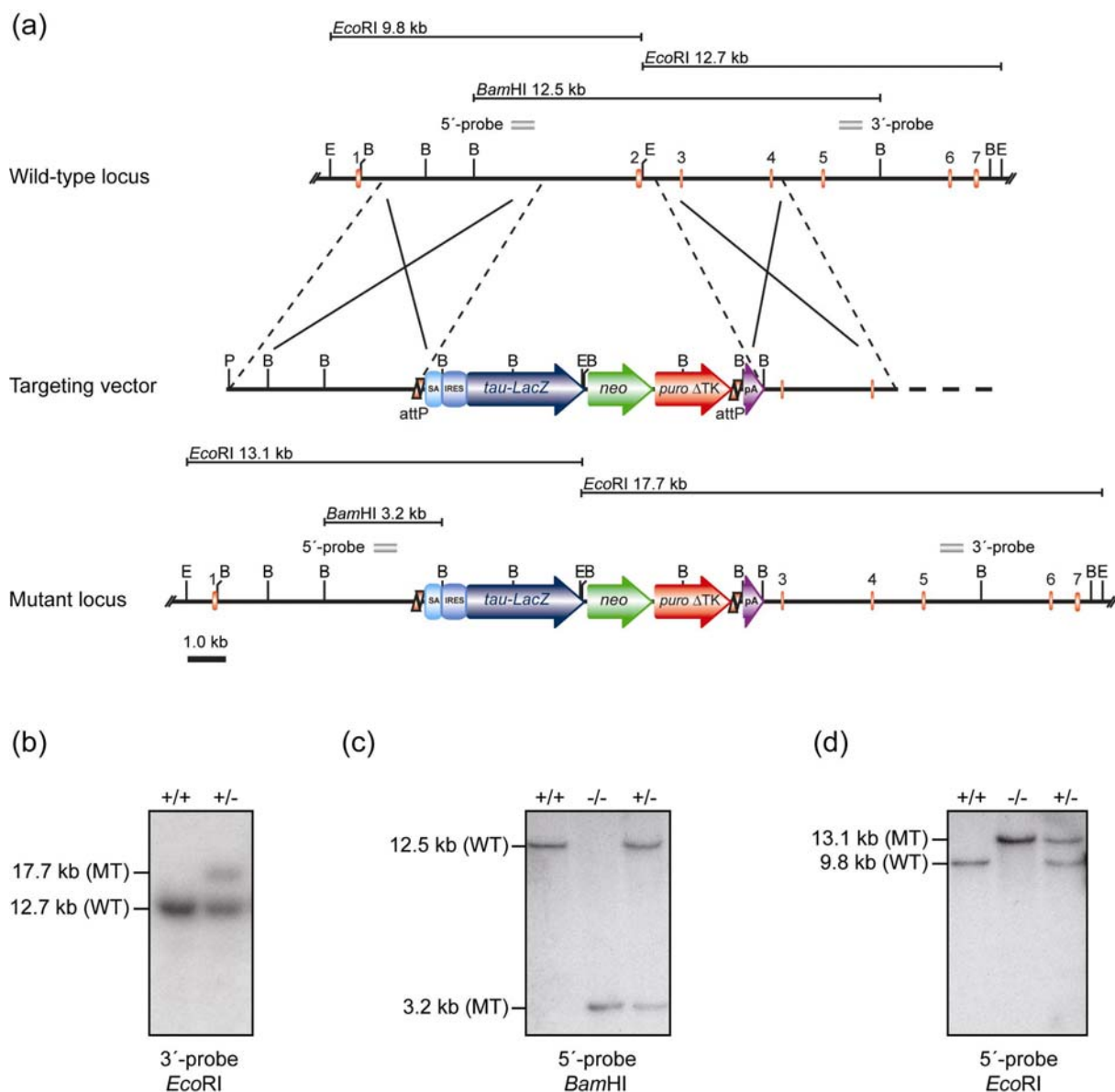


Fig. 12. Generation of *P2rx7* knockout mice. (a) Strategy for inactivation of the *P2rx7* gene. Partial restriction maps of the wild-type *P2rx7* locus, targeting vector and recombined locus (B, *Bam*HI; E, *Eco*RI; P, *Pac*I; SA, splice acceptor). (b) Southern blot analysis of wild-type and targeted ES cell clones. The 3'-probe was hybridized to *Eco*RI-digested genomic ES cell DNA. The targeted allele is indicated by the presence of an additional mutant 17.7 kb fragment. (c) Southern blot analysis of *Bam*HI-digested tail DNA of *P2rx7* mutant mice hybridized with the 5'-probe. The targeted allele is indicated by the presence of an additional mutant 3.2 kb fragment. (d) Southern blot analysis of *Eco*RI-digested tail DNA of *P2rx7* mutant mice hybridized with the 5'-probe. The targeted allele is indicated by the presence of an additional mutant 13.1 kb fragment. The hybridizing fragments obtained correspond to the indicated genotypes.

Targeting via homologous recombination in ES cells resulted in the deletion of a 2.3 kb segment of the *P2rx7* gene including exon 2. The loss of exon 2 and introduction of the reporter-selection cassette resulted not only in a frame shift but

also in a truncated *P2rx7* transcript due to introduction of a triple polyA sequence. The mutated *P2rx7* allele was successfully transmitted through the germline and in the F₂ generation homozygous *P2rx7*^{-/-} mutant mice were obtained at expected Mendelian frequency.

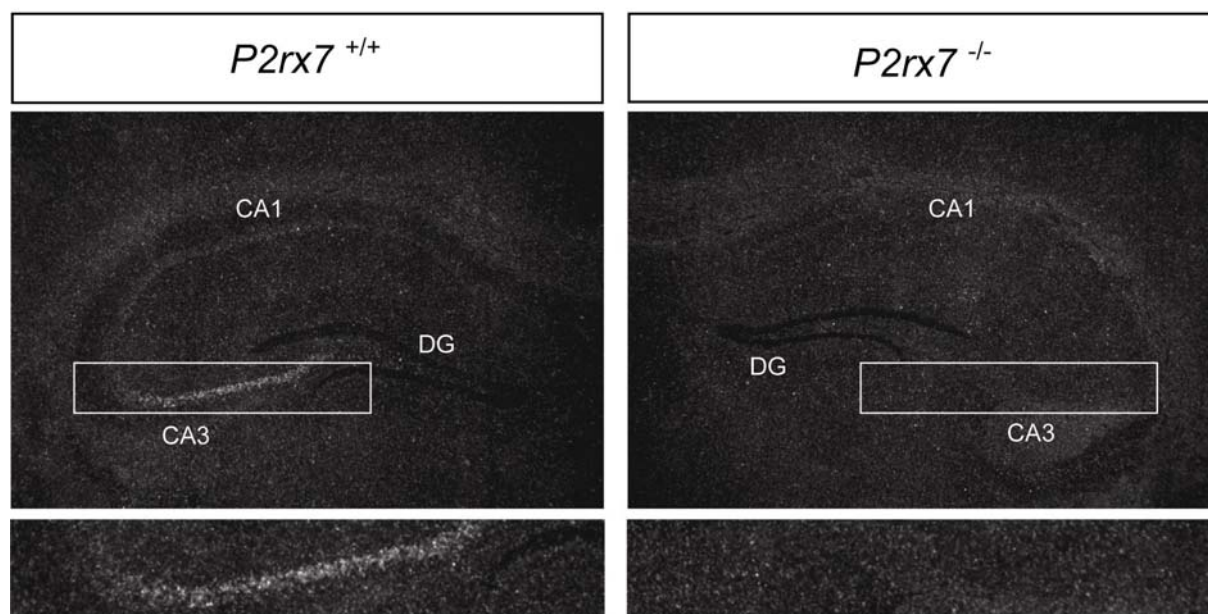
Homozygous *P2rx7* deficient mice exhibited normal development at birth. Postnatal development was also indistinguishable from that of heterozygous and wild-type littermates. Inspection of external and internal organs at different ages did not reveal any macroscopic abnormalities in *P2rx7*^{-/-} mice. No pathological alterations were detected upon histological examination of various organ systems including brain, heart, lung, liver, spleen, thymus, pancreas, stomach, intestine, ovary, kidney and skeletal muscle (data not shown). Homozygous mutant mice were fertile and reproduced normally.

3.1.1.2 Molecular characterization of *P2rx7* knockout mice

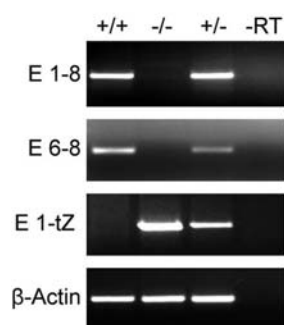
3.1.1.2.1 Expression analysis

To test for inactivation of the *P2rx7* gene in homozygous mutant mice, its expression was studied by *in situ* hybridization on brain sections as well as by RT-PCR. The characteristic expression pattern of *P2rx7* in the CA3 region of the hippocampus was observed in the brain of *P2rx7*^{+/+} mice, whereas no *P2rx7* transcript was detected in the brains of *P2rx7*^{-/-} animals indicating that the *P2rx7* gene was successfully disrupted (Fig. 13a). Along these lines, no *P2rx7*-specific transcript was detected in the brain of *P2rx7*^{-/-} animals by RT-PCR. Instead, a fusion transcript of exon 1 and the *tau-LacZ* reporter gene was detectable in heterozygous and homozygous mutant animals (Fig. 13b). In contrast to the findings in a previously established *P2rx7* deficient mouse line (Chessell et al., 2005; Nicke et al., 2009), neither *P2rx7(k)* nor any other known splice variants were detectable in the brain or peripheral tissues of *P2rx7*^{-/-} animals (Fig. 13c).

(a)



(b)



(c)

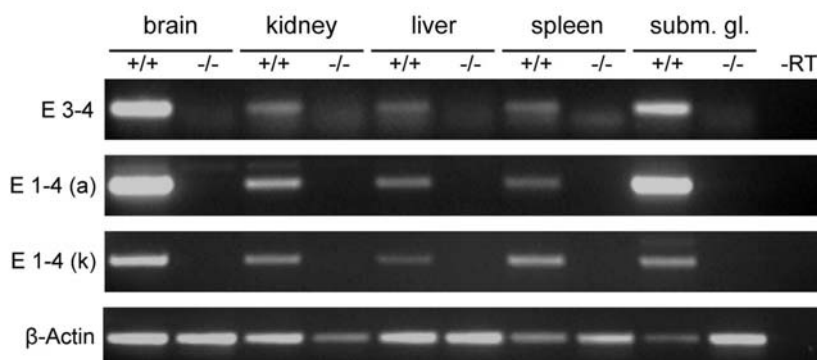


Fig. 13. Verification of successful disruption of *P2rx7*. (a) Disruption of *P2rx7* as demonstrated by *in situ* hybridization using a *P2rx7*-specific radiolabeled riboprobe detecting endogenous *P2rx7* mRNA expression. Depicted are representative dark-field photomicrographs of coronal brain sections of the hippocampus of *P2rx7* wild-type (*P2rx7*^{+/+}) and knockout (*P2rx7*^{-/-}) mice. Additionally, a magnification of the hippocampal CA3 region is shown below. *P2rx7*^{+/+} mice display the characteristic expression of *P2rx7* in the CA3 region of the hippocampus, whereas in *P2rx7*^{-/-} animals the expression is completely abolished. (b) Expression analysis of *P2rx7* in the adult brain as determined by RT-PCR using primers located in exons (E) 1 and 8, E 6 and 8 or in the *tau-lacZ* (tZ) reporter gene. Endogenous transcript levels are not detectable in *P2rx7*^{-/-} mice; instead of that the *tau-LacZ* reporter gene is expressed. A gene dosage-dependent expression is evident in heterozygous and homozygous *P2rx7* mutant animals. The RT-PCR for β -Actin demonstrates the utilization of identical amounts of cDNA derived from brain and liver RNA respectively (-RT, control without reverse transcription). (c) PCR on cDNA from the indicated tissues of *P2rx7*^{+/+} and *P2rx7*^{-/-} mice was performed using specific primer pairs located in indicated exons (E) amplifying either the *P2rx7*(a) or *P2rx7*(k) variant. The expression of *P2rx7* mRNA in *P2rx7*^{-/-} mice was fully abolished (subm. gl., submandibular gland).

3.1.1.2.2 Functional analysis

The successful disruption of *P2rx7* was functionally confirmed by the inability of peritoneal macrophages derived from *P2rx7*^{-/-} animals to mount a normal IL-1 β response upon LPS/BzATP stimulation, as determined by ELISA (Fig. 14a). Additionally, a significantly reduced calcium influx was measured upon BzATP treatment of peritoneal macrophages isolated from *P2rx7*^{-/-} mice. Stimulation of the cells with KCl was used as a positive control (ANOVA + post-hoc: wild-type basal vs. BzATP $p < 0.05$, wild-type basal vs. KCl $p < 0.001$; knockout basal vs. BzATP $p > 0.05$, knockout basal vs. KCl $p < 0.01$) (Fig. 14b).

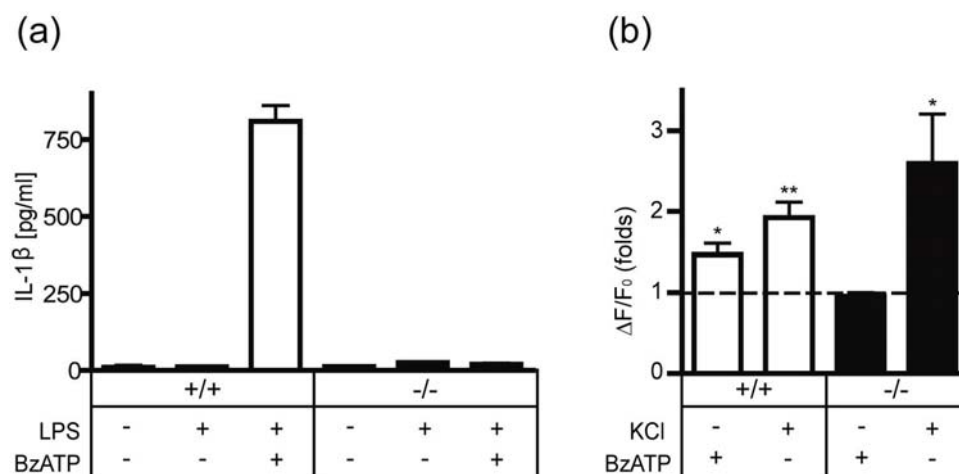


Fig. 14. Functional validation of *P2rx7* knockout. (a) IL-1 β release. Peritoneal macrophages of *P2rx7*^{-/-} mice fail to secrete IL-1 β in response to LPS stimulation and subsequent treatment with 2 mM of the P2RX7 agonist BzATP. Stimulation only with LPS or BzATP was used as negative control. Data are expressed as mean + S.E.M. (n = 4). (b) Calcium imaging. Peritoneal macrophages of *P2rx7*^{-/-} mice show a significantly reduced calcium influx in response to BzATP treatment. Calcium influx in peritoneal macrophages of *P2rx7*^{+/+} and *P2rx7*^{-/-} mice can be activated in a comparable manner upon KCl treatment (ANOVA + post-hoc: wild-type basal vs. BzATP $p < 0.05$, wild-type basal vs. KCl $p < 0.001$; knockout basal vs. BzATP $p > 0.05$, knockout basal vs. KCl $p < 0.01$). Calcium data are shown as $\Delta F/F_0$, where F_0 is the resting fluorescence (before stimulation) and ΔF is the peak change in fluorescence from resting levels. Data are expressed as mean + S.E.M. (n = 14).

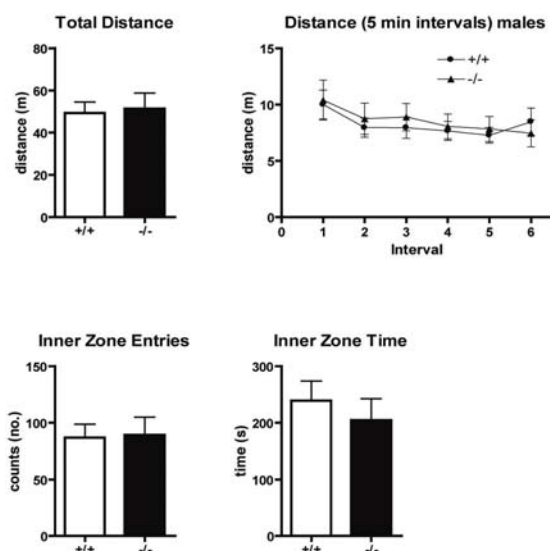
3.1.1.3 Behavioral characterization of *P2rx7* knockout mice

A comprehensive behavioral analysis was carried out in collaboration with Affectis Pharmaceuticals (Martinsried, Germany). A general assessment of physical habitus,

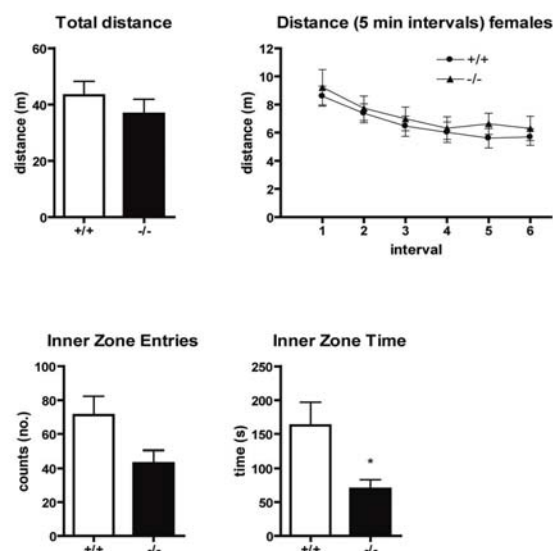
gait, grip strength, reaction to manipulation and other parameters did not yield differences between the genotypes, both in males and females (data not shown).

No differences in total activity between the genotypes were observed in the open field in both genders (Fig. 15a, b). In contrast to male knockout mice, knockout females made less inner zone entries ($p=0.0535$) and spent significantly less time in the inner zone than their wild-type counterparts ($p=0.0250$) (Fig. 15b). No significant differences between the genotypes could be detected in the dark/light box in both genders, however female knockout mice tended to spend less time in the lit compartment compared to wild-type animals ($p=0.0556$) (Fig. 15c, d).

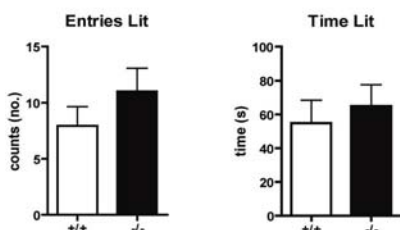
(a) Open field - males



(b) Open field - females



(c) Dark/light box - males



(d) Dark/light box - females

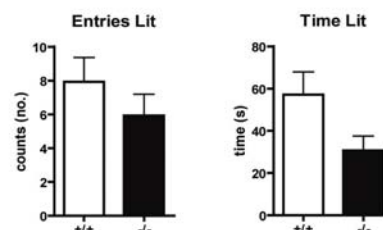


Fig. 15. Behavior of $P2rx7$ knockout mice in the open field and dark/light box test. Open field test (a, b): The graphs represent the covered distance both during the total 30 min testing period and split in 5 min intervals, and inner zone exploration of male (a) and female (b) $P2rx7$ wild-type ($P2rx7^{+/+}$; white bars) and knockout mice ($P2rx7^{-/-}$; black bars). Data are expressed as means + S.E.M. $n = 13-16$ per group. * $p < 0.05$ vs. $P2rx7^{+/+}$, t-test. Dark/light box test (c, d): The graphs represent the number of entries and time spent in the lit compartment of male (c) and female (d) $P2rx7^{+/+}$ and $P2rx7^{-/-}$ mice. Data are expressed as means + S.E.M. $n = 13-16$ per group.

While males did not significantly differ in behavior in the forced swim test (Fig. 16a), a significant increase in the floating time was detected in females ($p=0.0008$) (Fig. 16b).

(a) Forced Swim Test - males

(b) Forced Swim Test - females

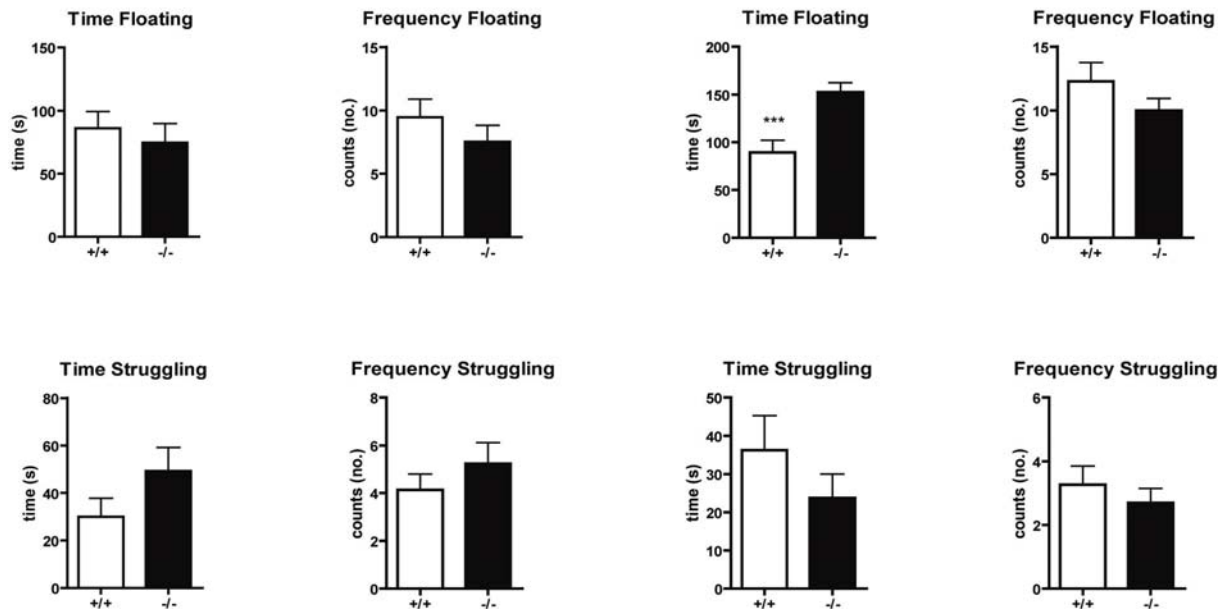
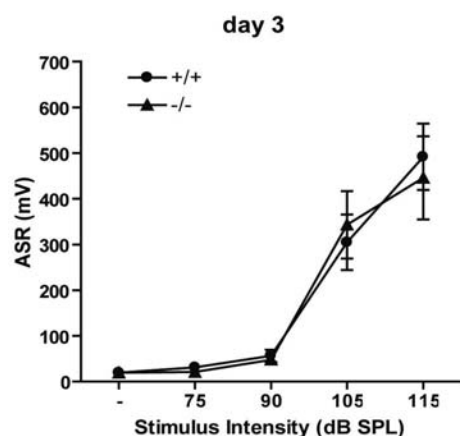


Fig. 16. Behavior of *P2rx7* knockout mice in the forced swim test. The graphs represent times and frequencies of struggling and floating behavior in the forced swim test of male (a) and female (b) *P2rx7* wild-type (*P2rx7*^{+/+}; white bars) and knockout (*P2rx7*^{-/-}; black bars) mice. Data are expressed as means + S.E.M. $n = 13-16$ per group. *** $p < 0.001$ vs. *P2rx7*^{+/+}, t-test.

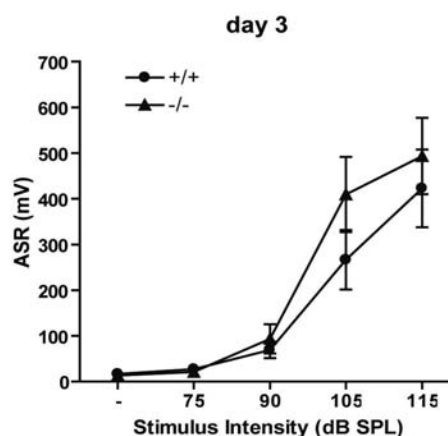
No differences between the genotypes were detected in body weight, water and saccharin consumption, novel food latency, marble burying, object recognition and on the modified hole board (data not shown).

The acoustic startle response did not significantly differ between the genotypes at different stimulus intensities of 75, 90, 105 and 115 dB for both males and females (Fig. 17a, b; third day of testing is shown). A similar result was obtained in the prepulse inhibition test at stimulus intensities of 55, 65, 75 dB (Fig. 17c, d; 75 dB condition is shown).

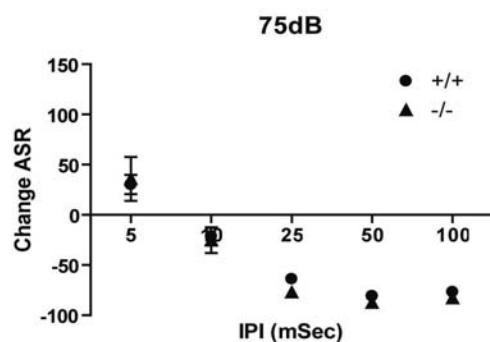
(a) Acoustic startle response - males



(b) Acoustic startle response - females



(c) Prepulse inhibition - males



(d) Prepulse inhibition - females

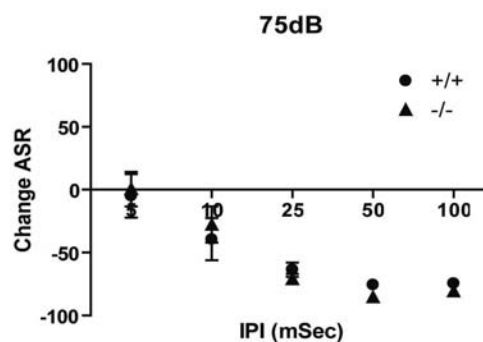


Fig. 17. Behavior of *P2rx7* knockout mice in the acoustic startle response and prepulse inhibition testing. Acoustic startle response (a, b): The data depicted on the graphs represent the mean peak startle amplitude in $mV \pm SEM$ in response to 30 pulses of each intensity, as well as 12 background noise (BG) measurements. Prepulse inhibition testing (c, d): The data depicted represent prepulse inhibition as a percentage change from baseline (without prepulse) for each interpulse interval. For both ASR and PPI, the intertrial interval ranged from 13 to 17 s.

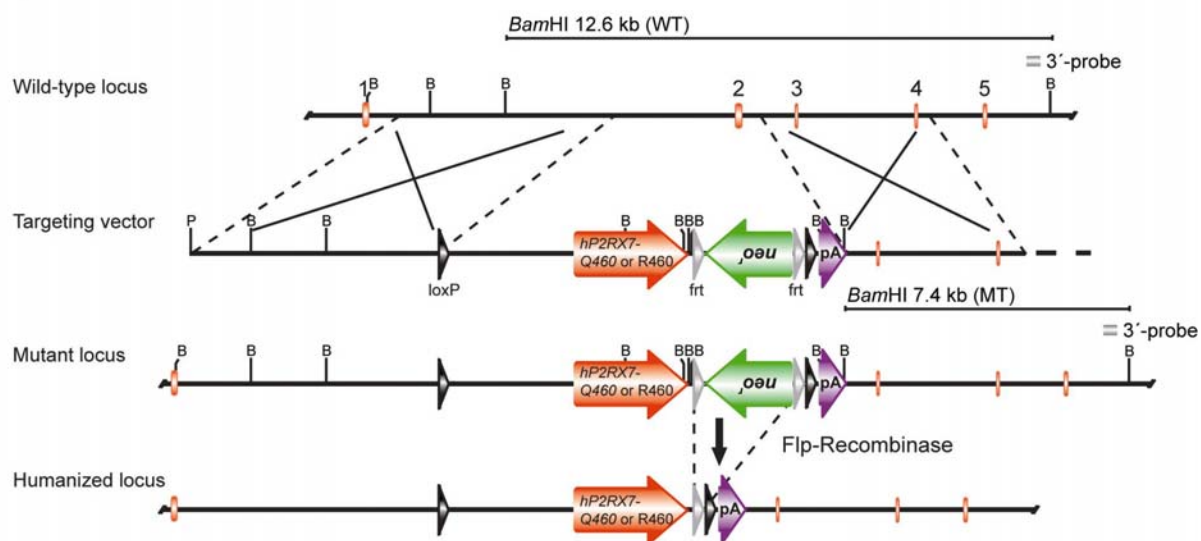
3.1.2 Generation and characterization of humanized *P2RX7* mouse mutants

3.1.2.1 Generation of humanized mouse mutants

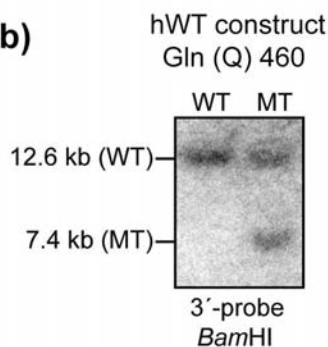
Homology arms were amplified by PCR from genomic DNA of TBV2 ES cells and cloned via the TOPO TA cloning kit. The 6.0 kb 5'-HA was amplified with primers containing a *PacI* and a *MfeI* restriction site, the 4.0 kb 3'-HA was amplified with primers containing an *Ascl* and an *EcoRI* restriction site. The sequence verified 5'-HA was inserted into a previously cloned shuttle vector via *PacI/MfeI*, and the 3'-HA via *Ascl/EcoRI*. The homology arms enframe (from 5' to 3'): a *loxP* site followed by the 3' end (1.4 kb) of mouse intron 1; the murine exon 2 is replaced by the human *P2RX7* cDNA comprising exons 2-13 of the wild-type (Gln460) or the mutant (Arg460) variant, respectively; a reverse oriented selection marker flanked by *frt* sites which consists of a phosphoglycerate kinase (PGK) promoter driven neomycin resistance gene equipped with a bovine growth hormone (bGH) poly A signal (pA), a second *loxP* site and finally a quadruple poly A signal consisting of a bGHpA, a PGK pA, and two SV40 pAs (Fig. 18a).

The linearized (via *PacI*) targeting vector was electroporated into TBV2 ES cells. Mutant ES cell clones were identified by Southern blot analysis of genomic ES cell DNA digested with *BamHI* using the 3' external probe (Fig. 18b, c). Mutant ES cells were used to generate chimeric mice by blastocyst injection. Germ-line transmission of the modified *P2rx7* allele was confirmed in offspring from male chimeras bred to wild-type C57BL/6J mice. Finally, the *frt* flanked selection cassette was removed by breeding to Flp-deleter mice (Rodriguez et al., 2000). Genotyping was performed by PCR and a subsequent restriction digest of the 557 bp PCR product with *PvuII*. Standard PCR conditions followed by *PvuII* digestion resulted in a 171 bp, 332 bp and 54 bp fragment for the human wild-type (Gln460) and a 503 bp and 54 bp fragment for the human mutant (Arg460) allele (Fig. 18d). Humanized mice, either homozygous for the wild-type hP2RX7-Gln460 ($P2rx7^{hGln460/hGln460}$, referred to as $P2rx7^{hWT}$) or for the mutant hP2RX7-Arg460 ($P2rx7^{hArg460/hArg460}$, referred to as $P2rx7^{hMT}$) were intercrossed to yield heterozygous $P2rx7^{hGln460/hArg460}$ (referred to as $P2rx7^{hWT/hMT}$) animals which were finally interbred to obtain $P2rx7^{hWT}$, $P2rx7^{hWT/hMT}$ and $P2rx7^{hMT}$ offspring at Mendelian rates (Fig. 19).

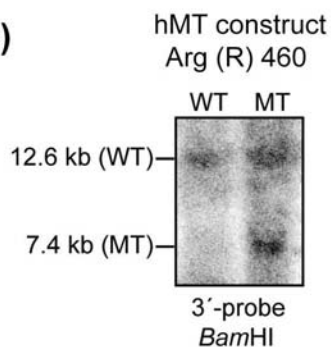
(a)



(b)



(c)



(d)

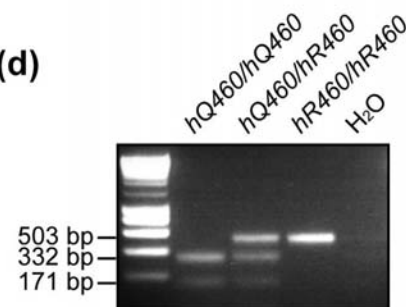


Fig. 18. Generation of humanized *P2RX7* (*hP2RX7*) mice. (a) Strategy for knockin of the human *P2RX7* gene. Partial restriction maps of the wild-type *P2rx7* locus, targeting vector, recombined locus and humanized locus after Flp recombinase-mediated deletion of the selection marker (B, *Bam*HI; P, *Pacl*; pA, polyadenylation signal). (b) Southern blot analysis of wild-type and targeted ES cell clones. The 3'-probe was hybridized to *Bam*HI-digested genomic ES cell DNA carrying the human wild-type construct. The targeted allele is indicated by the presence of an additional 7.4 kb fragment. (c) Southern blot analysis of *Bam*HI-digested ES cell DNA carrying the Q460R construct hybridized with the 3'-probe. The targeted allele is indicated by the presence of an additional 7.4 kb fragment. (d) Genotyping was performed by PCR and subsequent restriction digest of the 557 bp PCR product with *Pvu*II resulting in a 171 bp, 332 bp and 54 bp fragment for the human wild-type and a 503 bp and 54 bp fragment for the human mutant construct.

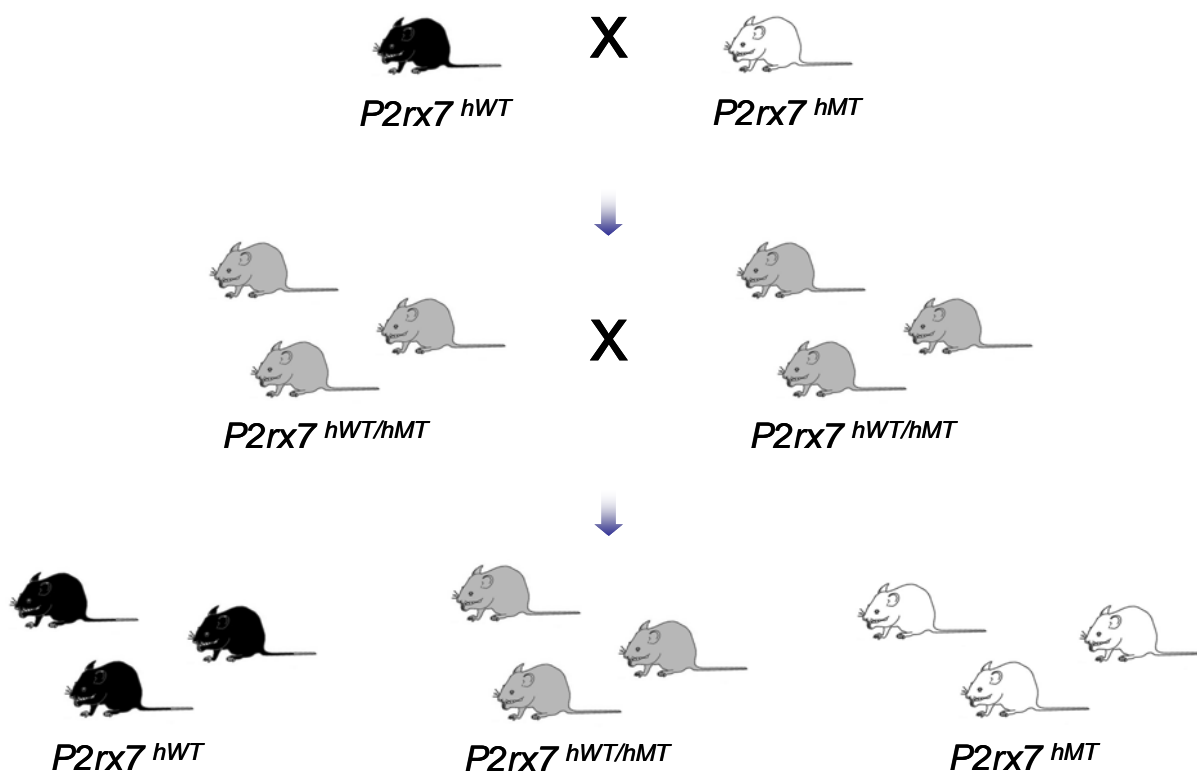


Fig. 19. Breeding scheme of *hP2RX7* mouse mutants. Humanized mice, either homozygous for the wild-type hP2RX7-Gln460 ($P2rx7^{hWT}$) or for the mutant hP2RX7-Arg460 ($P2rx7^{hMT}$) were intercrossed to yield heterozygous ($P2rx7^{hWT/hMT}$) animals which were finally interbred to obtain $P2rx7^{hWT}$, $P2rx7^{hWT/hMT}$ and $P2rx7^{hMT}$ offspring at Mendelian rates. All three genotypes were used for subsequent validation of the risk genotype.

3.1.2.2 Molecular characterization of humanized mouse mutants

3.1.2.2.1 Expression analysis

For verification of the knockin of the human *P2RX7* gene, its expression was studied by *in situ* hybridization on brain sections. A mouse-specific radiolabeled *P2rx7* riboprobe was used to detect endogenous *P2rx7* expression whereas a human-specific riboprobe was used to detect the expression of the knockin construct. $P2rx7^{+/+}$ mice display the characteristic expression of endogenous *P2rx7* in the CA3 region of the hippocampus, whereas the expression is completely abolished in homozygous $P2rx7^{hMT}$ animals (Fig. 20). Instead, the expression pattern of human *P2RX7* can be detected in knockin mice, and is identical to that of endogenous mouse *P2rx7* due to transcription from the endogenous *P2rx7* locus (Fig. 20).

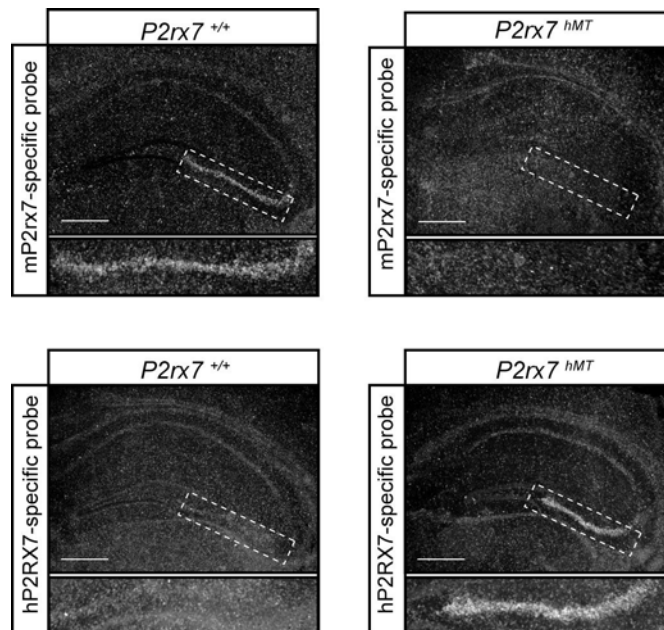


Fig. 20. The expression of human *P2RX7* in humanized knockin mice recapitulates endogenous expression of murine *P2rx7* as demonstrated by *in situ* hybridization. A mouse-specific radiolabeled *P2rx7* riboprobe was used to detect endogenous *mP2rx7* expression, whereas a human-specific riboprobe was used to detect the expression of *hP2RX7*. Depicted are representative dark-field photomicrographs of coronal brain sections of the hippocampus of *P2rx7* wild-type (*P2rx7*^{+/+}) and homozygous knockin mice expressing the mutant *P2RX7* Gln460Arg variant (*P2rx7*^{hMT}; scale bar 100 μ m).

3.1.2.2.2 Functional analysis

Functional validation was carried out via measurement of IL-1 β release from peritoneal macrophages derived from *hP2RX7* animals as determined by ELISA. In general, P2X7 receptors of all three genotypes were able to induce IL-1 β release from peritoneal macrophages stimulated with LPS/BzATP. Compared to *P2rx7*^{hWT}, peritoneal macrophages of *P2rx7*^{hWT/hMT} and *P2rx7*^{hMT} mice showed a significant increase in IL-1 β secretion in response to LPS stimulation and subsequent treatment with the P2RX7 agonist BzATP. Interestingly, *P2rx7*^{hWT/hMT} mice showed an even stronger increase than the *P2rx7*^{hMT} (Fig. 21).

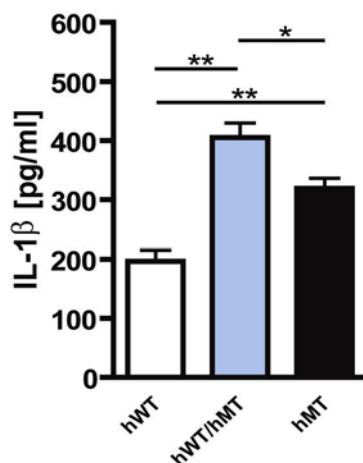


Fig. 21. Functional validation of *hP2RX7* mice via IL-1 β ELISA. Peritoneal macrophages of *P2rx7*^{hWT/hMT} and *P2rx7*^{hMT} mice showed a significant increase in IL-1 β secretion in response to LPS stimulation and subsequent treatment with 2 mM of the P2RX7 agonist BzATP compared to *P2rx7*^{hWT} mice. *P2rx7*^{hWT/hMT} mice showed an even stronger increase than the *P2rx7*^{hMT} mice (ANOVA + Newman-Keuls post-hoc: hWT vs. hWT/MT $p < 0.001$, hWT vs. hMT $p < 0.001$, hMT vs. hWT/MT $p < 0.01$). Data are expressed as mean + S.E.M. (Data of four independent experiments were pooled, each $n = 4$).

In order to investigate whether the different activation levels of P2RX7 impact the intracellular signaling cascade, we examined BzATP-induced ERK phosphorylation in primary hippocampal neurons derived from *hP2RX7* E18 embryos. In response to BzATP, neurons isolated from *P2rx7*^{hWT} animals showed a robust time-dependent ERK 1/2 phosphorylation. In contrast, the response to BzATP seemed to be diminished in neurons from *P2rx7*^{hWT/hMT} and *P2rx7*^{hMT} mice (Fig. 22).

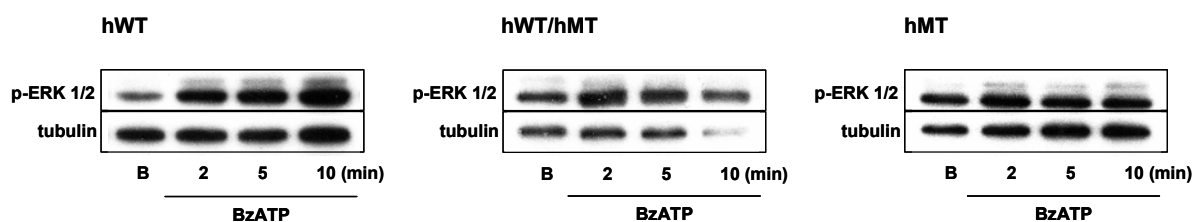


Fig. 22. Measurement of ERK 1/2 phosphorylation as determined by Western blot analysis. Neurons isolated from *P2rx7*^{hWT} animals showed a robust time-dependent ERK 1/2 phosphorylation in response to BzATP. In contrast, the response to BzATP seemed to be diminished in neurons from *P2rx7*^{hWT/hMT} and *P2rx7*^{hMT} mice. Primary hippocampal neurons (DIV14) isolated from *hP2RX7* E18 embryos were treated with 1 mM of the P2RX7 agonist BzATP for 2, 5 and 10 min (B, basal). Cells were harvested in RIPA lysis buffer and analyzed by Western blot using an anti-phospho-p44/42 MAPK (ERK 1/2) antibody (an anti-tyr-tubulin YL1/2 antibody was used to demonstrate the utilization of identical amounts of total protein).

3.1.2.3 Behavioral analysis of humanized mouse mutants

3.1.2.3.1 Basal characterization

Behavioral phenotyping of humanized mice did not reveal any significant differences in the open field (OF), elevated plus maze (EPM) or dark-light box under standard housing conditions (data not shown, compare Fig. 25). However, *P2rx7*^{hWT/hMT} mice showed a decreased acoustic startle response compared to their *P2rx7*^{hWT} and *P2rx7*^{hMT} littermates (Fig. 23).

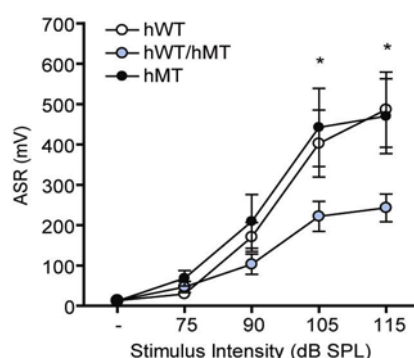


Fig. 23. Acoustic startle response. The acoustic startle response was significantly reduced in heterozygous animals at stimulus intensities greater than 90 dB (third day of testing; repeated measures ANOVA + post-hoc, $p < 0.05$).

3.1.2.3.2 Effects of chronic social defeat stress on *hP2RX7* mice

Since stress in combination with a genetic predisposition can act as a trigger for processes that result in an increased risk of developing mood disorders (de Kloet et al., 2005), we subjected *hP2RX7* mice to three weeks of chronic social defeat stress (Berton et al., 2006; Wagner et al., 2011) to assess whether the Gln460Arg polymorphism has any impact on the animals' stress response. All genotypes of *hP2RX7* mice showed similar characteristic physiological changes evoked by the CSDS (Fig. 24). These included a decrease in fur quality (Fig. 24a), a progressive increase in body weight (Fig. 24b), an enlargement of adrenal glands (Fig. 24c), an atrophy of the thymus (Fig. 24d) and a sensitization to a novel stressor (Fig. 24e).

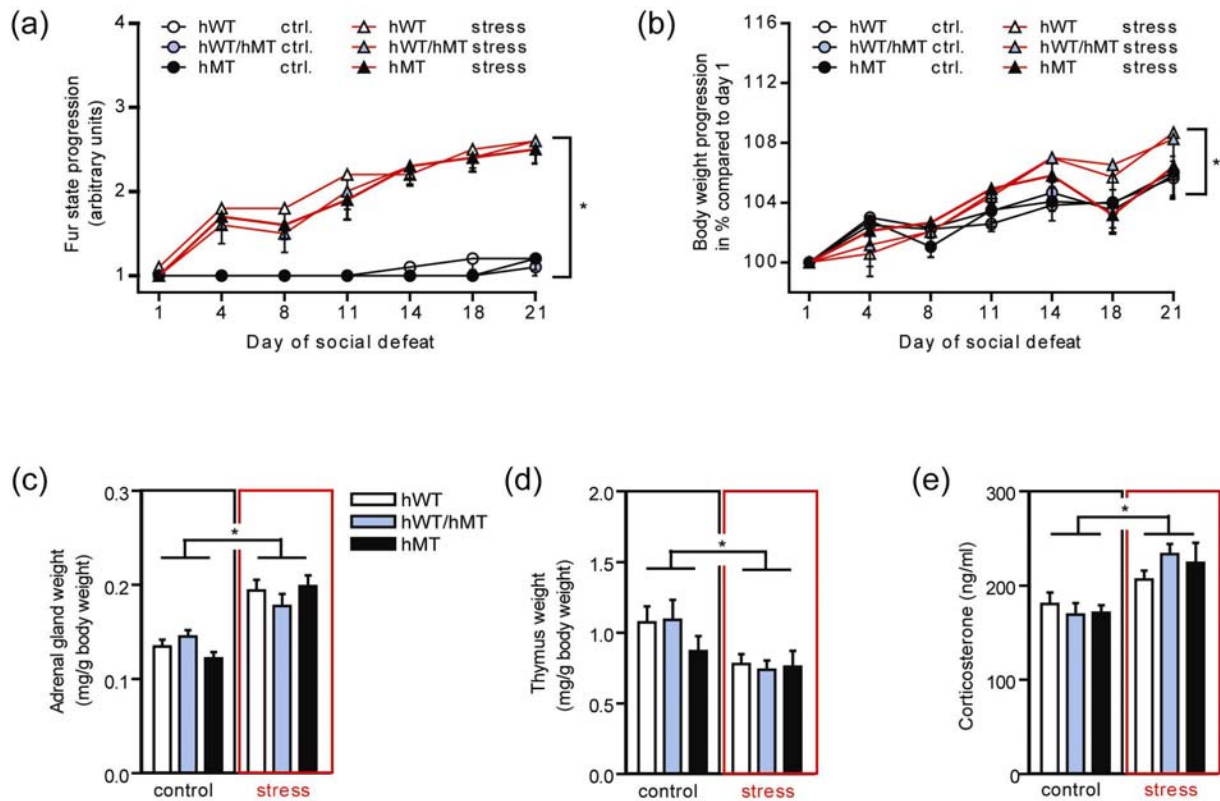


Fig. 24. Chronic social defeat stress induces robust physiological and neuroendocrine changes independent of genotypes. (a) CSDS led to a decrease in fur quality from day four onwards, depicted by an increase in fur state index (Repeated-measures ANOVA, $p < 0.0005$). (b) Stressed animals showed an increase in body weight gain compared to control littermates throughout the time course of the defeat (Repeated-measures ANOVA, $p < 0.05$). (c) An increase in relative adrenal weights was observed in mice subjected to CSDS (ANOVA, $p < 0.0005$). (d) Thymus weights were significantly reduced in stressed animals compared to their littermate controls (ANOVA, $p < 0.005$). (e) CSDS led to an enhanced corticosterone response following a forced swim challenge (ANOVA, $p < 0.0001$).

To further evaluate the effect of CSDS on behavioral endophenotypes related to mood disorders, stressed and control mice were subjected to a series of tests evaluating locomotion, anxiety-like behavior, sociability and social avoidance as well as hedonic behavior. In general, chronically stressed mice showed a decreased locomotion in the OF compared to unstressed mice. However, in the first 5 min of the OF stressed heterozygous $P2rx7^{hWT/hMT}$ mice did not show a decrease in locomotion (Fig. 25a). In response to CSDS heterozygous $P2rx7^{hWT/hMT}$ mice showed a significantly stronger decrease of the open arm time compared to $P2rx7^{hWT}$ and $P2rx7^{hMT}$ littermates (Fig. 25b).

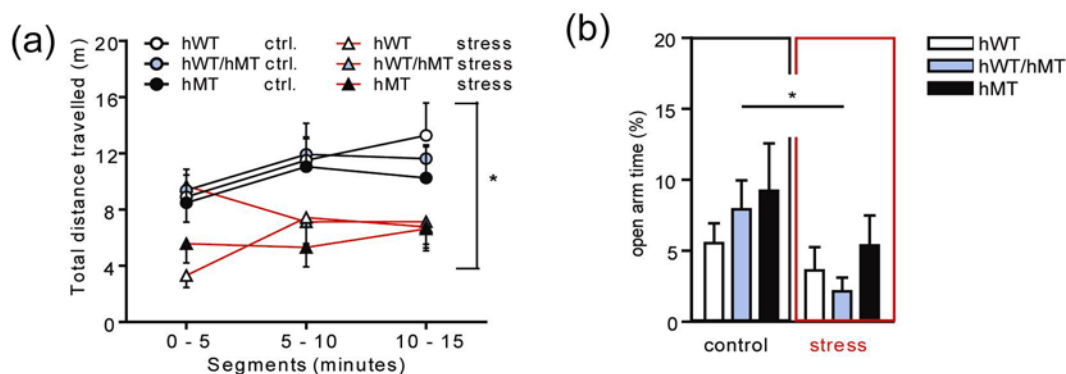


Fig. 25. Assessing anxiety-related behavior. (a) Chronically stressed mice displayed a decrease in locomotion during the open field test, compared to control animals (repeated measures ANOVA, $p < 0.005$). However, CSDS did not induce a decrease in locomotion in heterozygous $P2rx7^{hWT/hMT}$ mice during the first 5 min of the OF. (b) Heterozygous $P2rx7^{hWT/hMT}$ mice showed an enhanced anxiety response to CSDS in the EPM compared to $P2rx7^{hWT}$ and $P2rx7^{hMT}$ animals (ANOVA + post-hoc, $p < 0.05$).

A variety of neuropsychiatric disorders, including depression are characterized by disruption of social behavior (Nestler and Hyman, 2010). Along these lines, chronically stressed heterozygous $P2rx7^{hWT/hMT}$ mice developed a deficit in social behavior, as indicated by a significant decrease in preference for the social counterpart in the sociability test (Fig. 26a). A similar finding was observed in the social avoidance test. Upon CSDS $P2rx7^{hWT/hMT}$ mice spent significantly less time in close proximity to the social target compared to unstressed $P2rx7^{hWT/hMT}$ animals (Fig. 26b). In addition, only $P2rx7^{hWT/hMT}$ mice displayed this aversive response also in the presence of the novel object (Fig. 26c).

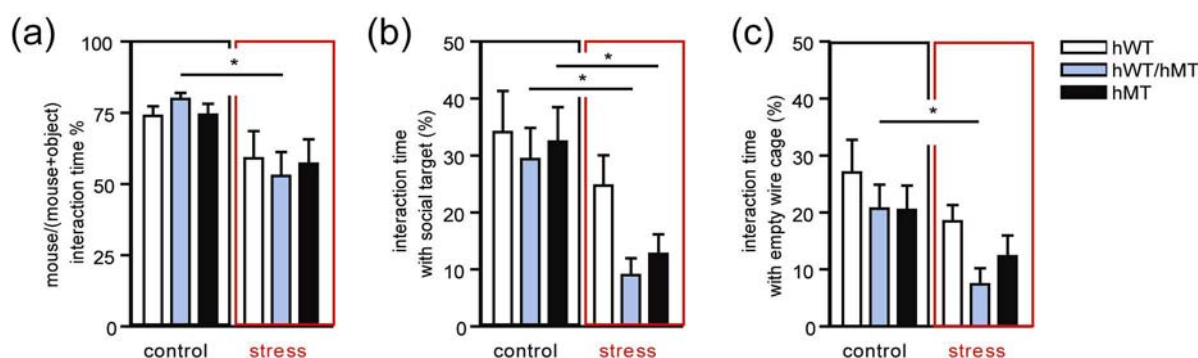


Fig. 26. Assessing social behavior. (a) Chronically stressed $P2rx7^{hWT/hMT}$ mice displayed reduced sociability, evident in decreased preference for a stranger mouse compared to an object (ANOVA + post hoc, $p < 0.05$). (b) CSDS evoked a decreased interaction time with the social target in heterozygous and homozygous mice during the social avoidance paradigm (ANOVA + post-hoc, $p < 0.05$). (c) Following CSDS, heterozygous mice spent significantly less time interacting with the empty wire cage during the first trial of the social avoidance task (ANOVA + post-hoc, $p < 0.05$).

To assess anhedonic behavior, which is a key feature of depression (Nestler and Hyman, 2010), we applied the female urine sniffing test (FUST). Again, only chronically stressed $P2rx7^{hWT/hMT}$ mice spent significantly less time sniffing female urine (Fig. 27b).

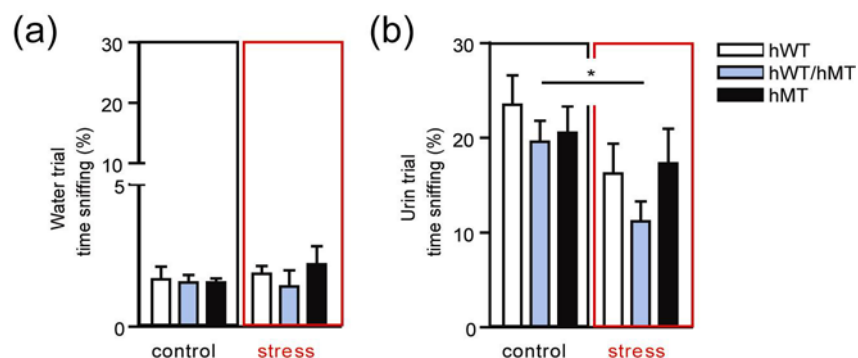


Fig. 27. Assessing anhedonic behavior. (a) No significant genotype and/or condition differences were detectable in the water trial of the FUST. (b) During the FUST, a significant decrease in time spent sniffing estrus female urine was only observed in stressed heterozygous animals compared to controls of the same genotype (ANOVA + post-hoc, $p < 0.05$).

Disturbances of the hypothalamic pituitary adrenocortical axis are one of the most robust findings shared by many depressed patients (Holsboer, 2000). Therefore, we investigated plasma corticosterone levels in controls and mice subjected to the CSDS. Heterozygous $P2rx7^{hWT/hMT}$ mice showed a significantly stronger fold increase in basal corticosterone secretion following CSDS, compared to $P2rx7^{hWT}$ and $P2rx7^{hMT}$ mice (Fig. 28).

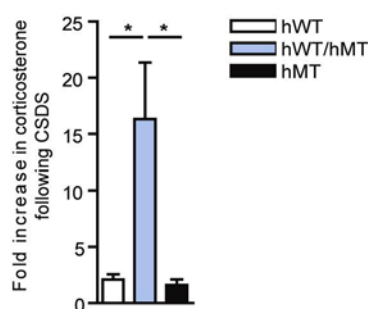


Fig. 28. Corticosterone measurement. CSDS lead to a significantly higher basal corticosterone fold increase in heterozygous compared to $P2rx7^{hWT}$ and $P2rx7^{hMT}$ mice; basal control values were set at 1 (ANOVA + post-hoc, $p < 0.005$).

3.1.2.4 Sleep pattern analysis of humanized mouse mutants

Besides neuroendocrine disturbance impaired sleep is one of the most reliable symptoms accompanying MDD, which even becomes manifest before diagnosis of the disease (Armitage, 2007;Modell et al., 2005;Rao et al., 2009;Steiger and Kimura, 2010). *hP2RX7* mice showed unaltered nocturnal sleep-wake behavior as indicated by the normal distribution of non-rapid eye movement sleep (NREMS) and rapid eye movement sleep (REMS; Fig. 29a, b). However, *P2rx7^{hWT/hMT}* mice showed a significantly higher number of episode entries to REMS during the light period (Fig. 29c), indicating a stronger drive towards REMS and more fragmented sleep cycles compared to *P2rx7^{hWT}* and *P2rx7^{hMT}* mice. Additionally, slow-wave activity (SWA) during NREMS, which measures the depth of NREMS, was constantly low in heterozygous mice (Fig. 29d). Accordingly, only a small amount of deep NREMS (SWS₂) was detected in *P2rx7^{hWT/hMT}* mice (Fig. 29e), suggesting a shallower NREMS. This finding is also reflected in the spectrograms where *P2rx7^{hWT/hMT}* mice exhibited reduced power densities in lower frequency activities of the electroencephalogram (EEG), especially during the light period (Fig. 29f).

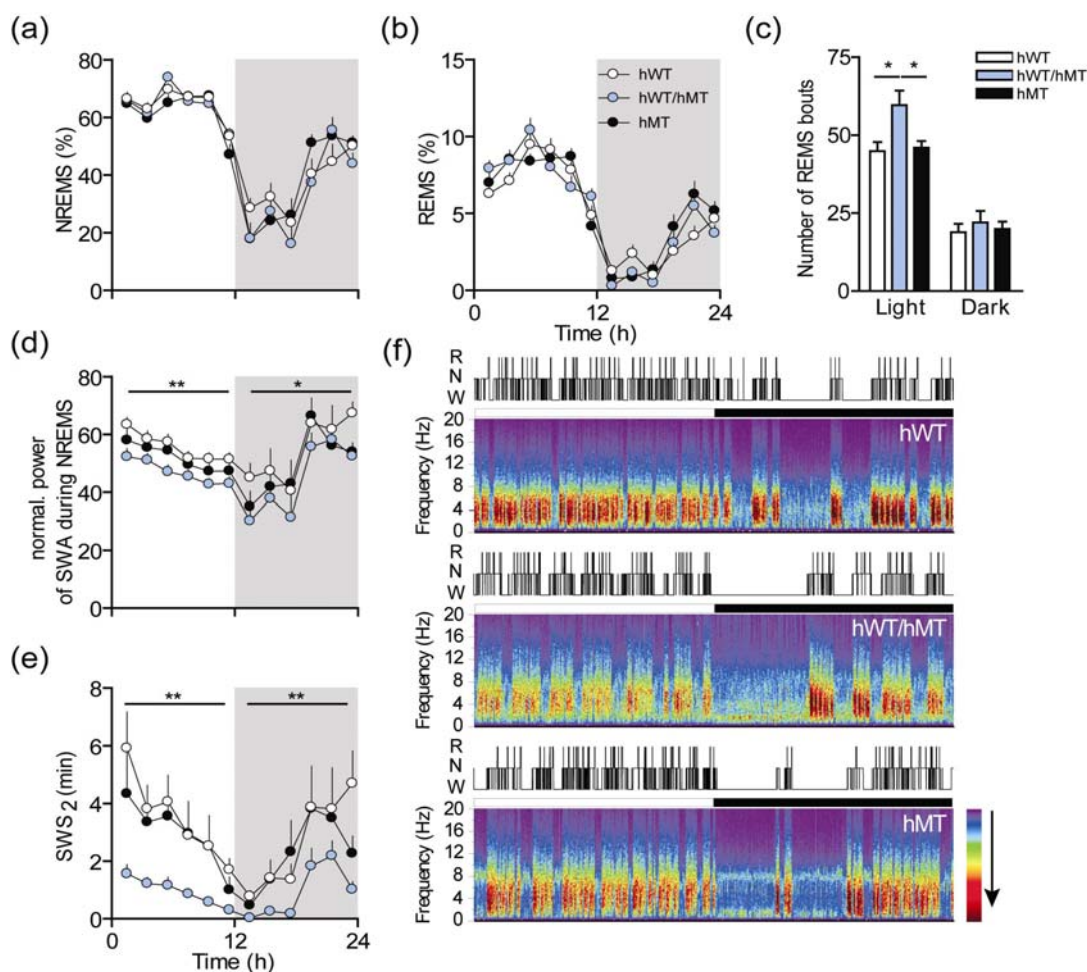


Fig. 29. Impaired sleep structures appear in heterozygous humanized *P2RX7* mutants. (a), (b) Time-course changes in NREMS and REMS during the baseline recording, respectively (2 h mean \pm s.e.m.; $n = 11$ in all groups). No particular genotype differences were observed in the amount of NREMS or REMS across the 24 h recording period. Areas with a grey background indicate the dark period. (c) Architecture of REMS was significantly altered. In heterozygous *P2rx7*^{hWT/hMT} mice which showed more frequent entries to the REMS epoch during the light period (12 h mean \pm s.e.m.; $n = 11$ in all groups; * $p < 0.05$). (d) In addition, slow-wave activity (SWA) during NREMS was significantly attenuated in heterozygous *P2rx7*^{hWT/hMT} mice although the amount of NREMS was comparable to that in other genotypes (2 h mean \pm s.e.m.; $n = 9$, *P2rx7*^{hWT} mice; $n = 11$, *P2rx7*^{hWT/hMT} and *P2rx7*^{hMT} mice; * $p < 0.05$, ** $p < 0.001$). (e) The impairment of NREMS became even clearer when SWS₂ (deeper NREMS that contains more than 50% of delta activity) was separately analyzed. *P2rx7*^{hWT/hMT} mice rarely entered SWS₂ across the whole 24 h. (2 h mean \pm s.e.m.; $n = 9$, *P2rx7*^{hWT} mice; $n = 11$, *P2rx7*^{hWT/hMT} and *P2rx7*^{hMT} mice; ** $p < 0.001$). (f) Hypnograms and spectrograms of a representative animal from each genotype. Dramatic suppression of the EEG power in lower frequency bands was evident in the *P2rx7*^{hWT/hMT} mouse during the light period in comparison to the other genotypes. However, this heterozygous animal showed normal sleep patterns according to its hypnogram. The power is higher towards the direction of the arrow in the color-code bar.

3.1.3 Comparison of mouse and human P2RX7

3.1.3.1 Breeding of littermates for behavioral testing

During handling and behavioral testing, *hP2RX7* animals exhibited signs of generally increased arousal and anxiety-like behavior across genotypes which was evidenced in respective test paradigms such as the OF, EPM or DaLi. Therefore, we compared the emotionality of mice expressing either the mouse or the human wild-type P2RX7, respectively. To this end, homozygous *P2rx7^{hWT}* mice were backcrossed in a first step with C57/BL6 wild-type animals, carrying the murine *P2rx7* gene on both alleles, to yield heterozygous *P2rx7^{+/hWT}* animals. To generate littermates for behavioral testing, heterozygous *P2rx7^{+/hWT}* mice were further intercrossed to obtain *P2rx7^{+/+}*, *P2rx7^{+/hWT}* and *P2rx7^{hWT}* offspring at Mendelian rates.

3.1.3.2 Behavioral characterization

To analyze differences between human and murine P2RX7 on phenotypic alterations, mice were subjected to a series of tests evaluating locomotion and anxiety-like behavior. In the OF, mice showed no difference in locomotion (Fig. 30a). However, *P2rx7^{hWT}* mice showed a significant decrease in the inner zone time (Fig. 30b) as well as in inner zone entries compared to *P2rx7^{+/+}* mice (Fig. 30c).

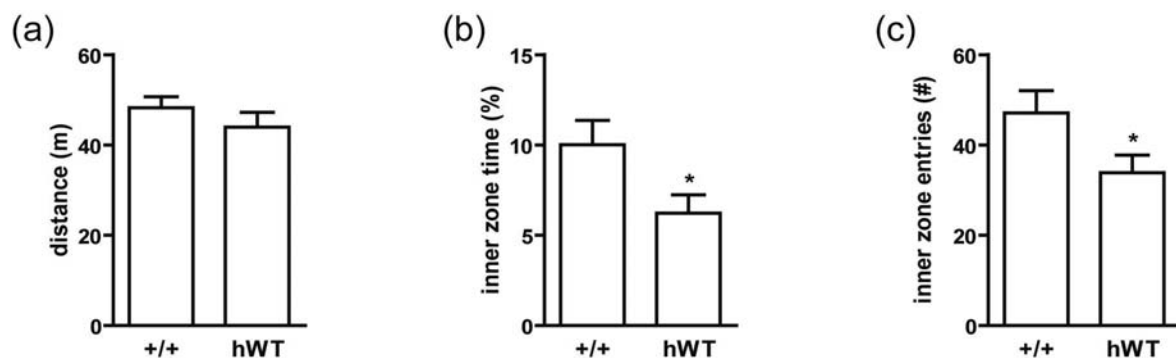


Fig. 30. *hP2RX7* mice exhibit increased anxiety-related behavior in the open field. *P2rx7^{hWT}* mice showed a significant decrease in the inner zone time as well as in inner zone entries compared to *P2rx7^{+/+}* mice (t-test, $p < 0.05$).

Accordingly, $P2rx7^{hWT}$ animals spent significantly less time on the open arms of the EPM (Fig. 31a) and entered these less frequently during the EPM (Fig. 31b). Again, no significant changes in locomotion between the genotypes could be detected during the EPM (Fig. 31c).

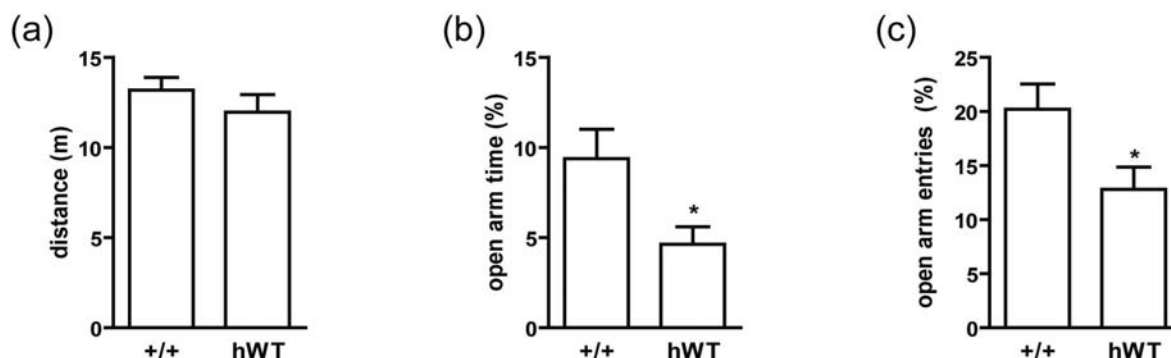


Fig. 31. $hP2RX7$ mice show increased anxiety-like behavior in the elevated plus maze. $P2rx7^{hWT}$ animals spent significantly less time on the open arms and entered these less frequently during the EPM (t-test, $p < 0.05$).

In the dark/light box, there were no differences between the genotypes, neither in the time spent in the lit compartment (Fig. 32a) nor in the number of entries into the lit compartment (Fig. 32b).

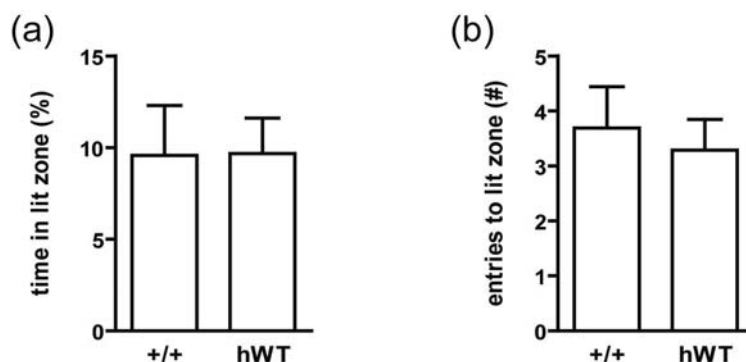


Fig. 32. Anxiety-related behavior is not affected in the dark/light box. No differences between the genotypes could be detected.

Measurement of corticosterone under basal conditions and following acute stress did not reveal any significant differences between $P2rx7^{+/+}$ and $P2rx7^{hWT}$ animals (Fig. 33).

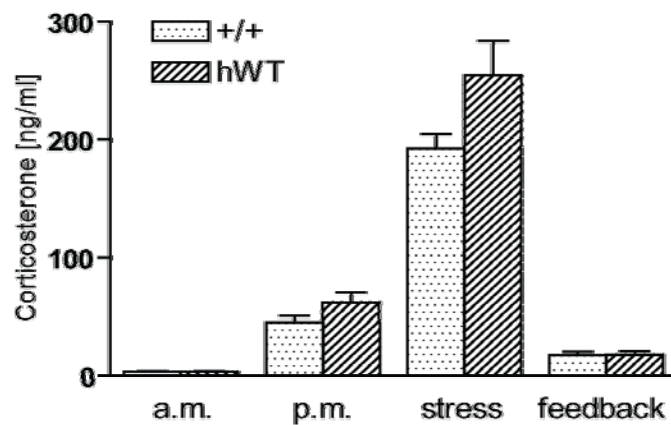


Fig. 33. Corticosterone levels are not altered between $P2rx7^{+/+}$ and $P2rx7^{hWT}$ mice. No significant changes in corticosterone were observed between $P2rx7^{+/+}$ and $P2rx7^{hWT}$ mice. (a.m. values were measured at 9:00 a.m., p.m. values were measured at 4:00 p.m.; acute restraint stress was applied for 10 min; feedback values were measured 90 min after restraint stress).

3.2 Validation of *TMEM132D* as a susceptibility gene for panic disorder and depression

3.2.1 Expression analysis of the *Tmem132* family

Since the expression and molecular function of TMEM132D is largely unknown, we investigated whether *Tmem132d* and other family members are expressed in the adult mouse brain. Therefore, RT-PCRs on RNA isolated from whole mouse brain tissue were performed. Expression of all *Tmem132* family members in the adult mouse brain was confirmed (Fig. 34).

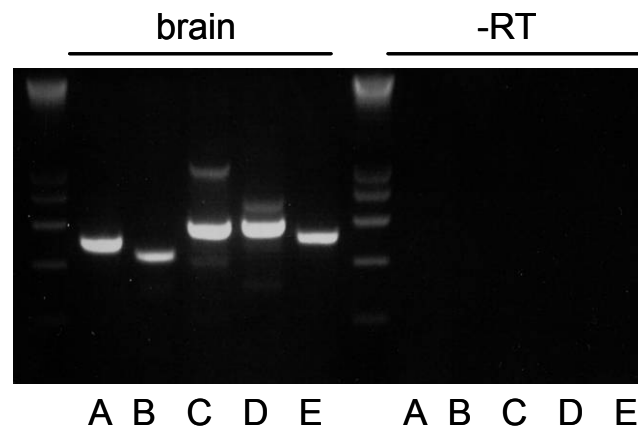


Fig. 34. Expression analysis of *Tmem132* family members using RT-PCR. All family members are expressed in the adult mouse brain.

Accordingly, a detailed expression pattern analysis of all *Tmem132* family members was carried out by *in situ* hybridization (Fig. 35). In general, *Tmem132* family members exhibited large differences in terms of expression pattern and strength in the central nervous system (CNS). *Tmem132a* is highly expressed throughout the entire brain, whereas *Tmem132c* and *Tmem132e* show only weak expression mainly in some thalamic nuclei. Expression of *Tmem132b* seems to be restricted to the forebrain. *Tmem132d* is expressed in the following brain regions: glomerular layer of the olfactory bulb, lateral septum, piriform cortex, cortex (mainly somatosensory cortex), CA1 region of the hippocampus, nuclei of the thalamus, dorsomedial hypothalamic nucleus, amygdala, periaqueductal grey, median raphe nucleus, motor nuclei in the hindbrain (Fig. 35).

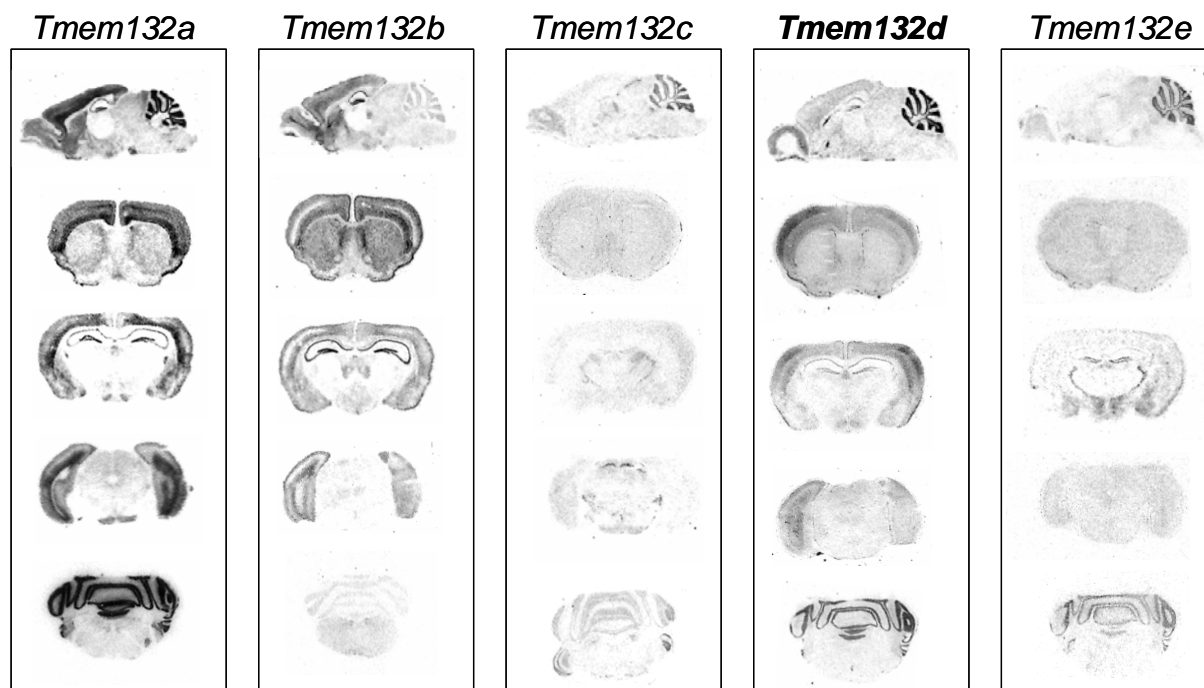


Fig. 35. Spatial distribution of *Tmem132* family members as determined by ISH. *Tmem132* family members show distinct expression patterns in the brain.

To analyze the expression of *Tmem132d* during development, ISH on brain slices of different postnatal stages was performed (Fig. 36). Interestingly, a strong expression of *Tmem132d* was observed in the subventricular zone at postnatal stages P8 and P10 compared to later developmental stages (P14, P21, P35). No changes were observed in other brain regions when comparing the expression of *Tmem132d* during different postnatal stages (data not shown).

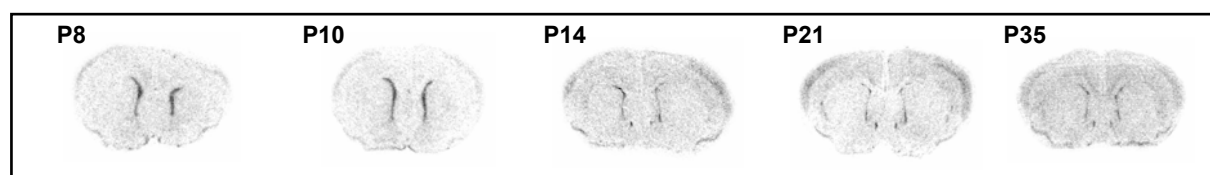


Fig. 36. Expression of *Tmem132d* during different postnatal stages as determined by ISH. A strong expression in the subventricular zone was observed in the brain of postnatal stages P8, P10.

3.2.2 *In vitro* studies

In silico studies analysing the protein sequence of TMEM132D indicate a potential single-pass type I (extracellular N-terminus) transmembrane protein structure. To further determine the intracellular localization of TMEM132D, a plasmid expressing a TMEM132D-GFP fusion protein carrying the GFP at the C-terminus was generated and transfected into human embryonic kidney (HEK293) cells. The TMEM132D-GFP fusion protein was located in the cellular membrane of HEK293 cells, whereas the GFP-N1 control plasmid was evenly expressed throughout the cytosol and the nucleus (Fig. 37).

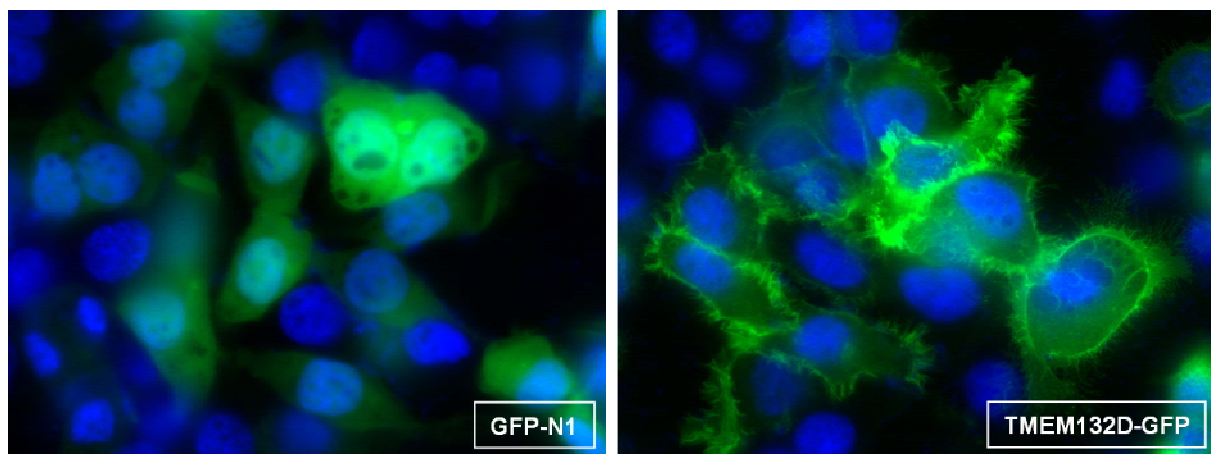


Fig. 37. TMEM132D is expressed in the cellular membrane. HEK293 cells were transfected with the GFP-N1 and a TMEM132D-GFP construct, respectively. Nuclei were counterstained with DAPI (blue).

Additionally, it seems that TMEM132D is localized in filopodia-like structures of HEK293 cells. For visualization of the cell processes, a phalloidin staining was carried out. Phalloidin is a toxin from the death cap and binds to actin filaments (Barden et al., 1987). Interestingly, we observed a strong co-localization of TMEM132D-GFP with actin filaments. Moreover, the cells transfected with TMEM132D-GFP seemed to develop an increased number of filopodia-like structures compared to cells transfected with the GFP-N1 control vector (Fig. 38).

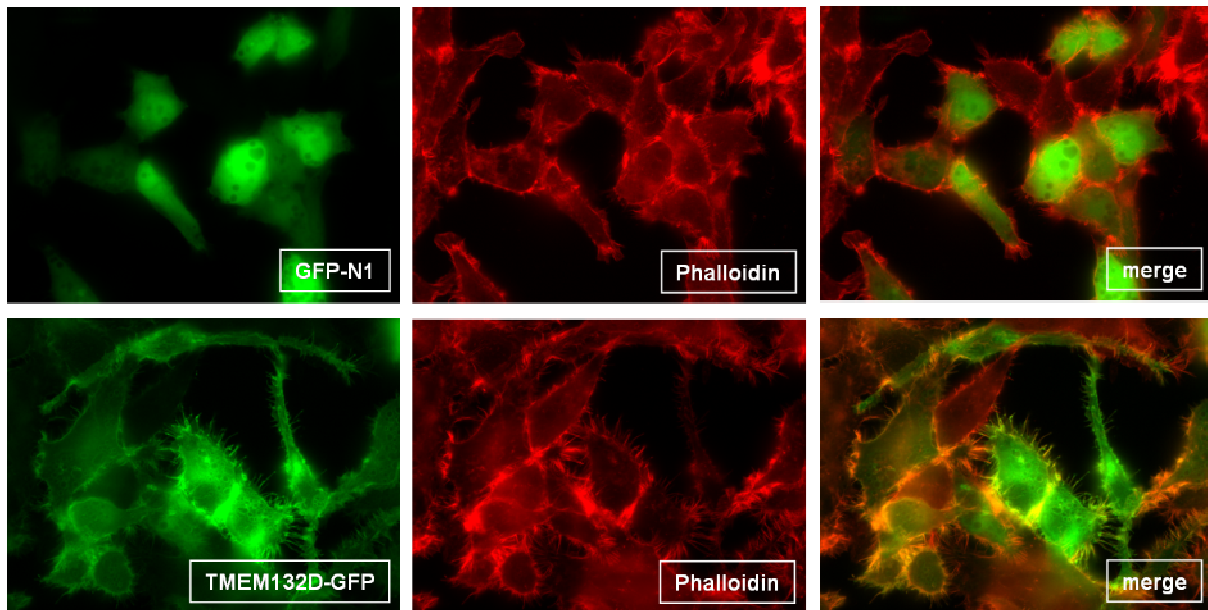


Fig. 38. TMEM132D co-localizes with actin and its overexpression leads to an increased number of filopodia-like structures. TMEM132D-GFP was transiently transfected into HEK293 cells. GFP-N1 was used as control. Cells were fixed with PFA and stained with rhodamine-phalloidin.

Since potential intracellular signaling cascades as well as agonists/antagonists of TMEM132D are entirely unknown, we performed a yeast two-hybrid (Y2H) membrane screen, based on the split-ubiquitin system (Stagljar et al., 1998;Thaminy et al., 2003), to identify proteins interacting with TMEM132D. Using this system, interactions of the full-length TMEM132D protein with other membrane proteins (Fig. 39A) or cytosolic proteins (Fig. 39B) can be detected *in situ* at the yeast membrane. Therefore, the *Tmem132d* cDNA was successfully cloned into the pBT3-SUC bait vector. The pBT3-SUC vector is appropriate for type I integral membrane proteins having a single transmembrane domain, a N_{out}/C_{in} topology and a N-terminal cleavable signal sequence. A signal sequence for the first 30 amino acids of the TMEM132D protein was predicted using SignalP 3.0 Server (<http://www.cbs.dtu.dk/services/SignalP/>) and SPdb: a signal peptide database (<http://proline.bic.nus.edu.sg/spdb/>). Since signal sequences of mammalian type I proteins are not always recognized by the yeast translocation machinery, the sequence encoding the N-terminal signal sequence was removed from the *Tmem132d* cDNA and the truncated cDNA was cloned into the pBT3-SUC vector which provides a yeast signal sequence derived from the *SUC2* (invertase) gene of *Saccharomyces cerevisiae*. The sequence-verified bait construct was transformed into the supplied NMY51 yeast strain and the correct expression was analyzed by

Western blot of total yeast extracts. However, only pCCW-Alg5 used as control bait could be detected in the Western blot.

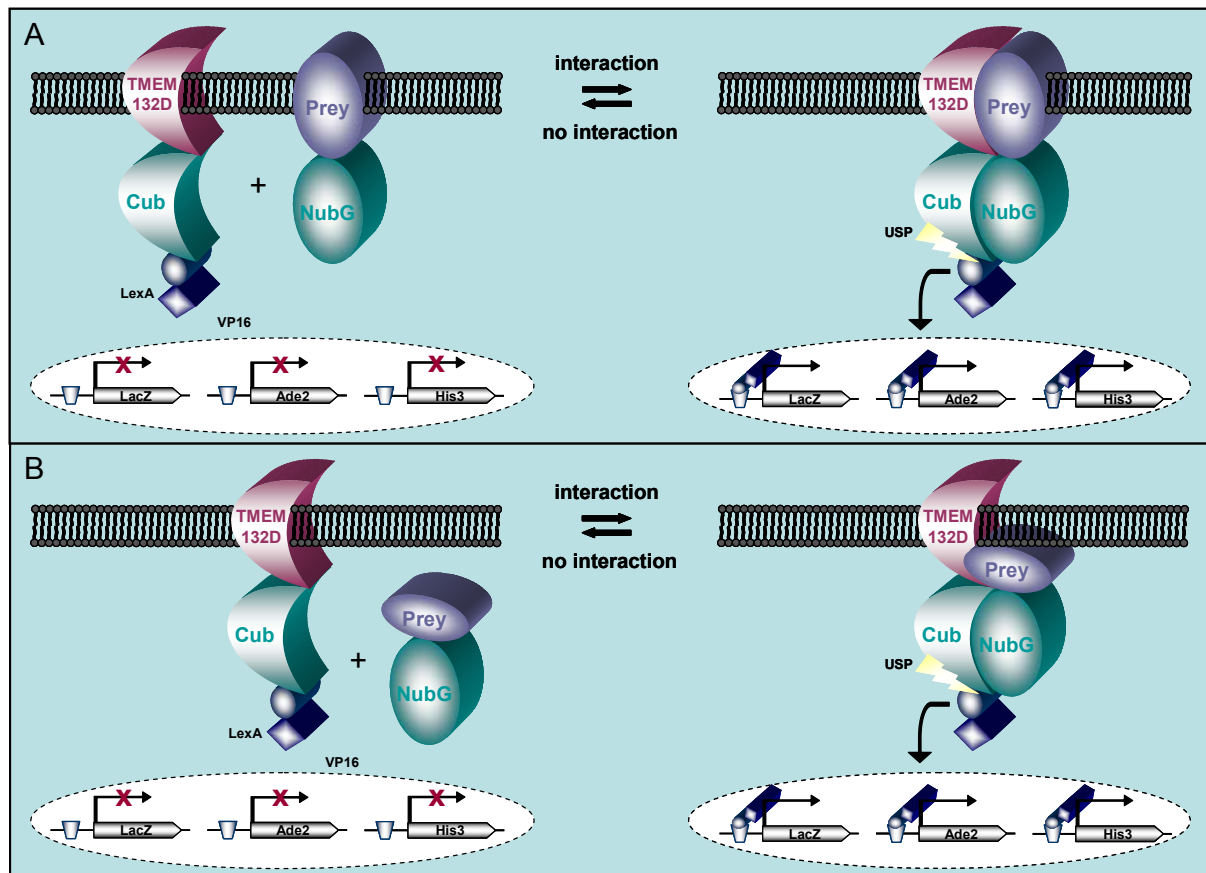


Fig. 39. Identification of TMEM132D interacting proteins via Y2H membrane screening. TMEM132D – the bait protein – is fused to the C-terminal half of ubiquitin (Cub) and the artificial transcription factor LexA-VP16. The prey protein – either another membrane protein (A) or a cytosolic protein (B) – is fused to the mutated N-terminal half of ubiquitin (NubG), in which the isoleucine (I) at position 3 of the protein is exchanged for a glycine (G). Only if TMEM132D and a prey interact, are NubG and Cub forced into close proximity, resulting in the reconstitution of split-ubiquitin. The reconstituted ubiquitin is recognized by ubiquitin-specific proteases (USP) which cleave the polypeptide chain between Cub and LexA-VP16. The artificial transcription factor is released from the membrane and translocates to the nucleus where it binds to the LexA operators upstream of a reporter gene. This leads to transcriptional activation of reporter genes, two auxotrophic growth markers (*HIS3* and *ADE2*), whose activation enables the yeast to grow on defined minimal medium lacking histidine or adenine, and *lacZ*, encoding the enzyme β -galactosidase, whose expression leads to color development in a β -galactosidase assay.

Nevertheless, following the recommendations of the protocol, we proceeded with the control assay. Therefore, the bait was co-transformed with the supplied control prey plasmids pAI-Alg5 (expressing wild-type NubI) and pDL2-Alg5 (expressing the

mutated form NubG). Co-expression of the bait with pAI-Alg5 should result in reconstitution of split-ubiquitin through the strong affinity of wild-type Nubl for Cub and the subsequent activation of reporter genes. Growth of yeast expressing the bait and the pAI-Alg5 control indicates that the bait is functional in the Y2H membrane system. Co-expression of the bait together with pDL2-Alg5 should not activate the reporter genes, as the mutated NubG moiety has no affinity for Cub. Calculation of percentage of growth of yeast bearing pBT3-SUC-Tmem132d and pAI-Alg5 under selection resulted in 10% on average. Although growth of 20-100% under selective conditions – depending on the expression level of the bait – is recommended, we decided to proceed with a pilot screen to optimize the basic screening conditions.

The pilot screen was performed to determine whether the bait displays any activation of reporter genes in the absence of a protein-protein interaction when transformed together with an empty library vector. Therefore, the bait construct was co-transformed with the empty library vector and assayed on selective plates of increasing stringency. Additionally, plates were supplemented with different amounts of 3-aminotriazole (3-AT), a competitive inhibitor of the *HIS3* gene product meaning that increasing levels of 3-AT simultaneously increase the stringency of *HIS3* selection. Selective plates not displaying any growth were selected for the library screen, in this case ALHW plates (lacking adenine, leucine, histidine and tryptophan) supplemented with 5 mM 3-AT. At this stringency, the bait will still be able to interact with the Alg5-Nubl control prey and will not display any background when co-expressed with NubG alone.

To screen the bait against a NubG-fused mouse adult brain cDNA library (NubG-X), the cDNA library was transformed into NMY51 expressing the bait and interactors were selected using the stringency conditions determined in the pilot screen. The transformation efficiency was in the expected range of 5×10^5 to 2×10^6 clones/ μ g DNA. As mammalian cDNA libraries have complexities around 2×10^6 independent clones, this transformation efficiency is sufficient to cover the cDNA library at least 2-3 times. 192 positive colonies were picked, taking advantage of the *ADE2* phenotype of the NMY51 yeast strain (Fig. 40), and re-streaked using the same selective conditions as used in the library screen.

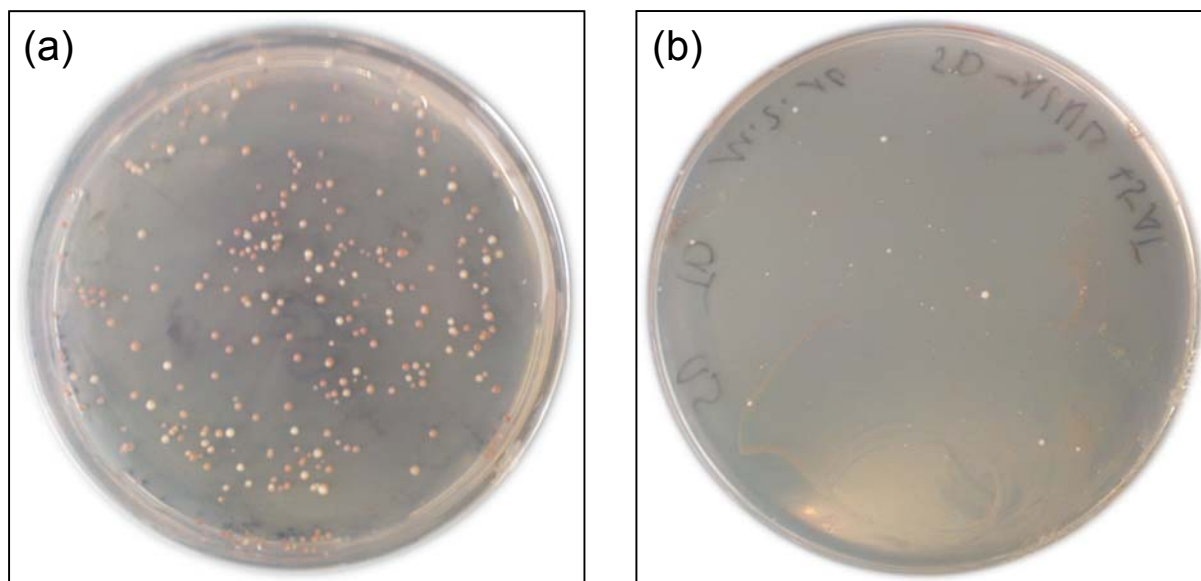


Fig. 40. ADE2 phenotype of the NMY51 yeast strain. (a) Yeast colonies transformed with *Tmem132d*-pBT3-SUC exhibit a pinkish color. (b) Yeast transformed with *Tmem132d*-pBT3-SUC and a mouse adult brain cDNA library display a faint pink to white color, depending on the strength of interaction.

Only white colonies were used to perform a β -galactosidase assay (Fig. 41) in order to select the strongest interactors from the screen. β -galactosidase activity was quantified by measuring the optical density using the freely available computer program ImageJ (<http://rsbweb.nih.gov/ij/>).



Fig. 41. Detection of strongest interactors via β -galactosidase assay. 48 clones with the strongest β -galactosidase activity (deep blue) were selected for plasmid isolation.

Library plasmids from the 48 strongest interactors were isolated and re-transformed into *E. coli*. Due to problems during DNA isolation from yeast, not all of the 48 clones could be re-transformed. For each original yeast clone, two independent colonies

were picked and plasmid DNA was prepared. The insert size of each clone was determined by restriction digest. Isolated plasmids were sequenced to determine the identity of the cDNA encoding the interactor using the primer sequences provided in the protocol (see supplementary data). The sequenced clones were analyzed by Dualsystems Biotech for false-positive interactors (Table 4).

Table 4. BlastX analysis of preys. BlastX against UniProtKB/Swiss-Prot (dark-blue, screen-specific interactors (not occurred in any other screen yet); light-blue, interactors which occurred in some screens in the past; white, interactors which occur in 20-50% of all performed screens; ER, endoplasmatic reticulum). Occurrence is indicated for the actual screen (right column).

Prey-ID	Uniprot ID	Protein name (description)	Subcellular localization	Occurrence
Fkbp8	O35465	Peptidyl-prolyl cis-trans isomerase FKBP8	Mitochondrion membrane	1
Glx5	Q80Y14	Glutaredoxin-related protein 5	Mitochondrion	2
Rgs10	Q9CQE5	Regulator of G-protein signaling 10		1
Rtn1	Q8K0T0	Reticulon-1	ER membrane	2
Sumo2	P61957	Small ubiquitin-related modifier 2	Nucleus	1
Uba52	P62984	Ubiquitin-60S ribosomal protein L40	Cytoplasm, Nucleus	1
Gpsn2	Q9CY27	Trans-2,3-enoyl-CoA reductase	ER membrane	7
Rnf41	Q8BH75	E3 ubiquitin-protein ligase NRDP1		1
Serp2	Q6TAW2	Stress-associated endoplasmic reticulum protein 2	Membrane, ER membrane	5
Tmem11	Q8BK08	Transmembrane protein 11	Membrane	3
Selk	Q9JLJ1	Selenoprotein K		3
Spcs1	Q9D958	Signal peptidase complex subunit 1	Microsome, ER membrane	1

Further validation of the identified interactors using independent methods has to be carried out in the future.

3.2.3 Generation and characterization of *Tmem132d* knockout mice

3.2.3.1 Generation of knockout mice

To analyze the effects of a constitutive loss of *Tmem132d* function on depression- and anxiety-related behavior, *Tmem132d* knockout animals were generated. Additionally, these knockout mice, carrying a *LacZ* reporter gene, were used to analyze cell-type specific expression of TMEM132D in the brain.

Conventional knockout mice were generated using ES cell clones (clone ID E302C11; cell line E14TG2a.4 (ES cells 129P2)) received from the German Genetrap Consortium (GGTC). The GGTC provides a gene trap database representing a repository of sequences produced in a large scale gene trap screen by insertional mutations in mouse ES cells using various gene trap vectors which are

delivered either by electroporation or retroviral infection. In this case, a retroviral enhanced conditional gene trap vector, eFlipRosa β geo, was used, comprising the following components (from 5' to 3'): a long terminal repeat (LTR) followed by osteopontin enhancer elements (OPE), flanked by heterotypic FLPe recombinase target sequences frt/F3; a splice acceptor (SA) followed by a β -galactosidase/neomycinphosphotransferase fusion gene (β geo) and a polyadenylation sequence (pA). The entire reporter-selection cassette is flanked by heterotypic Cre recombinase target sequences loxP/lox5171 followed again by frt/F3 sites and a long terminal repeat (Fig. 42). The insertion of the osteopontin enhancer into a conventional gene trap vector significantly increases the gene trapping efficiency in high-throughput screens and facilitates the recovery of poorly expressed genes (Schnutgen et al., 2008).

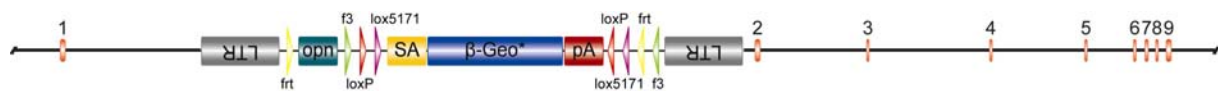


Fig. 42. Conditional gene trap vector eFlipRosa β geo. The vector was retrovirally inserted into intron 1 of the *Tmem132d* gene (integration site: 164.452-164.453 bp of intron 1).

After integration into intron 1 of the *Tmem132d* gene (integration site: 164.452-164.453 bp of intron 1), transcripts initiated at the endogenous promoter should be spliced from the splice donor of the endogenous exon 1 to the SA of the SA β geo pA cassette. Thereby, the β geo reporter gene is expressed and the endogenous transcript is captured and prematurely terminated at the cassette's pA causing a mutation (Schnutgen et al., 2005). Importantly, integration of the gene trap vector into intron 1 ensures disruption of the signal peptide of the TMEM132D protein. Therefore, β -gal-neo is not secreted but confers resistance to neomycin. Additionally, the vector relies on directional site-specific recombination systems (FLPe/Cre-mediated systems) that can repair and re-induce gene trap mutations when activated in succession to produce conditional gene disruption (Schnutgen et al., 2005).

Mutant ES cells were used to generate chimeric mice by blastocyst injection. Germ-line transmission of the modified *Tmem132d* allele was confirmed in the offspring from male chimeras bred to wild-type C57BL/6J mice. In the F₂ generation homozygous *Tmem132d*^{-/-} mutant mice were obtained at the expected Mendelian frequency.

Homozygous *Tmem132d*^{-/-} mice exhibited normal development at birth. Also postnatal development was indistinguishable from that of heterozygous and wild-type littermates. Inspection of external and internal organs at different ages did not reveal any macroscopic abnormalities in *Tmem132d*^{-/-} mice. Homozygous mutant mice were fertile and reproduced normally.

3.2.3.2 Molecular characterization of knockout mice

3.2.3.2.1 Expression analysis

To test for inactivation of the *Tmem132d* gene in homozygous mutant mice, its expression was studied by *in situ* hybridization on brain sections as well as by LacZ staining. Using a *Tmem132d*-specific ISH probe covering the 3'UTR, an almost complete loss of *Tmem132d* expression was detected in the brain of knockout animals. Instead, mRNA expression of the *LacZ* reporter gene was observed which was confirmed by X-Gal staining detecting β -galactosidase activity (Fig. 43).

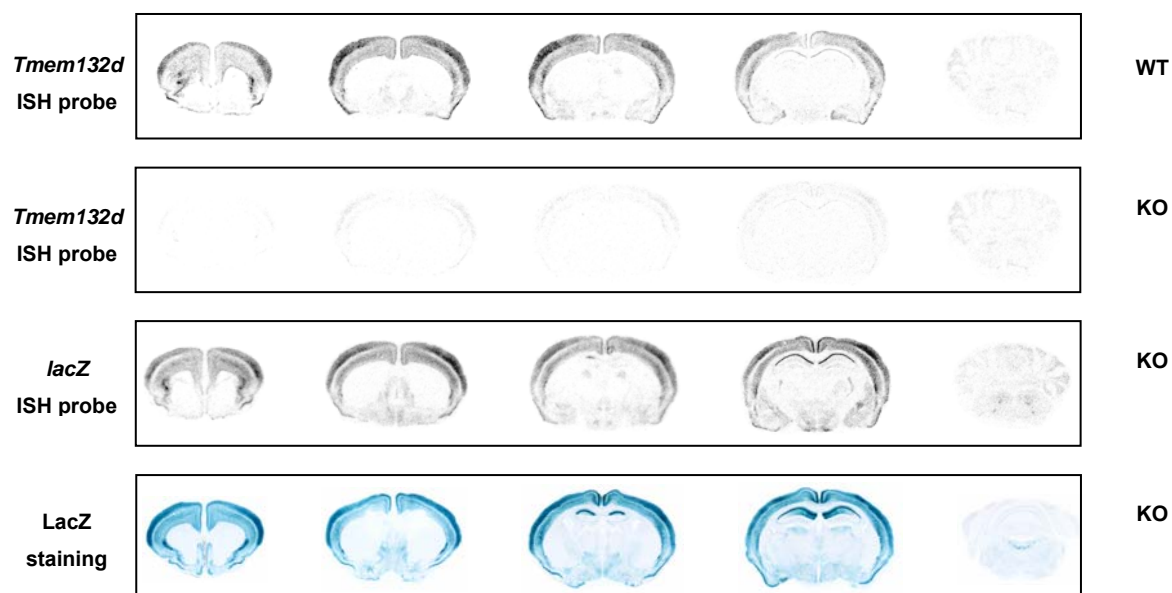


Fig. 43. Expression analysis of *Tmem132d* knockout (KO) mice as determined by ISH and LacZ staining. *Tmem132d* expression is strongly decreased in the brain of homozygous KO mice. Specific expression of the *LacZ* reporter gene was analyzed by X-Gal staining confirming the results obtained by ISH.

Additionally, expression of the closest relatives, *Tmem132b* and *Tmem132c*, was analyzed in homozygous *Tmem132d*^{-/-} mice to assess potential compensatory

regulation of *Tmem132* family members located on the same chromosome. No differences in expression of other *Tmem132* members could be observed between WT and KO animals (Fig. 44).

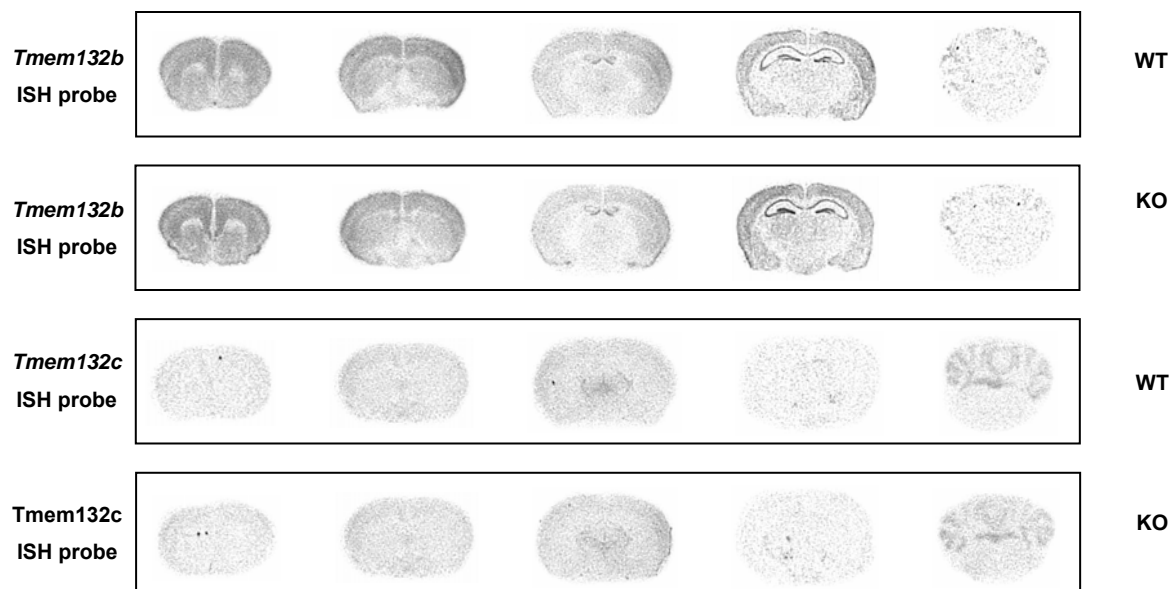


Fig. 44. Expression analysis of *Tmem132b* and *Tmem132c* in *Tmem132d* knockout mice as determined by ISH. Expression of *Tmem132* family members located on the same chromosome is not affected in mutant mice.

3.2.3.2.2 Co-localization studies using neuronal markers

To further analyze the expression of TMEM132D in neuronal cells, immunohistochemical stainings were performed taking advantage of the knockout animals expressing the *LacZ* reporter gene. Since antibodies for TMEM132D are not available, we used an anti- β Gal antibody detecting the LacZ reporter protein in KO mice representing endogenous TMEM132D expression. Co-staining of the neuronal marker NeuN and LacZ – representing expression of TMEM132D – revealed a strong co-localization in the CA1 region of the hippocampus, the basolateral amygdala and the piriform cortex (Fig. 45). Additionally, co-expression was observed in the somatosensory cortex, the cingulate cortex, in some thalamic nuclei and motor nuclei in the hindbrain (data not shown).

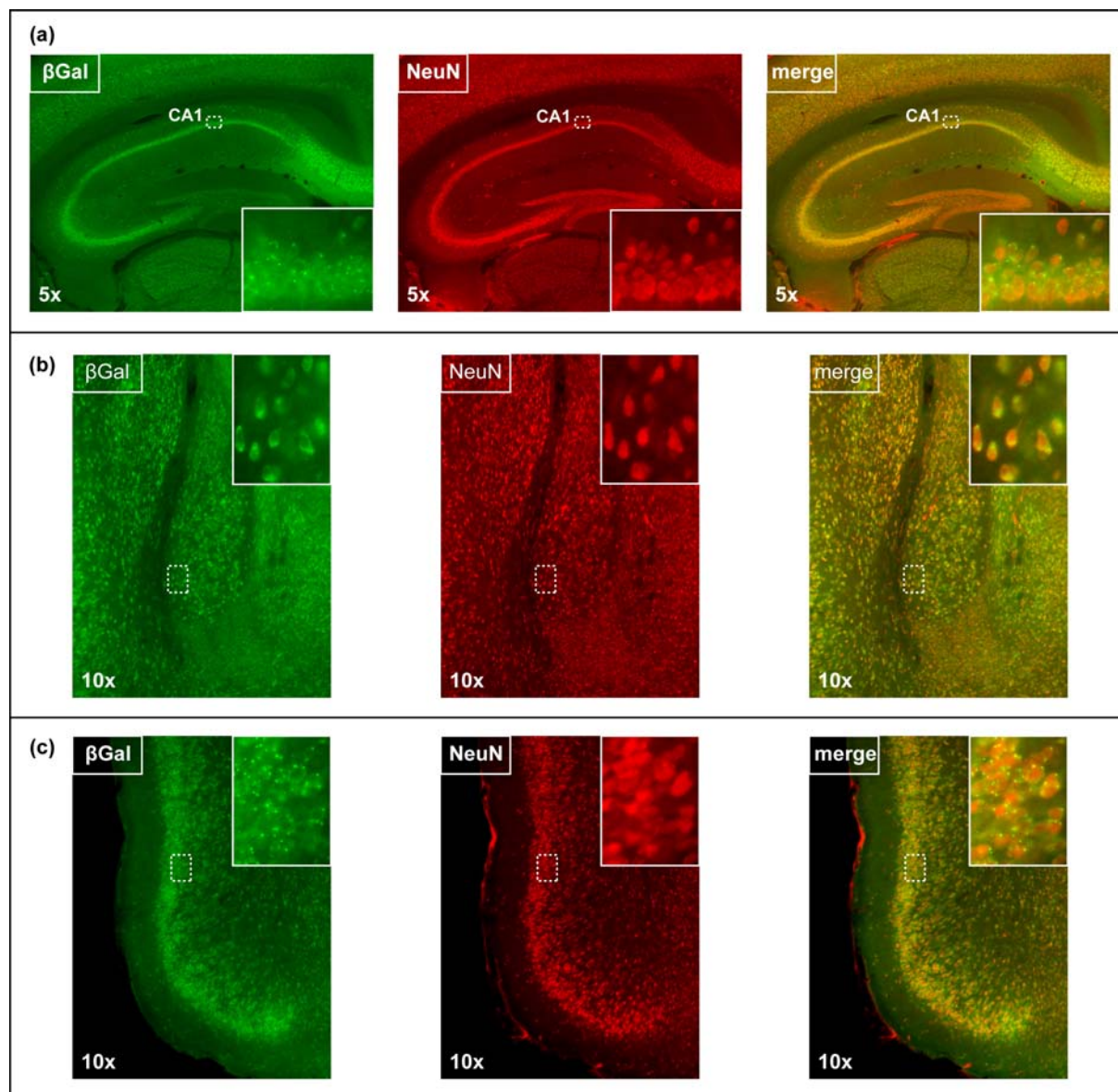


Fig. 45. TMEM132D colocalizes with the neuronal marker NeuN. Co-expression (a) in the CA1 region of the hippocampus, (b) the basolateral amygdala and (c) the piriform cortex of *Tmem132d*^{-/-} brains was observed as determined by immunohistochemical stainings using anti-NeuN and anti-βGal antibodies. In the inlays, a magnification of a representative region is shown illustrating co-localizing cells.

Cell-type specificity was further analyzed using markers for glutamatergic (anti-Glu) and GABAergic (anti-GAD67) neurons. Co-stainings of glutamatergic neurons with the β-galactosidase reporter, representing TMEM132D expression, resulted in co-localization in glutamatergic cells of the CA1 region of the hippocampus, the basolateral amygdala and the piriform cortex (Fig. 46) as well as in glutamatergic neurons of the cortex (data not shown).

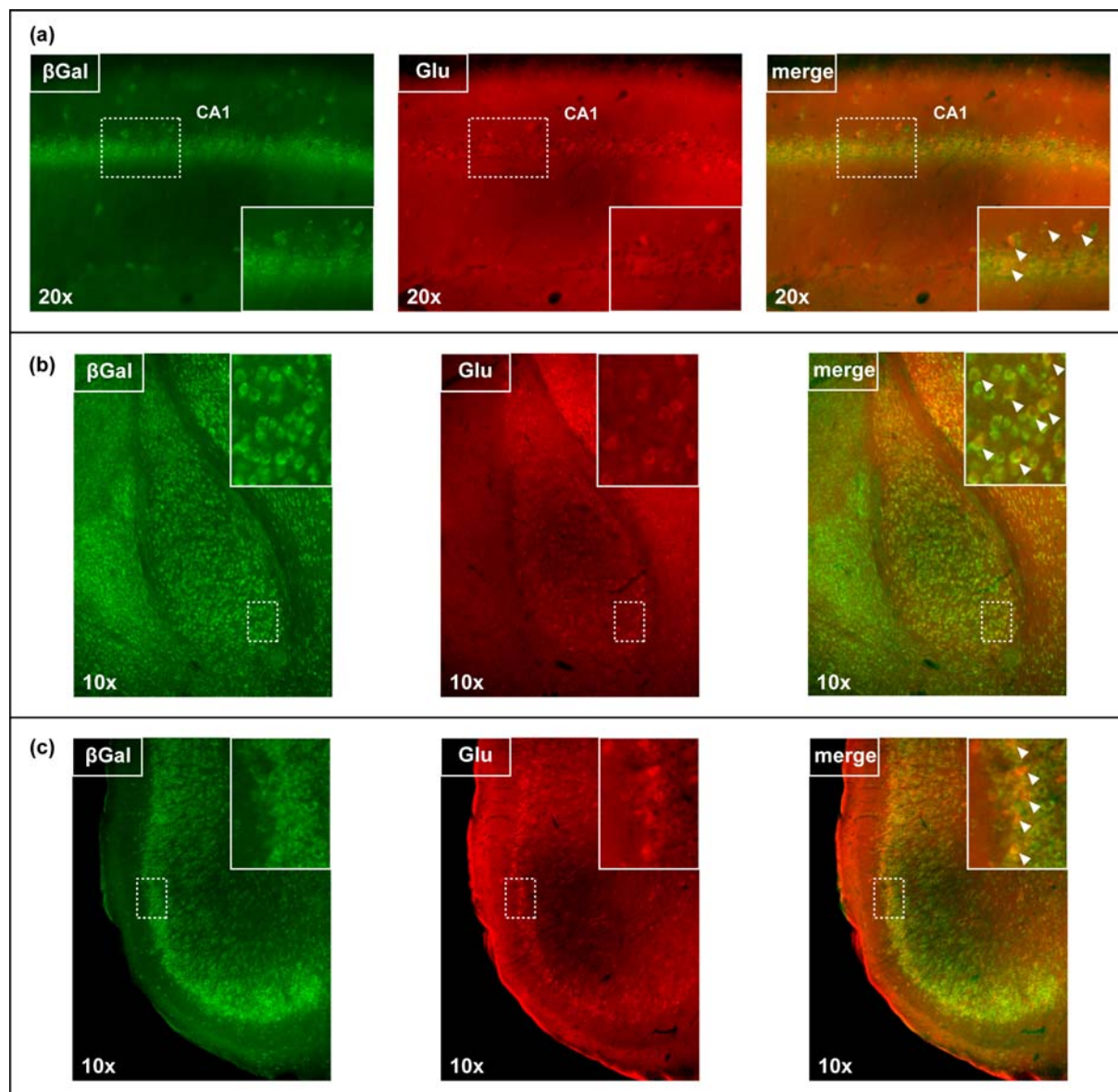


Fig. 46. TMEM132D is expressed in glutamatergic neurons. Co-expression (a) in the CA1 region of the hippocampus, (b) the basolateral amygdala and (c) the piriform cortex of *Tmem132d*^{-/-} brains was observed as determined by immunohistochemical stainings using anti-Glu and anti-βGal antibodies. In the inlays, a magnification of a representative region is shown illustrating co-localizing cells indicated by the white arrows.

Analysis of the expression of the β-galactosidase reporter, representing TMEM132D expression, and GAD67, a marker for GABAergic neurons, did not reveal significant co-localization in the piriform cortex (Fig. 47b) and other brain regions. Only slight co-expression of the LacZ reporter with GABAergic neurons was seen in the CA1 stratum oriens (o) and the stratum moleculare (m) of the hippocampus of *Tmem132d*^{-/-} mice (Fig. 47a).

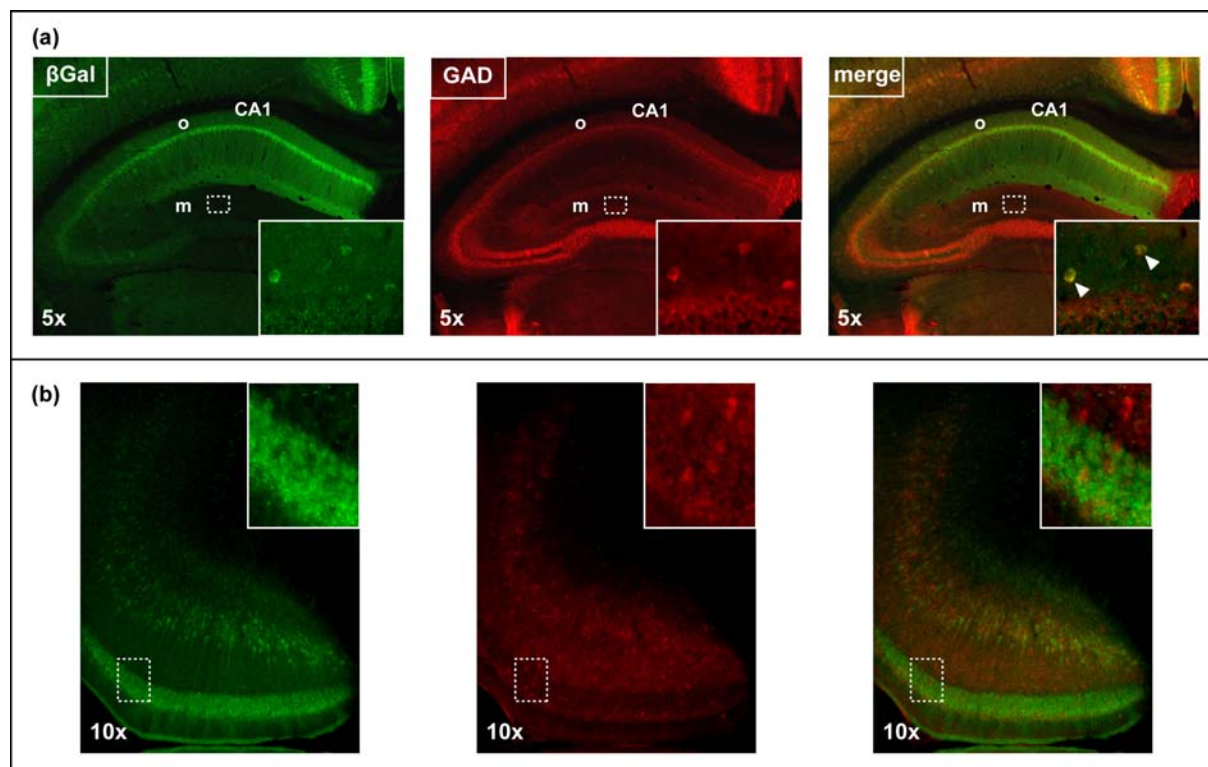
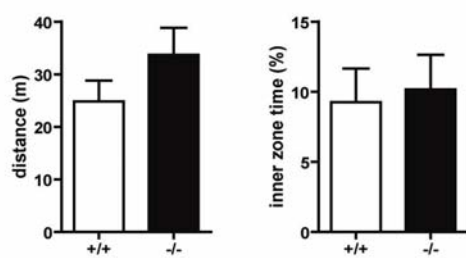


Fig. 47. TMEM132D is rarely co-expressed in GABAergic neurons. (a) Co-expression was observed in the CA1 stratum oriens (o) and the stratum moleculare (m) of the hippocampus of *Tmem132d*^{-/-} mice. (b) No co-localization was seen in the piriform cortex of *Tmem132d*^{-/-} brains as determined by immunohistochemical stainings using anti-GAD67 and anti-βGal antibodies. In the inlays, a magnification of a representative region is shown illustrating co-localizing cells indicated by the white arrows.

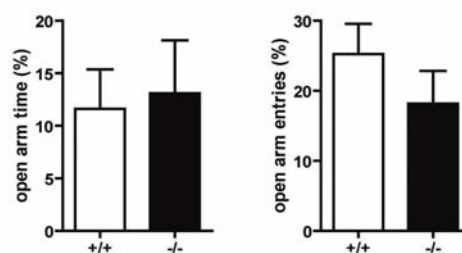
3.2.3.3 Behavioral analysis of knockout mice

An initial behavioral screen assessing locomotion and anxiety-like behavior did not reveal any differences between *Tmem132d* knockout and wild-type mice under basal conditions (Fig. 48a, b, c). Remarkably, *Tmem132d*^{-/-} animals showed a significant increase in struggling time compared to *Tmem132d*^{+/+} littermates in the FST. Accordingly, knockout mice spent significantly less time floating (Fig. 48d).

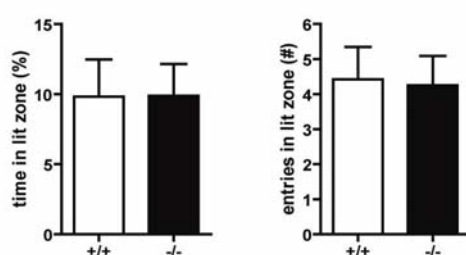
(a) Open Field



(b) Elevated Plus Maze



(c) Dark/Light box



(d) Forced Swim Test

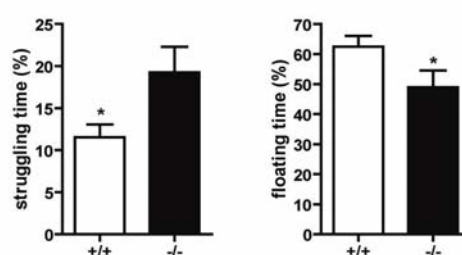


Fig. 48. Behavioral analysis of *Tmem132d*-KO mice. (a, b, c) No changes between the genotypes were observed in the OF, EPM and DaLi box. (d) Knockout animals showed a significant increase in struggling time and a significant decrease in floating time in the FST.

4 Discussion

4.1 Validation of *P2RX7* as a susceptibility gene for mood disorders using genetic mouse models

4.1.1 Generation and analysis of *P2rx7* knockout mice

To get more insights into the general effects of P2RX7 with regard to depression and anxiety, a conventional *P2rx7* knockout mouse line previously established in our group was analyzed. Successful disruption of the *P2rx7* gene was confirmed by ISH and PCR. In addition, we determined the absence of active *P2rx7* splice variants in our *P2rx7* knockout mouse line. This is in contrast to the findings in previously established *P2rx7* deficient mouse lines. Recent publications reported the presence of functionally active truncated variants of P2RX7 (Marin-Garcia et al., 2008; Masin et al., 2011; Sanchez-Nogueiro et al., 2005) in one of the published *P2rx7* knockout strains (Solle et al., 2001). In an additional *P2rx7* knockout strain (Chessell et al., 2005) the expression of an alternative, functionally active *P2rx7* splice variant in specific tissue of *P2rx7* knockout mice was reported (Nicke et al., 2009; Taylor et al., 2009). However, the comprehensive analysis of *P2rx7* transcripts in our knockout animals suggests that the strategy followed in the present study resulted in a true null allele for *P2rx7*. The knockout was functionally validated by the failure of peritoneal macrophages to release interleukin-1 β in response to LPS stimulation and subsequent treatment with the P2RX7 agonist BzATP (Basso et al., 2009; Chessell et al., 2005; Solle et al., 2001). In addition, we were able to confirm the functional disruption of P2RX7 by the measurement of a significantly impaired calcium influx of peritoneal macrophages derived from knockout animals upon BzATP treatment.

Furthermore, the behavioral consequences of a total *P2rx7* knockout were analyzed in both genders in a range of test paradigms developed to model endophenotypes of psychiatric disorders. Assessment of anxiety-related behavior revealed that female knockout mice displayed a significantly decreased inner zone exploration in the open field test while locomotor activity was not altered. In the dark/light box test, female knockouts tended to spend less time in the lit compartment than the wild-types. These data suggest an increased anxiety-related phenotype caused by deletion of *P2rx7*. Female *P2rx7* knockout mice also exhibited significantly increased passive

stress-coping behavior in the forced swim test supporting the notion that *P2rx7* impairment might increase the risk to develop depression-like endophenotypes. However, the difference between the genotypes was only seen in females, not in males. Gender differences in the effects of genetic manipulations on depression-like behavior have been reported before (Monteggia et al., 2007) and go along with the clinical observation that depression and anxiety disorder are more prevalent in females (Grigoriadis and Robinson, 2007). Several explanations for this dimorphism have been proposed, such as hormonal, anatomic and neurochemical differences between the sexes (Cahill, 2006;Palanza, 2001). No differences were observed in the acoustic startle response and with respect to prepulse inhibition (PPI) neither in males nor in females. The acoustic startle response is commonly used as readout for posttraumatic stress disorder (PTSD) and hyperarousal (Golub et al., 2009), whereas the PPI is used as readout for schizophrenia revealing deficits in sensory motor gating (Amann et al., 2010). In addition to the knockout mouse line kept on a mixed background, we also analyzed behavioral effects of *P2rx7*^{-/-} mice bred on a pure 129S2/SvPas background. Opposed to our expectations, no differences were detected in any test paradigm rendering interpretations rather difficult.

Moreover, two other knockout lines were studied with respect to anxiety- and depression-related behaviors (Basso et al., 2009;Boucher et al., 2011). In contrast to our results, a previous publication reported a significantly decreased passive stress coping behavior of male *P2rx7* knockout mice in the forced swim test as well as in the tail suspension test. Examination of anxiety-related behavior did not reveal any differences, neither in the elevated plus maze nor in the novelty-suppression of feeding paradigm (Basso et al., 2009). Unfortunately, female behavior was not assessed. Although the mice used in the two studies were bred on a similar (mainly C57BL/6J) background, there were several methodological differences of which a major distinction was the strategy of how the experimental animals were generated. While Basso and co-workers applied homozygous breeding to produce two independent lines of pure *P2rx7* wild-type and knockout breeding colonies, in our study a heterozygous breeding scheme was used. The latter approach bears the advantage that it provides the possibility to compare littermates of the distinct genotypes in the respective behavioral tests. This excludes the risk that observed differences are not primarily due to the genetic manipulation, but might be a consequence of e.g. genetic drift, divergent environmental conditions, maternal care,

stress susceptibility, housing conditions or dominance hierarchy in the cage. In another recent study, female knockout mice, originally generated by Solle and colleagues (Solle et al., 2001), exhibited a significantly decreased immobility time compared to the wild-types in the forced swim test, however only at day 2 and 3 of testing. In contrast to that, increased anxiety-related behavior was observed in the elevated plus maze in female *P2rx7*^{-/-} mice, but not in the light-dark emergence test where only an effect in locomotor activity was detected (Boucher et al., 2011). Although the anxiety phenotype is in line with our observations, the results of the forced swim test are contradictory to our data. As mentioned before, truncated P2RX7 variants are functionally active (Marin-Garcia et al., 2008; Masin et al., 2011; Sanchez-Nogueiro et al., 2005) in the *P2rx7* knockout strain established by Solle and colleagues (Solle et al., 2001) suggesting compensatory mechanisms adopted by the truncated version possibly leading to misinterpretation of behavioral readouts. A comparison of behavioral effects obtained from the different knockout lines is summarized in Table 5.

Table 5. Behavioral readouts in existing *P2rx7* knockout mouse lines. The mouse line analyzed by Basso et al., 2009 was obtained from Lexicon Genetics, the knockout line investigated by Boucher et al. was originally generated by Solle et al., 2001. Behavior of another knockout strain (Chessell et al., 2005) has not been conducted. TST, tail suspension test; NSF, novelty-suppression of feeding paradigm; LDE, light-dark emergence test.

knockout mouse line (origin)	gender	active stress-coping	anxiety	locomotion
Basso et al., 2009 (Lexicon Genetics)	♂	↑ (TST, FST)	no difference (EPM, NSF)	no difference (OF)
Boucher et al., 2011 (Pfizer/Solle et al.)	♀	↑ (FST, day 2 and 3)	↑ (EPM), no difference (LDE)	↓ (LDE)
generated line (see 3.1.1.1)	♂	no difference (FST)	no difference (OF, DaLi)	no difference (OF)
generated line (see 3.1.1.1)	♀	↓ (FST)	↑ (OF, DaLi)	no difference (OF)

Considering all the data, an involvement of the *P2rx7* deletion in mood-related endophenotypes still remains unclear. To trigger processes that result in an increased risk of developing mood disorders, an environmental challenge, such as chronic social defeat stress (Berton et al., 2006; Wagner et al., 2011), in combination with the genetic modification may be needed (de Kloet et al., 2005). Another strategy could be to generate conditional knockout lines by breeding the *hP2RX7* mice carrying a floxed *P2RX7* gene with different Cre mouse lines. Utilization of a Cre-deleter line, resulting in a loss of human *P2RX7* in the whole body, would allow for direct comparison of *P2rx7*^{hWT} and knockout mice. In addition, this knockout line

could be further backcrossed with C57BL/6J wild-type animals in order to obtain offspring carrying again the murine *P2rx7* gene or the knockout allele, respectively. Considering the behavioral results obtained by comparison of mouse and human P2RX7 (see 3.1.3), we would be able to address directly the circuits underlying the increased anxiety-related behavior by using neurotransmitter-type-specific Cre mouse lines. Such a conditional approach would also allow for circumvention of potential compensatory effects due to life long disruption of *P2rx7*. Another interesting tool might be a glia-specific Cre line, in order to investigate whether the observed behavioral effects are due to expression of P2RX7 in neurons or in glial cells.

Nevertheless, *P2rx7* knockout animals may not be the proper model to unravel the functional relevance of P2RX7 and in particular of the Q460R polymorphism with regard to mood disorders. For that reason, we generated transgenic mice in which the mouse *P2rx7* gene was substituted by the human *P2RX7* wild-type or the *hP2RX7*-Gln460Arg variant, respectively.

4.1.2 Generation and characterization of humanized *P2RX7* mouse mutants

Several studies have investigated associations of SNPs in the *P2RX7* gene with bipolar disorder and major depression, most of them considering the Gln460Arg polymorphism. While some studies reported association of this SNP with BD or MDD (Hejjas et al., 2009;Lucae et al., 2006;McQuillin et al., 2009;Soronen et al., 2011) other studies did not detect significant associations (Green et al., 2009;Grigoriou-Serbanescu et al., 2009;Lavebratt et al., 2010;Viikki et al., 2011). Hence, there is currently no consensus as to whether this SNP confers susceptibility to mood disorders. One explanation for these diverse findings could be that the phenotype and the clinical picture of mood disorders are still difficult to define. Patient samples used for a GWAS are often rather heterogeneous with regard to sex, age, symptoms, environmental factors and other issues, often leading to inconsistent results obtained by independent association studies analyzing the same polymorphisms. Pooling all GWAS data available for a certain disease enlarge the sample size, and thereby increase the statistical power of GWAS. Therefore, a meta-analysis was performed revealing significant effects of rs2230912 on MDD/BD case-control status which can be explained by a dominant or a heterozygous-disadvantage model. These findings suggest a role of *P2RX7* in mood disorders, but the functional relevance of the polymorphism *in vivo* as well as the true risk genotype associated with the disease still has to be determined.

To study the functional relevance of the non-synonymous *P2RX7* SNP in an appropriate *in vivo* model, we generated transgenic mice in which the mouse *P2rx7* gene (*mP2rx7*) was substituted by human *P2RX7* (*hP2RX7*)-wild-type (WT) or *hP2RX7*-Gln460Arg, respectively. Therefore, we used a knockin strategy based on homologous recombination in embryonic stem cells. These humanized mouse mutants were then analyzed for gene expression and changes in molecular function of *P2RX7* as well as basal behavior. Since an environmental challenge together with a certain genetic predisposition can trigger processes which can enhance the risk to develop mood disorders, we additionally applied a chronic social stress paradigm in these mice, followed by comprehensive behavioral screening covering anxiety-related, anhedonic and social behavior. Finally, considering that sleep disturbances

are one of the main endophenotypes of depression (Armitage, 2007;Modell et al., 2005;Rao et al., 2009;Steiger and Kimura, 2010), a comprehensive analysis of sleep pattern and sleep architecture was conducted. Using all these different approaches, we were able to validate the human association data evidenced by the GWAS and to identify the Gln460Arg polymorphism as a risk genotype associated with the disease. Analysis of human *P2RX7* mRNA expression in *hP2RX7* mice revealed that the spatial expression of *hP2RX7* is identical to the endogenous expression pattern of *mP2rx7*. These data indicate that the knockin successfully substituted *mP2rx7* by *hP2RX7*. Functional validation was carried out by measuring the release of IL-1 β of peritoneal macrophages derived from *hP2RX7* animals. Macrophages of *P2rx7*^{hWT/hMT} and *P2rx7*^{hMT} mice showed a significant increase in IL-1 β secretion in response to LPS/BzATP stimulation compared to *P2rx7*^{hWT}, whereas the *P2rx7*^{hWT/hMT} mice showed a stronger increase compared to *P2rx7*^{hMT}. These results indicate that the Q460R polymorphism alters the functionality of the receptor regarding cytokine secretion but the molecular mechanisms leading to these changes still have to be determined. There are several publications describing an increase of pro-inflammatory cytokines in depressed patients (Maes, 2008;Miller et al., 2009). Excessive secretion of cytokines such as IL-1 β , TNF- α and IFN- γ could also be one reason for the high prevalence of depression in infectious, autoimmune and neurodegenerative diseases. In addition, clinical use of cytokines induces depressive-like symptoms that can be attenuated with antidepressants. Patients suffering from major depression often show elevations in the density of microglia, as well as enhanced levels of circulating pro-inflammatory cytokines. In animals, central or systemic administration of pro-inflammatory cytokines can induce a so-called sickness behavior characterized by physiological and behavioral changes associated with depression. Altogether, these data suggest that cytokines may well be involved in the etiopathogenesis of depression. In fact, several antidepressants decrease the release of pro-inflammatory cytokines both *in vitro* and *in vivo* at therapeutically effective concentrations. Antidepressants also attenuate the behavioral and emotional disturbances triggered by (1) activation of the immune response, (2) cytokine administration to humans and rodents, (3) increased production of pro-inflammatory cytokines seen in depressed patients. Therefore, it is tempting to speculate that P2X7 receptor antagonism may represent a novel target for the treatment of depression (Skaper et al., 2010). In contrast to our results, previous

studies did not reveal major functional effects of the Q460R polymorphism itself on IL-1 β secretion (Stokes et al., 2010). In a recent study, Stokes and colleagues analyzed 3430 Caucasian subjects with bipolar disorder resulting in the identification of four common *P2RX7* haplotype blocks in addition to the most frequent one considered as wild-type. One haplotype block uniquely contained the Q460R SNP which was co-inherited with the gain of function SNP A348T and in most cases is in strong linkage disequilibrium with two other gain of function SNPs, H155Y and H270R (Fig. 49).

	76	150	155	270	276	307	348	357	460	496	568	Population Frequency
P2X7-1	Val	Gly	His	His	Arg	Arg	Ala	Thr	Gln	Glu	Ile	0.342
P2X7-2	Val	Gly	His	His	Arg	Arg	Thr	Thr	Gln	Glu	Ile	0.232
P2X7-4	Val	Gly	Tyr	Arg	Arg	Arg	Thr	Thr	Arg	Glu	Ile	0.169

Fig. 49. Illustration of the amino acid sequence at 11 positions for the 3 haplotypes of interest. P2X7-1 represents the most frequent haplotype block in the Caucasian population. P2X7-2 contains the Ala348Thr polymorphism in isolation, whereas P2X7-4 additionally contains the Gln460Arg variant (red box) as well as the His155Tyr and the His270Arg polymorphism. P2X7-3 and P2X7-5 contain SNPs which are known to confer loss of function, Glu496Ala and Thr357Ser (not shown) (Stokes et al., 2010).

In cell culture experiments, this haplotype led to a significant increase in ethidium⁺ uptake, ATP-induced currents and IL-1 β release compared to the wild-type haplotype. Thus, it was proposed that the combination of these gain of function SNPs, frequently co-inherited with the Q460R SNP, may have functional effects in the pathophysiology of affective disorders and may give rise to increased pro-inflammatory cytokines rather than single SNPs in isolation (Sluyter et al., 2010; Stokes et al., 2010). However, using peritoneal macrophages derived from *hP2RX7* mice, we were able to show that cells isolated from heterozygous and homozygous animals exhibited a significantly elevated IL-1 β response upon LPS/BzATP treatment suggesting that the Q460R SNP itself indeed has a functional effect on IL-1 β secretion, but mainly in heterozygotes. One obvious explanation for these divergent results is that, besides the homozygote allele carriers, the heterozygous genotype represents a possible risk genotype determined by the meta-analysis, which has never been considered in previous functional studies. For further validation, IL-1 β secretion should be determined in primary microglia cultured from

hP2RX7 mice to analyze the functionality of the receptor also in the brain. As another functional readout, investigation of BzATP-induced ERK phosphorylation was used to study how the different activation levels of P2RX7 affect the intracellular signaling cascade. Neurons isolated from *P2rx7^{hWT}* animals showed a robust time-dependent ERK 1/2 phosphorylation. In contrast, the response to BzATP seemed to be diminished in neurons from *P2rx7^{hWT/hMT}* and *P2rx7^{hMT}* mice, possibly due to altered P2RX7 function. Notably, this loss of function phenotype seems to be contradictory to the observations revealed during measurement of IL-1 β secretion. However, it has to be considered that IL-1 β release was monitored in peripheral immunocompetent cells, whereas ERK phosphorylation was determined in primary hippocampal neurons – two completely different cell types orchestrating totally different pathways. To overcome this problem, both assays should be conducted in primary microglia, where both pathways are active and therefore could be measured in the same cell type: on the one hand, ATP-stimulated P2RX7 triggers K⁺ efflux from cells activating the inflammasome which, in turn, activates caspase-1 leading to maturation of IL-1 β and subsequent release from the cell. Additionally, P2RX7 activation also results in activation of phospholipases A2 and D as well as tyrosine phosphorylation and activation of mitogen-activated protein kinase (MAPK) pathway proteins (MEK, ERK 1/2) which can influence the activity of transcription factors (Skaper et al., 2010).

Characterization of behavior under standard housing conditions revealed only differences in the acoustic startle reflex which is considered to reflect aspects of anxiety (Holmes et al., 2001). *P2rx7^{hWT/hMT}* mice showed a decreased acoustic startle response compared to their *P2rx7^{hWT}* and *P2rx7^{hMT}* littermates. A similar behavior has been observed in rats selectively bred for high anxiety (Yilmazer-Hanke et al., 2004) suggesting a generally altered stress response or coping strategy of *P2rx7^{hWT/hMT}* mice. In many cases an environmental challenge in combination with a genetic predisposition is needed to trigger processes that result in an increased risk of developing mood disorders (de Kloet et al., 2005). Therefore, we subjected *hP2RX7* mice to three weeks of chronic social defeat stress (Berton et al., 2006;Wagner et al., 2011) to assess whether the Gln460Arg polymorphism has any impact on the animals' stress response. The successful application of chronic stress was evidenced by changes in physiological and neuroendocrine parameters as expected from the literature (Berton et al., 2006;Wagner et al., 2011). In the OF,

chronically stressed mice showed a decreased locomotion compared to unstressed mice also confirming the successful application of chronic stress. In the first 5 min of the OF stressed heterozygous *P2rx7*^{hWT/hMT} mice did not show a decrease in locomotion suggesting a state of increased arousal. In response to CSDS heterozygous *hP2RX7* mice showed a significantly stronger decrease of the open arm time indicating increased anxiety-like behavior compared to *P2rx7*^{hWT} and *P2rx7*^{hMT} littermates. A variety of neuropsychiatric disorders, including depression are characterized by disruption of social behavior (Nestler and Hyman, 2010). Accordingly, chronically stressed heterozygous *P2rx7*^{hWT/hMT} mice developed a deficit in social behavior, as indicated by a significant decrease in preference for the social counterpart in the sociability test. A similar finding was observed in the social avoidance test with the difference that also the homozygous mice displayed a decreased interaction time with the social target. Upon CSDS *P2rx7*^{hWT/hMT} mice spent significantly less time in close proximity to the social target compared to unstressed *P2rx7*^{hWT/hMT} animals. In addition, only *P2rx7*^{hWT/hMT} mice displayed this aversive response also in the presence of the object alone implying increased anxiety-like behavior. To assess anhedonic behavior, which is a key feature of depression (Nestler and Hyman, 2010), we applied the female urine sniffing test. Again, only chronically stressed *P2rx7*^{hWT/hMT} mice spent significantly less time sniffing female urine, which indicates anhedonic behavior. The increase in basal corticosterone levels in response to CSDS in *P2rx7*^{hWT/hMT} mice also indicated an increased vulnerability to stress. Taken together, *hP2RX7* mice provide strong evidence that mainly the *P2RX7*-WT/*P2RX7*-Gln460Arg heterozygosis conveys an increased vulnerability to develop depression-related endophenotypes in response to chronic stress.

Impaired sleep is one of the most reliable symptoms accompanying MDD, which even becomes manifest before diagnosis of the disease, and more than 80% of the patients with major depression complain about insomnia (Armitage, 2007;Modell et al., 2005;Rao et al., 2009;Steiger and Kimura, 2010). In our studies, *P2rx7*^{hWT/hMT} mice showed a significantly higher number of episode entries to REMS during the light period, indicating a stronger drive towards REMS and more fragmented sleep cycles compared to *P2rx7*^{hWT} and *P2rx7*^{hMT} mice. Additionally, slow-wave activity during NREMS, which measures the depth of NREMS, was constantly low in heterozygous mice. Accordingly, only a small amount of deep NREMS (SWS₂) was

detected in $P2rx7^{hWT/hMT}$ mice, suggesting a shallower NREMS. These results indicate that heterozygous $P2rx7^{hWT/hMT}$ mice have an altered sleep architecture and attenuated quality of sleep compared to $P2rx7^{hWT}$ and $P2rx7^{hMT}$ littermates which can be viewed as equivalent to sleep changes in mood disorders. In subjects with MDD, characteristic changes in the sleep EEG can be observed: (1) impaired sleep continuity, (2) disinhibition of REM sleep (shortened REM latency or REM onset periods, prolonged first REM period, elevated REM sleep density), (3) changes of NREM sleep (decrease of SWS, sleep stage 2 and SWA) (Armitage, 2007;Modell et al., 2005;Rao et al., 2009;Steiger and Kimura, 2010). Moreover, our data further propose that mainly the heterozygous genotype gives rise to an increased susceptibility to develop endophenotypes associated with depression.

However, the potential underlying molecular mechanisms are still not understood. To selectively address P2RX7 function *in vivo* is virtually impossible due to the lack of specific tools, e.g. selective agonists and antagonists, respectively (North and Surprenant, 2000) or specific antibodies (Anderson and Nedergaard, 2006;Sim et al., 2004). Another difficulty is related to the broad co-expression with other P2X receptors such as the P2RX4, which renders the discrimination of P2RX7-specific effects almost impossible. To overcome these limitations one could use *in vitro* cellular models i.e. a HEK293 cell line that does not endogenously express P2RX7 stably transfected with P2RX7 variants. By making use of this strategy, Aprile-Garcia and colleagues were able to show that BzATP induced a similar rapid increase in intracellular calcium and in currents in whole-cell patch clamp analysis in cells expressing either hP2RX7-WT or hP2RX7-Gln460Arg. This is in agreement with previous publications, where the P2RX7-Gln460Arg variant showed no differences compared to P2RX7-WT with respect to ATP-activated ion channel function and pore formation (Cabrini et al., 2005;Roger et al., 2010). In order to address the outcome of co-expression of P2RX7-WT and P2RX7-Gln460Arg, which would reflect the heterozygous genotype, cells were co-transfected with both variants. Cells co-expressing both hP2RX7-WT and hP2RX7-Gln460Arg variants showed a significant reduction of normal receptor function in terms of calcium uptake and whole cell currents. As another signaling pathway downstream of P2RX7 activation of ERK 1/2 was assessed. In response to BzATP, cells stably expressing either hP2RX7-WT or hP2RX7-Gln460Arg showed a robust time-dependent ERK 1/2 phosphorylation. In contrast, a diminished response to BzATP in hP2RX7-WT and hP2RX7-Gln460Arg

co-expressing cells could be observed. Aprile-Garcia and colleagues further analyzed whether this phenotype may be the result of the physical interaction between P2RX7-WT and P2RX7-Gln460Arg subunits by co-immunoprecipitation and FRET experiments. Indeed, their results provide clear evidence for a physical interaction of the subunits (Aprile-Garcia et al., submitted).

Notably, the results obtained during the analysis of *hP2RX7* animals do not completely reflect the *in vitro* data. During analysis of IL-1 β release, ERK 1/2 phosphorylation and social avoidance behavior, not only *P2rx7*^{*hWT/hMT*} but also *P2rx7*^{*hMT*} mice provided evidence for an altered P2RX7 function. However, there are remarkable differences when comparing the *in vivo* experiments to the *in vitro* approaches: It has been shown that P2RX4, which is broadly expressed in the adult mouse brain, is able to form hetero-oligomers with P2RX7 (Antonio et al., 2011;Dubyak, 2007) possibly leading to molecular mechanisms in the brain of *hP2RX7* mice which are not present in cell culture. Additionally, ATP and BzATP are no selective agonists for P2RX7, but also for other P2X receptors and, by conversion into adenosine, for adenosine receptors widely expressed in the brain (Kukley et al., 2004;Sperlagh et al., 2006).

In summary, mainly heteromerization of the WT P2RX7 with the mutant Gln460Arg P2RX7 variant causes significant alterations of normal receptor function. The *in vitro* experiments as well as the behavioral results of *hP2RX7* mice strongly support the functional relevance of the mutation in heterozygosity and provide a mechanistic basis for the heterozygote disadvantage model emerging from the human association studies.

Therefore, the animal model described in this work significantly contributes to unravel the functional relevance of the Q460R polymorphism with regard to depression-associated endophenotypes. This is certainly due to the fact that our mouse model fulfills a broad spectrum of the criteria required for a valid animal model (Fig. 50) as described by McKinney and Bunney (McKinney, Jr. and Bunney, Jr., 1969): Construct validity was successfully achieved through knockin of a human gene variant potentially associated with depression leading to changes in intracellular mechanisms such as increased IL-1 β secretion which is also often observed in depressed patients (Maes, 2008;Miller et al., 2009). This genetic modification was further combined with an environmental trigger, in this case a chronic social defeat stress paradigm, since it has been shown that an environmental challenge in

combination with a genetic predisposition can trigger processes that result in an increased risk of developing mood disorders (de Kloet et al., 2005). Our model exhibited sufficient face validity as indicated by depression-related endophenotypes determined by analysis of sleep and behavior, as well as by neuroendocrine alterations occurring in subjects suffering from mood disorders (Holsboer and Barden, 1996).

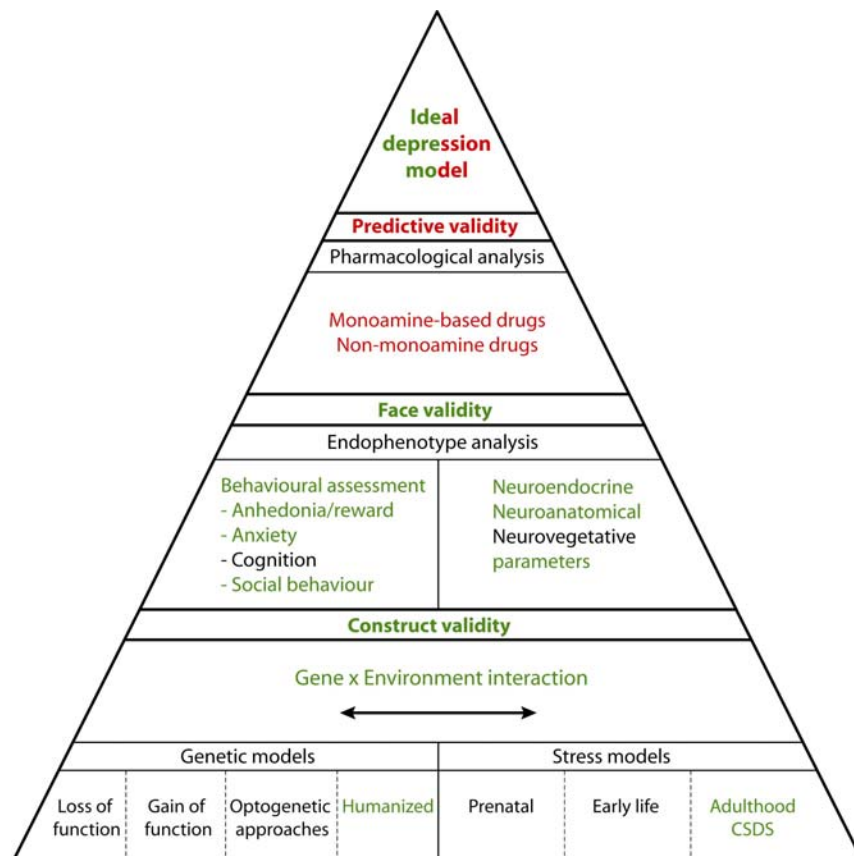


Fig. 50. Towards an ideal mouse model of depression – a reconsideration. Criteria fulfilled by *hP2RX7* mice are depicted in green. In red, criteria to be determined are shown (Dedic et al., 2011).

To test for predictive validity, meaning the response of this mouse model to antidepressant treatment, one could use classical antidepressants or P2RX7 antagonists.

4.1.3 Comparison of mouse and human P2RX7

Since we observed signs of increased arousal and anxiety-like behavior during behavioral testing of *hP2RX7* mice, independent of the genotype, we assessed the impact of human and murine P2RX7 on different phenotypic readouts. Indeed, *P2rx7^{hWT}* mice showed a significant decrease in the inner zone time as well as in inner zone entries in the OF test compared to *P2rx7^{+/+}* mice. Similarly, *P2rx7^{hWT}* animals spent significantly less time on the open arm and entered less often to the open arm during the EPM test. In both tests, increased anxiety-related behavior was independent of locomotor activity. No differences were detected in the dark/light box. This can be explained by the assumption that, compared to the other tests, the dark/light box may be more aversive for the mice and thus may measure a different type of anxiety. Therefore, additional anxiety tests should be performed to assess this issue more accurately. No differences in plasma corticosterone were measured implying that the changes in behavior are not HPA-axis dependent. Altogether, *P2rx7^{hWT}* mice showed a significantly increased anxiety-related behavior compared to *P2rx7^{+/+}* animals.

The observed changes could be due to species-specific differences of P2RX7 in terms of kinetic properties. It was shown that current growth, a progressive increase in current in response to repeated agonist application, as well as channel dilatation appear more rapid at the human than at the mouse P2X7 receptor upon BzATP stimulation (Hibell et al., 2000; Hibell et al., 2001).

Our results emphasize the importance of using the appropriate control for an animal model. By usage of *P2rx7^{hWT}* mice as control animals we were able to exclude the appearance of unspecific effects which are not caused by the mutation itself.

In general, species-specific differences should be considered during the generation of a suitable genetic animal model, in particular for the validation of human association data. One prominent example for the modeling of neuropsychiatric disease-relevant human SNPs in mice is the Val66Met polymorphism in the *BDNF* gene. This SNP only exists in humans and is not found in other species. *BDNF* transgenic mice were established by introducing a point mutation into the murine *Bdnf* gene leading to a change of valine to methionine at amino acid position 66 (Blendy, 2011; Chen et al., 2006). Although the protein sequence of human and murine BDNF is rather homologous, it may have been more appropriate to generate

transgenic knockin mice expressing either the wild-type or the disease-associated human BDNF variant since the polymorphism does not exist in mice.

4.2 Validation of *TMEM132D* as a susceptibility gene for panic disorder and depression

The second candidate gene, *TMEM132D*, was found to be associated with panic disorder and anxiety symptoms in depressed patients in a recent association study (Erhardt et al., 2011) as well as with attention-deficit/hyperactivity disorder (ADHD) in children as recently shown by Mick and colleagues (Mick et al., 2011) suggesting *TMEM132D* as a new candidate gene for mood and anxiety disorders. Unfortunately, the expression and function of *TMEM132D* in the brain has not been characterized at all and the SNPs which were found to be associated are all intronic rendering a validation of *TMEM132D* as a susceptibility gene rather difficult. Therefore, we applied *in vitro* and *in vivo* approaches to get more insights into the role of *TMEM132D* in the brain.

First of all, we analyzed the expression of *Tmem132d* and other *Tmem132* family members during different postnatal stages and in the adult mouse brain. We were able to show that all *Tmem132* family members are expressed in the adult mouse brain, and furthermore, to provide an overview of the expression patterns of all family members. So far, only the expression of *Tmem132a* has been confirmed in the rat brain (Oh-hashii et al., 2003). *Tmem132a* and *Tmem132e* expression is also documented in the Allen brain atlas (<http://www.brain-map.org/>). An expression analysis for *Tmem132b* and *Tmem132c* has not been described before. Comparing the expression of all family members revealed large differences considering the expression level and pattern, thus suggesting diverse functions of *Tmem132* members in the adult mouse brain. The expression pattern of *Tmem132d*, for example in the CA1 region of the hippocampus, indicates expression in neuronal cells. This in contrast to findings of Nomoto and colleagues proposing a specific expression of *TMEM132D* in mature oligodendrocytes in the brain (Nomoto et al., 2003). Interestingly, expression analysis of different postnatal stages demonstrated a strong expression of *Tmem132d* in the subventricular zone (SVZ) of the lateral ventricle of postnatal stages P8 and P10. In the adult brain, the SVZ is the main site of continuous neurogenesis. Neural precursors migrate as chains from the SVZ along the rostral migratory stream (RMS) to the olfactory bulb, where they differentiate into neurons. It has been shown that integrins play a critical role in the production of cell

protrusions and cell migration at different developmental stages and in the adult brain. Particularly $\beta 1$ integrins have been identified as important regulators of cell chain formation and migration of neural precursors in the RMS (Belvindrah et al., 2007; Emsley and Hagg, 2003; Jacques et al., 1998; Murase and Horwitz, 2002). Notably, expression stages of $\beta 1$ integrins in the RMS during postnatal development are comparable to the expression time course of *Tmem132d* in the SVZ. As mentioned in the introduction, *in silico* analysis of sites/motifs in the TMEM132D protein resulted in the detection of a potential RGD cell attachment sequence which is usually recognized by integrins (Ruoslahti, 1996) suggesting a potential connection between integrins and TMEM132D.

Analysis of the intracellular localization of the TMEM132D protein confirmed its localization in the cellular membrane as proposed by *in silico* studies. Additionally, overexpression of TMEM132D in HEK293 cells led to an increase in filopodia-like structures. Interestingly, TMEM132D strongly co-localized with actin filaments as shown by phalloidin staining. Actin and accordingly the actin cytoskeleton are key components for the assembly, maturation and turnover of protrusion and adhesion structures. Actin implements different organizations in lamellipodia and filopodia, the two main types of protrusive structures. Membrane extension by protrusion, adhesion formation and cell-body translocation are key steps in the highly complex process of cell migration in the RMS, in which intracellular and extracellular signals act in concert to produce a coordinated response. Thereby, the integrins act as kind of a molecular clutch. They bind to extracellular ligands via their outer domains, whereas their cytoplasmic domains are linked to numerous structural/signaling molecules as well as the actin cytoskeleton. These integrin-mediated adhesions serve as traction points for contractile or tensional forces through their interaction with actin (Vicente-Manzanares et al., 2009). Therefore, our findings suggest a role of TMEM132D in adhesion/migration which is also in line with the expression data and the findings of the *in silico* screen and should therefore be analyzed further in detail.

A potential molecular mechanism of TMEM132D function taking into account all current findings is depicted in Fig. 51.

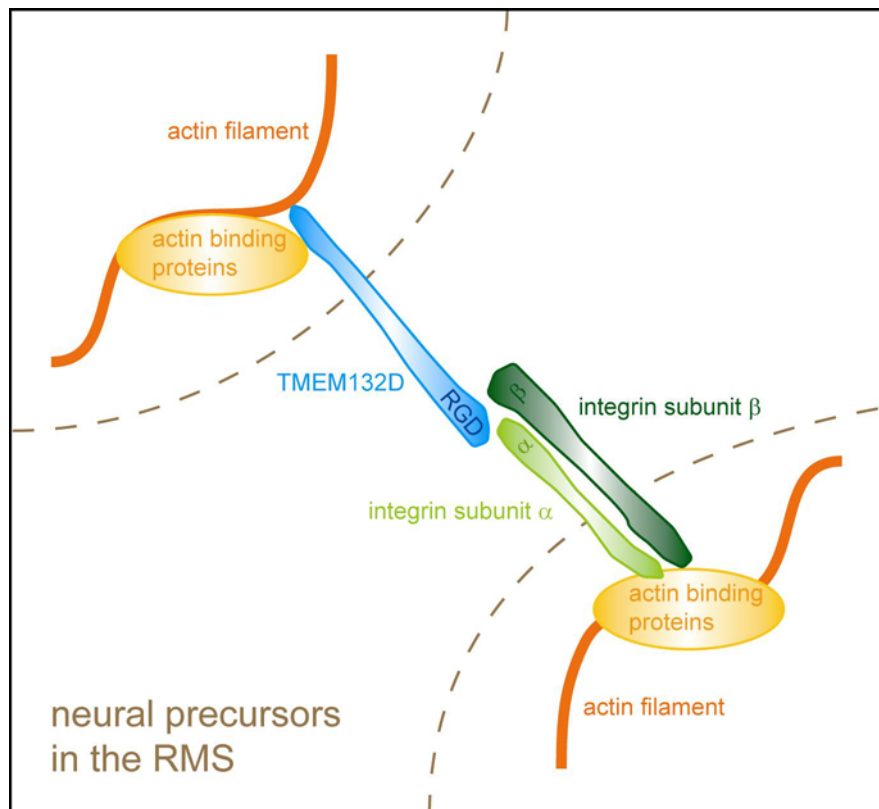


Fig. 51 Hypothesis of TMEM132D function. TMEM132D is expressed in the SVZ, the main site of neurogenesis, and may interact with $\beta 1$ integrins, via its potential RGD sequence, which regulate migration of neural precursors in the RMS. In addition, TMEM132D may affect the formation of cell protrusions and might interact with actin which is important for adhesion assembly during migration and the formation of protrusions orchestrated by integrins.

Since the identification of interacting proteins could also account for unraveling the molecular function of TMEM132D, a Y2H membrane screen was performed. A great advantage of this type of Y2H is that interaction analysis of full-length proteins, including membrane proteins, cytosolic proteins or membrane-anchored proteins, takes place at the cellular membrane. The bulk of preys identified in the screen were associated with the mitochondrial membrane or the membrane of the endoplasmic reticulum. These results indicate that trafficking of the bait protein to the cellular membrane was not very successful, and that the bait may have ectopically integrated into the membranes of cell organelles. This could be due to the instability of the bait which was already evidenced by the negative results in the Western blot and the low growth under selective conditions in the control assay. In some cases, failure to detect expression of the bait protein may be connected with inefficient translation of the fusion protein by yeast. To clarify if the identified proteins could be real interaction

partners, the results of the Y2H membrane screen have to be validated in an independent experiment, for instance by co-immunoprecipitation.

Additionally, *Tmem132d* reporter knockout animals were generated using a gene trap strategy (GGTC). Expression analysis of *Tmem132d*^{-/-} mice revealed that *Tmem132d* was almost fully abolished in the gene trap mice. Only a weak residual expression was observed which most likely can be attributed to partial splicing around of the splice donor of the endogenous exon 1 to the splice acceptor (SA) of the endogenous exon 2 instead of splicing to the SA of the SAβgeopA cassette. This is often the case when using gene trap vectors for insertional mutagenesis and should be considered when analyzing any results obtained from the knockout mice. Expression analysis further confirmed that the LacZ reporter fully reflects the endogenous *Tmem132d* expression indicating that the *LacZ* gene is solely controlled by the endogenous promoter elements of *Tmem132d*. In addition, the expression of *Tmem132b* and *Tmem132c* was determined in the brain of *Tmem132d* knockout animals to control for potential compensatory mechanisms. These closely related family members are located on the same chromosome as *Tmem132d* and their function is also fully unknown. Comparison of their expression in brains of wild-type and *Tmem132d*^{-/-} mice did not reveal any differences in the expression pattern or level suggesting that no compensatory regulation of these family members caused by *Tmem132d* depletion had occurred.

Since there is no antibody for TMEM132D available, we took advantage of the *Tmem132d* gene trap mice using the LacZ reporter to analyze cell-type specific expression of TMEM132D. Co-staining of the reporter protein with the neuronal marker NeuN proved the expression of TMEM132D in neurons as suggested by the expression pattern obtained by ISH. These results are in contradiction to the findings of Nomoto and colleagues who proposed TMEM132D as specific marker for mature oligodendrocytes (Nomoto et al., 2003), and therefore suggest a completely different function of TMEM132D in the brain. For further dissection we used neuronal markers for different neurotransmitter systems corresponding to the expression pattern observed by ISH. Using markers for glutamatergic and GABAergic neurons indicated an enriched expression of TMEM132D in glutamatergic neurons. To validate the functional and behavioral consequences of this cell-type specific expression, conditional knockout mice could be generated by breeding the animals containing the conditional gene trap vector with mice expressing the Cre recombinase under cell

type-specific promoters for glutamatergic (Nex-Cre) and GABAergic (Dlx-Cre) neurons. This is possible due to the directional site-specific recombination systems (FLPe/Cre-mediated systems) of the gene trap vector that can repair and re-induce gene trap mutations when activated in succession to produce conditional gene disruption. In a first step, FLP inverts the SA β geopA cassette into a nonmutagenic antisense orientation. This inversion reactivates normal splicing between the endogenous splice sites, thereby repairing the mutation. In a second step, Cre-mediated inversion then repositions the SA β geopA cassette back into its mutagenic sense orientation (Schnutgen et al., 2005).

Behavioral analysis of *Tmem132d*^{-/-} mice resulted in an increased active stress-coping behavior as indicated by an increase in the struggling time and decreased floating time in the FST implying a role of TMEM132D in the regulation of mood and depression-related behavior. To further confirm this phenotype, a second FST as well as a tail suspension test (TST), which is considered to be a similar behavioral readout, may be performed using an independent batch of animals. Additionally, investigation of the reaction of *Tmem132d*^{-/-} mice in response to antidepressant treatment during FST might be of interest. To further analyze the endophenotype of these knockout mice with regard to mood disorders, additional tests should be applied assessing also changes in social and anhedonic behavior such as the sociability test or FUST. Moreover, an environmental challenge such as a chronic social stress paradigm should be applied prior to behavioral testing. Because of the expression of TMEM132D in the subventricular zone and its possible interaction with integrins, which are important for migration of neural precursors in the RMS, olfaction may also be an interesting issue to be investigated.

Unfortunately, a direct *in vivo* validation of the human association data in terms of a humanized mouse model carrying the associated SNPs is not possible. The problem for this undertaking is that all identified polymorphisms are located in intronic regions of the *TMEM132D* gene which are not conserved between humans and rodents. Therefore, the conditional knockout lines mentioned above may represent a preferably appropriate alternative to study the impact of TMEM132D on the risk to develop mood and anxiety disorders in the future.

5 Conclusion

The presented work aimed at the validation of new candidate genes for mood disorders – *P2RX7* and *TMEM132D* – identified by linkage and/or association studies as potential novel therapeutic targets. To address the functional consequences of the *P2RX7*-Gln460Arg polymorphism, which is associated with unipolar and bipolar depression, we generated transgenic humanized *P2RX7* mice. Our results indicate that mainly the *P2RX7*-WT/*P2RX7*-Gln460Arg heterozygosity conveys an increased vulnerability to develop depression-related endophenotypes in response to chronic stress. Furthermore, only heterozygous *hP2RX7* mice have an altered sleep architecture and attenuated quality of sleep which is reminiscent of mood disorders. Altogether, heteromerization of the WT *P2RX7* with the mutant Gln460Arg *P2RX7* variant causes significant alterations of normal receptor function. The behavioral results of *hP2RX7* mice as well as the *in vitro* experiments strongly support the functional relevance of the mutation in heterozygosity and provide a mechanistic basis for the heterozygote disadvantage model emerging from the human association studies. The identification of SNPs in *TMEM132D*, associated with symptoms of depression and anxiety in subjects with panic disorder, unipolar depression or attention-deficit/hyperactivity disorder, raised the necessity to unravel its previously unknown function using *in vitro* and *in vivo* approaches. To our knowledge, this is the first study showing a potential functional role of *TMEM132D* in the brain. Our results evidence that *TMEM132D* may be involved in the migration of neural progenitors born in the subventricular zone through the rostral migratory stream during postnatal development and/or adult neurogenesis. This possible functional role may be based on the interaction with $\beta 1$ integrins via its potential RGD sequence as well as on the regulation of formation of cell protrusions via the interaction with actin, a key component for adhesion assembly during migration and protrusion formation mediated by integrins. Moreover, the behavioral results of the knockout mice suggest an involvement of *TMEM132D* in the development of mood-related endophenotypes. In summary, it is tempting to speculate that the candidate genes analyzed in this study might represent potential new targets for the treatment of mood disorders, and are thus worth to be investigated in more detail in the future.

6 Supplementary data

Supplementary Table S 1. Motif scan results for mouse TMEM132D (http://myhits.isb-sib.ch/cgi-bin/motif_scan). Database of motifs: PeroxiBase profiles [perox], HAMAP profiles [hamap], PROSITE patterns [pat], More profiles [pre], Pfam HMMs (local models) [pfam_fs], Pfam HMMs (global models) [pfam_ls], PROSITE patterns (frequent match producers) [freq_pat], PROSITE profiles [prf].

motif	AA start	AA end
freq_pat:AMIDATION [?]	209	212
freq_pat:ASN_GLYCOSYLATION [?]	72	75
freq_pat:ASN_GLYCOSYLATION [?]	94	97
freq_pat:ASN_GLYCOSYLATION [?]	313	316
freq_pat:ASN_GLYCOSYLATION [?]	804	807
freq_pat:ASN_GLYCOSYLATION [?]	967	970
freq_pat:CAMP_PHOSPHO_SITE [?]	212	215
freq_pat:CAMP_PHOSPHO_SITE [?]	780	783
freq_pat:CAMP_PHOSPHO_SITE [?]	856	859
freq_pat:CAMP_PHOSPHO_SITE [?]	1041	1044
freq_pat:CK2_PHOSPHO_SITE [?]	77	80
freq_pat:CK2_PHOSPHO_SITE [?]	340	343
freq_pat:CK2_PHOSPHO_SITE [?]	371	374
freq_pat:CK2_PHOSPHO_SITE [?]	420	423
freq_pat:CK2_PHOSPHO_SITE [?]	455	458
freq_pat:CK2_PHOSPHO_SITE [?]	473	476
freq_pat:CK2_PHOSPHO_SITE [?]	512	515
freq_pat:CK2_PHOSPHO_SITE [?]	530	533
freq_pat:CK2_PHOSPHO_SITE [?]	554	557
freq_pat:CK2_PHOSPHO_SITE [?]	630	633
freq_pat:CK2_PHOSPHO_SITE [?]	656	659
freq_pat:CK2_PHOSPHO_SITE [?]	663	666
freq_pat:CK2_PHOSPHO_SITE [?]	720	723
freq_pat:CK2_PHOSPHO_SITE [?]	735	738
freq_pat:CK2_PHOSPHO_SITE [?]	885	888
freq_pat:CK2_PHOSPHO_SITE [?]	912	915
freq_pat:CK2_PHOSPHO_SITE [?]	980	983
freq_pat:CK2_PHOSPHO_SITE [?]	987	990
freq_pat:CK2_PHOSPHO_SITE [?]	1052	1055
freq_pat:CK2_PHOSPHO_SITE [?]	1066	1069
freq_pat:CK2 PHOSPHO_SITE [?]	1088	1091

freq_pat:MYRISTYL [?]	32	37
freq_pat:MYRISTYL [?]	185	190
freq_pat:MYRISTYL [?]	247	252
freq_pat:MYRISTYL [?]	333	338
freq_pat:MYRISTYL [?]	367	372
freq_pat:MYRISTYL [?]	460	465
freq_pat:MYRISTYL [?]	590	595
freq_pat:MYRISTYL [?]	626	631
freq_pat:MYRISTYL [?]	674	679
freq_pat:MYRISTYL [?]	684	689
freq_pat:MYRISTYL [?]	797	802
freq_pat:MYRISTYL [?]	846	851
freq_pat:MYRISTYL [?]	894	899
freq_pat:MYRISTYL [?]	955	960
freq_pat:MYRISTYL [?]	973	978
freq_pat:MYRISTYL [?]	1019	1024
freq_pat:MYRISTYL [?]	1056	1061
freq_pat:MYRISTYL [?]	1077	1082
freq_pat:PKC_PHOSPHO_SITE [?]	87	89
freq_pat:PKC_PHOSPHO_SITE [?]	181	183
freq_pat:PKC_PHOSPHO_SITE [?]	209	211
freq_pat:PKC_PHOSPHO_SITE [?]	243	245
freq_pat:PKC_PHOSPHO_SITE [?]	297	299
freq_pat:PKC_PHOSPHO_SITE [?]	320	322
freq_pat:PKC_PHOSPHO_SITE [?]	351	353
freq_pat:PKC_PHOSPHO_SITE [?]	368	370
freq_pat:PKC_PHOSPHO_SITE [?]	420	422
freq_pat:PKC_PHOSPHO_SITE [?]	443	445
freq_pat:PKC_PHOSPHO_SITE [?]	482	484
freq_pat:PKC_PHOSPHO_SITE [?]	546	548
freq_pat:PKC_PHOSPHO_SITE [?]	685	687
freq_pat:PKC_PHOSPHO_SITE [?]	779	781
freq_pat:PKC_PHOSPHO_SITE [?]	791	793
freq_pat:PKC_PHOSPHO_SITE [?]	825	827
freq_pat:PKC_PHOSPHO_SITE [?]	854	856
freq_pat:PKC_PHOSPHO_SITE [?]	966	968
freq_pat:PKC_PHOSPHO_SITE [?]	1037	1039
freq_pat:RGD [?]	235	237
freq_pat:TYR_PHOSPHO_SITE [?]	370	377
freq_pat:TYR_PHOSPHO_SITE [?]	480	487
pfam_fs:Spot_14 [?]	692	713
pfam_fs:TSP_3 [?]	472	486

Supplementary Table S 2. Motif scan results for human TMEM132D (http://myhits.isb-sib.ch/cgi-bin/motif_scan). Database of motifs: PeroxiBase profiles [perox], HAMAP profiles [hamap], PROSITE patterns [pat], More profiles [pre], Pfam HMMs (local models) [pfam_fs], Pfam HMMs (global models) [pfam_ls], PROSITE patterns (frequent match producers) [freq_pat], PROSITE profiles [prf].

motif	AA start	AA end
freq_pat:AMIDATION [?]	210	213
freq_pat:ASN_GLYCOSYLATION [?]	72	75
freq_pat:ASN_GLYCOSYLATION [?]	94	97
freq_pat:ASN_GLYCOSYLATION [?]	314	317
freq_pat:ASN_GLYCOSYLATION [?]	505	508
freq_pat:ASN_GLYCOSYLATION [?]	805	808
freq_pat:ASN_GLYCOSYLATION [?]	821	824
freq_pat:ASN_GLYCOSYLATION [?]	969	972
freq_pat:CAMP_PHOSPHO_SITE [?]	212	215
freq_pat:CAMP_PHOSPHO_SITE [?]	277	280
freq_pat:CAMP_PHOSPHO_SITE [?]	781	784
freq_pat:CAMP_PHOSPHO_SITE [?]	828	831
freq_pat:CK2_PHOSPHO_SITE [?]	77	80
freq_pat:CK2_PHOSPHO_SITE [?]	160	163
freq_pat:CK2_PHOSPHO_SITE [?]	222	225
freq_pat:CK2_PHOSPHO_SITE [?]	255	258
freq_pat:CK2_PHOSPHO_SITE [?]	280	283
freq_pat:CK2_PHOSPHO_SITE [?]	315	318
freq_pat:CK2_PHOSPHO_SITE [?]	341	344
freq_pat:CK2_PHOSPHO_SITE [?]	421	424
freq_pat:CK2_PHOSPHO_SITE [?]	456	459
freq_pat:CK2_PHOSPHO_SITE [?]	462	465
freq_pat:CK2_PHOSPHO_SITE [?]	474	477
freq_pat:CK2_PHOSPHO_SITE [?]	513	516
freq_pat:CK2_PHOSPHO_SITE [?]	531	534
freq_pat:CK2_PHOSPHO_SITE [?]	555	558
freq_pat:CK2_PHOSPHO_SITE [?]	657	660
freq_pat:CK2_PHOSPHO_SITE [?]	664	667
freq_pat:CK2_PHOSPHO_SITE [?]	721	724
freq_pat:CK2_PHOSPHO_SITE [?]	736	739
freq_pat:CK2_PHOSPHO_SITE [?]	855	858
freq_pat:CK2_PHOSPHO_SITE [?]	870	873
freq_pat:CK2_PHOSPHO_SITE [?]	897	900
freq_pat:CK2_PHOSPHO_SITE [?]	914	917
freq_pat:CK2_PHOSPHO_SITE [?]	982	985
freq_pat:CK2_PHOSPHO_SITE [?]	989	992
freq_pat:CK2_PHOSPHO_SITE [?]	1054	1057
freq_pat:CK2_PHOSPHO_SITE [?]	1068	1071

freq_pat:MYRISTYL [?]	32	37
freq_pat:MYRISTYL [?]	190	195
freq_pat:MYRISTYL [?]	233	238
freq_pat:MYRISTYL [?]	249	254
freq_pat:MYRISTYL [?]	334	339
freq_pat:MYRISTYL [?]	368	373
freq_pat:MYRISTYL [?]	591	596
freq_pat:MYRISTYL [?]	632	637
freq_pat:MYRISTYL [?]	675	680
freq_pat:MYRISTYL [?]	685	690
freq_pat:MYRISTYL [?]	798	803
freq_pat:MYRISTYL [?]	835	840
freq_pat:MYRISTYL [?]	848	853
freq_pat:MYRISTYL [?]	957	962
freq_pat:PKC_PHOSPHO_SITE [?]	87	89
freq_pat:PKC_PHOSPHO_SITE [?]	120	122
freq_pat:PKC_PHOSPHO_SITE [?]	182	184
freq_pat:PKC_PHOSPHO_SITE [?]	275	277
freq_pat:PKC_PHOSPHO_SITE [?]	280	282
freq_pat:PKC_PHOSPHO_SITE [?]	298	300
freq_pat:PKC_PHOSPHO_SITE [?]	321	323
freq_pat:PKC_PHOSPHO_SITE [?]	352	354
freq_pat:PKC_PHOSPHO_SITE [?]	421	423
freq_pat:PKC_PHOSPHO_SITE [?]	444	446
freq_pat:PKC_PHOSPHO_SITE [?]	483	485
freq_pat:PKC_PHOSPHO_SITE [?]	547	549
freq_pat:PKC_PHOSPHO_SITE [?]	686	688
freq_pat:PKC_PHOSPHO_SITE [?]	780	782
freq_pat:PKC_PHOSPHO_SITE [?]	823	825
freq_pat:PKC_PHOSPHO_SITE [?]	857	859
freq_pat:PKC_PHOSPHO_SITE [?]	968	970
freq_pat:PKC_PHOSPHO_SITE [?]	1008	1010
freq_pat:PKC_PHOSPHO_SITE [?]	1039	1041
freq_pat:RGD [?]	236	238
freq_pat:TYR_PHOSPHO_SITE [?]	481	488
pfam_fs:Big_2 [?]	786	807
pfam_ls:MORN [?]	841	863

Supplementary Table S 3. Complete list of sequence-verified clones identified in the Y2H membrane screening.

Clone-ID	Prey-ID	Protein name (description)
6	Rtn1	reticulon 1, transcript variant 2
8	Serp2	stress-associated endoplasmic reticulum protein family member 2
9	Rgs10	regulator of G-protein signalling 10
10	Serp2	stress-associated endoplasmic reticulum protein family
11	Rnf41	ring finger protein 41
12A	Tmem11	transmembrane protein 11
12B	Serp2	stress-associated endoplasmic reticulum protein family member 2
14	Tmem11	transmembrane protein 11
15	Gpsn2	glycoprotein, synaptic 2
16	Tmem41b	transmembrane protein 41B
18	Selk	selenoprotein K
19	Selk	selenoprotein K
20	Gpsn2	glycoprotein, synaptic 2
26	Rtn1	reticulon 1, transcript variant 2
27	Glrx5	glutaredoxin 5 homolog (S. cerevisiae)
28	Sumo2	SMT3 suppressor of mif two 3 homolog 2 (yeast)
29	Fkbp8	FK506 binding protein 8
30A	Snx27	sorting nexin family member 27 isoform 1/2
30B	Glrx5	glutaredoxin 5 homolog (S. cerevisiae)
31	Serp2	stress-associated endoplasmic reticulum protein family member 2
32	Gpsn2	glycoprotein, synaptic 2
33A	Gpsn2	glycoprotein, synaptic 2
33B	Rps14	ribosomal protein S14
36	Gpsn2	glycoprotein, synaptic 2
37	Spcs1	signal peptidase complex subunit 1 homolog (S. cerevisiae)
38	Gpsn2	glycoprotein, synaptic 2
39	Tmem11	transmembrane protein 11
40	Uba52	ubiquitin A-52 residue ribosomal protein fusion product 1
42	Gpsn2	glycoprotein, synaptic 2
43	Selk	selenoprotein K
45	Serp2	stress-associated endoplasmic reticulum protein family member 2
46	Map1lc3a	microtubule-associated protein 1 light chain 3 alpha

7 References

- Adams JC (2001) Thrombospondins: multifunctional regulators of cell interactions. *Annu Rev Cell Dev Biol* 17:25-51.
- Adriouch S, Dox C, Welge V, Seman M, Koch-Nolte F, Haag F (2002) Cutting edge: a natural P451L mutation in the cytoplasmic domain impairs the function of the mouse P2X7 receptor. *J Immunol* 169:4108-4112.
- Ainsworth K, Smith SE, Sharp T (1998) Repeated administration of fluoxetine, desipramine and tranylcypromine increases dopamine D2-like but not D1-like receptor function in the rat. *J Psychopharmacol* 12:252-257.
- Althoff RR, Rettew DC, Ayer LA, Hudziak JJ (2010a) Cross-informant agreement of the Dysregulation Profile of the Child Behavior Checklist. *Psychiatry Res* 178:550-555.
- Althoff RR, Verhulst FC, Rettew DC, Hudziak JJ, van der EJ (2010b) Adult outcomes of childhood dysregulation: a 14-year follow-up study. *J Am Acad Child Adolesc Psychiatry* 49:1105-1116.
- Amann LC, Gandal MJ, Halene TB, Ehrlichman RS, White SL, McCarren HS, Siegel SJ (2010) Mouse behavioral endophenotypes for schizophrenia. *Brain Res Bull* 83:147-161.
- Anderson CM, Nedergaard M (2006) Emerging challenges of assigning P2X7 receptor function and immunoreactivity in neurons. *Trends Neurosci* 29:257-262.
- Angold A, Costello EJ, Erkanli A (1999) Comorbidity. *J Child Psychol Psychiatry* 40:57-87.
- Antonio LS, Stewart AP, Xu XJ, Varanda WA, Murrell-Lagnado RD, Edwardson JM (2011) P2X4 receptors interact with both P2X2 and P2X7 receptors in the form of homotrimers. *Br J Pharmacol* 163:1069-1077.
- Armitage R (2007) Sleep and circadian rhythms in mood disorders. *Acta Psychiatr Scand Suppl* 104-115.
- Ayer L, Althoff R, Ivanova M, Rettew D, Waxler E, Sulman J, Hudziak J (2009) Child Behavior Checklist Juvenile Bipolar Disorder (CBCL-JBD) and CBCL Posttraumatic Stress Problems (CBCL-PTSP) scales are measures of a single dysregulatory syndrome. *J Child Psychol Psychiatry* 50:1291-1300.
- Baracchi F, Opp MR (2008) Sleep-wake behavior and responses to sleep deprivation of mice lacking both interleukin-1 beta receptor 1 and tumor necrosis factor-alpha receptor 1. *Brain Behav Immun* 22:982-993.
- Barden JA, Miki M, Hambly BD, dos Remedios CG (1987) Localization of the phalloidin and nucleotide-binding sites on actin. *Eur J Biochem* 162:583-588.
- Barden N, Harvey M, Gagne B, Shink E, Tremblay M, Raymond C, Labbe M, Villeneuve A, Rochette D, Bordeleau L, Stadler H, Holsboer F, Muller-Myhsok B (2006) Analysis of single nucleotide polymorphisms in genes in the chromosome 12Q24.31 region points to P2RX7 as a susceptibility gene to bipolar affective disorder. *Am J Med Genet B Neuropsychiatr Genet* 141B:374-382.
- Basso AM, Bratcher NA, Harris RR, Jarvis MF, Decker MW, Rueter LE (2009) Behavioral profile of P2X7 receptor knockout mice in animal models of depression and anxiety: relevance for neuropsychiatric disorders. *Behav Brain Res* 198:83-90.
- Baum AE, Akula N, Cabanero M, Cardona I, Corona W, Klemens B, Schulze TG, Cichon S, Rietschel M, Nothen MM, Georgi A, Schumacher J, Schwarz M, Abou JR, Hofels S, Propping P, Satagopan J, tera-Wadleigh SD, Hardy J, McMahon FJ (2008) A genome-wide association study implicates

- diacylglycerol kinase eta (DGKH) and several other genes in the etiology of bipolar disorder. *Mol Psychiatry* 13:197-207.
- Belvindrah R, Hankel S, Walker J, Patton BL, Muller U (2007) Beta1 integrins control the formation of cell chains in the adult rostral migratory stream. *J Neurosci* 27:2704-2717.
- Berton O, McClung CA, Dileone RJ, Krishnan V, Renthal W, Russo SJ, Graham D, Tsankova NM, Bolanos CA, Rios M, Monteggia LM, Self DW, Nestler EJ (2006) Essential role of BDNF in the mesolimbic dopamine pathway in social defeat stress. *Science* 311:864-868.
- Berton O, Nestler EJ (2006) New approaches to antidepressant drug discovery: beyond monoamines. *Nat Rev Neurosci* 7:137-151.
- Biederman J, Newcorn J, Sprich S (1991) Comorbidity of attention deficit hyperactivity disorder with conduct, depressive, anxiety, and other disorders. *Am J Psychiatry* 148:564-577.
- Biederman J, Petty CR, Monuteaux MC, Evans M, Parcell T, Faraone SV, Wozniak J (2009) The Child Behavior Checklist-Pediatric Bipolar Disorder profile predicts a subsequent diagnosis of bipolar disorder and associated impairments in ADHD youth growing up: a longitudinal analysis. *J Clin Psychiatry* 70:732-740.
- Blendy JA (2011) Modeling neuropsychiatric disease-relevant human SNPs in mice. *Neuropsychopharmacology* 36:364-365.
- Boucher AA, Arnold JC, Hunt GE, Spiro A, Spencer J, Brown C, McGregor IS, Bennett MR, Kassiou M (2011) Resilience and reduced c-Fos expression in P2X7 receptor knockout mice exposed to repeated forced swim test. *Neuroscience* 189:170-177.
- Bradford MD, Soltoff SP (2002) P2X7 receptors activate protein kinase D and p42/p44 mitogen-activated protein kinase (MAPK) downstream of protein kinase C. *Biochem J* 366:745-755.
- Brown GW, Bifulco A, Harris TO (1987) Life events, vulnerability and onset of depression: some refinements. *Br J Psychiatry* 150:30-42.
- Cabrini G, Falzoni S, Forchap SL, Pellegatti P, Balboni A, Agostini P, Cuneo A, Castoldi G, Baricordi OR, Di VF (2005) A His-155 to Tyr polymorphism confers gain-of-function to the human P2X7 receptor of human leukemic lymphocytes. *J Immunol* 175:82-89.
- Cahill L (2006) Why sex matters for neuroscience. *Nat Rev Neurosci* 7:477-484.
- Chadman KK, Yang M, Crawley JN (2009) Criteria for validating mouse models of psychiatric diseases. *Am J Med Genet B Neuropsychiatr Genet* 150B:1-11.
- Chen YT, Bradley A (2000) A new positive/negative selectable marker, puDeltak, for use in embryonic stem cells. *Genesis* 28:31-35.
- Chen ZY, Jing D, Bath KG, Ieraci A, Khan T, Siao CJ, Herrera DG, Toth M, Yang C, McEwen BS, Hempstead BL, Lee FS (2006) Genetic variant BDNF (Val66Met) polymorphism alters anxiety-related behavior. *Science* 314:140-143.
- Chessell IP, Hatcher JP, Bountra C, Michel AD, Hughes JP, Green P, Egerton J, Murfin M, Richardson J, Peck WL, Grahames CB, Casula MA, Yiangou Y, Birch R, Anand P, Buell GN (2005) Disruption of the P2X7 purinoceptor gene abolishes chronic inflammatory and neuropathic pain. *Pain* 114:386-396.
- Cichon S, Craddock N, Daly M, Faraone SV, Gejman PV, Kelsoe J, Lehner T, Levinson DF, Moran A, Sklar P, Sullivan PF (2009) Genomewide association studies: history, rationale, and prospects for psychiatric disorders. *Am J Psychiatry* 166:540-556.

- Covington HE, III, Maze I, LaPlant QC, Vialou VF, Ohnishi YN, Berton O, Fass DM, Renthal W, Rush AJ, III, Wu EY, Ghose S, Krishnan V, Russo SJ, Tammimga C, Haggarty SJ, Nestler EJ (2009) Antidepressant actions of histone deacetylase inhibitors. *J Neurosci* 29:11451-11460.
- Craddock N, O'Donovan MC, Owen MJ (2008) Genome-wide association studies in psychiatry: lessons from early studies of non-psychiatric and psychiatric phenotypes. *Mol Psychiatry* 13:649-653.
- Crellin R, Bottiglieri T, Reynolds EH (1993) Folates and psychiatric disorders. Clinical potential. *Drugs* 45:623-636.
- D'Aquila PS, Collu M, Gessa GL, Serra G (2000) The role of dopamine in the mechanism of action of antidepressant drugs. *Eur J Pharmacol* 405:365-373.
- de Kloet ER, Joels M, Holsboer F (2005) Stress and the brain: from adaptation to disease. *Nat Rev Neurosci* 6:463-475.
- Dedic, Walser, Deussing (2011) Mouse Models of Depression. *Psychiatric Disorders - Trends and Developments*, Toru Uehara (Ed)185-222.
- Denlinger LC, Fiset PL, Sommer JA, Watters JJ, Prabhu U, Dubyak GR, Proctor RA, Bertics PJ (2001) Cutting edge: the nucleotide receptor P2X7 contains multiple protein- and lipid-interaction motifs including a potential binding site for bacterial lipopolysaccharide. *J Immunol* 167:1871-1876.
- Denlinger LC, Sommer JA, Parker K, Gudipaty L, Fiset PL, Watters JW, Proctor RA, Dubyak GR, Bertics PJ (2003) Mutation of a dibasic amino acid motif within the C terminus of the P2X7 nucleotide receptor results in trafficking defects and impaired function. *J Immunol* 171:1304-1311.
- Deuchars SA, Atkinson L, Brooke RE, Musa H, Milligan CJ, Batten TF, Buckley NJ, Parson SH, Deuchars J (2001) Neuronal P2X7 receptors are targeted to presynaptic terminals in the central and peripheral nervous systems. *J Neurosci* 21:7143-7152.
- Deussing (2006) Animal models of depression. *Drug Discovery Today: Disease Models* 3.
- Di Virgilio (2007) Liaisons dangereuses: P2X(7) and the inflammasome. *Trends Pharmacol Sci* 28:465-472.
- Dubyak GR (2007) Go it alone no more--P2X7 joins the society of heteromeric ATP-gated receptor channels. *Mol Pharmacol* 72:1402-1405.
- Dunner DL, Patrick V, Fieve RR (1979) Life events at the onset of bipolar affective illness. *Am J Psychiatry* 136:508-511.
- Emsley JG, Hagg T (2003) alpha6beta1 integrin directs migration of neuronal precursors in adult mouse forebrain. *Exp Neurol* 183:273-285.
- Erhardt A, et al. (2011) TMEM132D, a new candidate for anxiety phenotypes: evidence from human and mouse studies. *Mol Psychiatry* 16:647-663.
- Fava M, Kendler KS (2000) Major depressive disorder. *Neuron* 28:335-341.
- Ferrari D, Chiozzi P, Falzoni S, Dal SM, Melchiorri L, Baricordi OR, Di VF (1997a) Extracellular ATP triggers IL-1 beta release by activating the purinergic P2Z receptor of human macrophages. *J Immunol* 159:1451-1458.
- Ferrari D, Chiozzi P, Falzoni S, Hanau S, Di VF (1997b) Purinergic modulation of interleukin-1 beta release from microglial cells stimulated with bacterial endotoxin. *J Exp Med* 185:579-582.
- Ferreira MA, et al. (2008) Collaborative genome-wide association analysis supports a role for ANK3 and CACNA1C in bipolar disorder. *Nat Genet* 40:1056-1058.

- Franken P, Malafosse A, Tafti M (1998) Genetic variation in EEG activity during sleep in inbred mice. *Am J Physiol* 275:R1127-R1137.
- Fuller SJ, Stokes L, Skarratt KK, Gu BJ, Wiley JS (2009) Genetics of the P2X7 receptor and human disease. *Purinergic Signal* 5:257-262.
- Goltser-Dubner T, Galili-Weisstub E, Segman RH (2010) Genetics of unipolar major depressive disorder. *Isr J Psychiatry Relat Sci* 47:72-82.
- Golub Y, Mauch CP, Dahlhoff M, Wotjak CT (2009) Consequences of extinction training on associative and non-associative fear in a mouse model of Posttraumatic Stress Disorder (PTSD). *Behav Brain Res* 205:544-549.
- Green EK, Grozeva D, Raybould R, Elvidge G, Macgregor S, Craig I, Farmer A, McGuffin P, Forty L, Jones L, Jones I, O'Donovan MC, Owen MJ, Kirov G, Craddock N (2009) P2RX7: A bipolar and unipolar disorder candidate susceptibility gene? *Am J Med Genet B Neuropsychiatr Genet* 150B:1063-1069.
- Grigoriadis DE (2005) The corticotropin-releasing factor receptor: a novel target for the treatment of depression and anxiety-related disorders. *Expert Opin Ther Targets* 9:651-684.
- Grigoriadis S, Robinson GE (2007) Gender issues in depression. *Ann Clin Psychiatry* 19:247-255.
- Grigoriou-Serbanescu M, et al. (2009) Variation in P2RX7 candidate gene (rs2230912) is not associated with bipolar I disorder and unipolar major depression in four European samples. *Am J Med Genet B Neuropsychiatr Genet* 150B:1017-1021.
- Gu BJ, Sluyter R, Skarratt KK, Shemon AN, Dao-Ung LP, Fuller SJ, Barden JA, Clarke AL, Petrou S, Wiley JS (2004) An Arg307 to Gln polymorphism within the ATP-binding site causes loss of function of the human P2X7 receptor. *J Biol Chem* 279:31287-31295.
- Hasler G, Drevets WC, Manji HK, Charney DS (2004) Discovering endophenotypes for major depression. *Neuropsychopharmacology* 29:1765-1781.
- Hejjas K, Szekely A, Domotor E, Halmai Z, Balogh G, Schilling B, Sarosi A, Faludi G, Sasvari-Szekely M, Nemoda Z (2009) Association between depression and the Gln460Arg polymorphism of P2RX7 gene: a dimensional approach. *Am J Med Genet B Neuropsychiatr Genet* 150B:295-299.
- Hibell AD, Kidd EJ, Chessell IP, Humphrey PP, Michel AD (2000) Apparent species differences in the kinetic properties of P2X(7) receptors. *Br J Pharmacol* 130:167-173.
- Hibell AD, Thompson KM, Simon J, Xing M, Humphrey PP, Michel AD (2001) Species- and agonist-dependent differences in the deactivation-kinetics of P2X7 receptors. *Naunyn Schmiedebergs Arch Pharmacol* 363:639-648.
- Holmes A, Hollon TR, Gleason TC, Liu Z, Dreiling J, Sibley DR, Crawley JN (2001) Behavioral characterization of dopamine D5 receptor null mutant mice. *Behav Neurosci* 115:1129-1144.
- Holsboer F (2000) The corticosteroid receptor hypothesis of depression. *Neuropsychopharmacology* 23:477-501.
- Holsboer F (2001) Stress, hypercortisolism and corticosteroid receptors in depression: implications for therapy. *J Affect Disord* 62:77-91.
- Holsboer F (2005) The future of antidepressant pharmacogenetics is arriving. Introduction. *Prog Neuropsychopharmacol Biol Psychiatry* 29:996-998.
- Holsboer F, Barden N (1996) Antidepressants and hypothalamic-pituitary-adrenocortical regulation. *Endocr Rev* 17:187-205.

- Jacques TS, Relvas JB, Nishimura S, Pytela R, Edwards GM, Streuli CH, French-Constant C (1998) Neural precursor cell chain migration and division are regulated through different beta1 integrins. *Development* 125:3167-3177.
- Jakubcakova V, Flachskamm C, Deussing JM, Kimura M (2011) Deficiency of corticotropin-releasing hormone type-2 receptor alters sleep responses to bacterial lipopolysaccharide in mice. *Brain Behav Immun*.
- Kataoka A, Tozaki-Saitoh H, Koga Y, Tsuda M, Inoue K (2009) Activation of P2X7 receptors induces CCL3 production in microglial cells through transcription factor NFAT. *J Neurochem* 108:115-125.
- Keck ME (2006) Corticotropin-releasing factor, vasopressin and receptor systems in depression and anxiety. *Amino Acids* 31:241-250.
- Kessler RC, Berglund P, Demler O, Jin R, Koretz D, Merikangas KR, Rush AJ, Walters EE, Wang PS (2003) The epidemiology of major depressive disorder: results from the National Comorbidity Survey Replication (NCS-R). *JAMA* 289:3095-3105.
- Khakh BS, North RA (2006) P2X receptors as cell-surface ATP sensors in health and disease. *Nature* 442:527-532.
- Kimura M, Muller-Preuss P, Lu A, Wiesner E, Flachskamm C, Wurst W, Holsboer F, Deussing JM (2010) Conditional corticotropin-releasing hormone overexpression in the mouse forebrain enhances rapid eye movement sleep. *Mol Psychiatry* 15:154-165.
- Kukley M, Stausberg P, Adelman G, Chessell IP, Dietrich D (2004) Ecto-nucleotidases and nucleoside transporters mediate activation of adenosine receptors on hippocampal mossy fibers by P2X7 receptor agonist 2'-3'-O-(4-benzoylbenzoyl)-ATP. *J Neurosci* 24:7128-7139.
- Lavebratt C, Aberg E, Sjöholm LK, Forsell Y (2010) Variations in FKBP5 and BDNF genes are suggestively associated with depression in a Swedish population-based cohort. *J Affect Disord* 125:249-255.
- Lenertz LY, Gavala ML, Zhu Y, Bertics PJ (2011) Transcriptional control mechanisms associated with the nucleotide receptor P2X7, a critical regulator of immunologic, osteogenic, and neurologic functions. *Immunol Res* 50:22-38.
- Levinson DF (2006) The genetics of depression: a review. *Biol Psychiatry* 60:84-92.
- Lopez-Leon S, Janssens AC, Gonzalez-Zuloeta Ladd AM, Del-Favero J, Claes SJ, Oostra BA, van Duijn CM (2008) Meta-analyses of genetic studies on major depressive disorder. *Mol Psychiatry* 13:772-785.
- Louis RP, Lee J, Stephenson R (2004) Design and validation of a computer-based sleep-scoring algorithm. *J Neurosci Methods* 133:71-80.
- Lu A, Steiner MA, Whittle N, Vogl AM, Walser SM, Ableitner M, Refojo D, Ekker M, Rubenstein JL, Stalla GK, Singewald N, Holsboer F, Wotjak CT, Wurst W, Deussing JM (2008) Conditional mouse mutants highlight mechanisms of corticotropin-releasing hormone effects on stress-coping behavior. *Mol Psychiatry* 13:1028-1042.
- Lucae S, Salyakina D, Barden N, Harvey M, Gagne B, Labbe M, Binder EB, Uhr M, Paez-Pereda M, Sillaber I, Ising M, Bruckl T, Lieb R, Holsboer F, Muller-Myhsok B (2006) P2RX7, a gene coding for a purinergic ligand-gated ion channel, is associated with major depressive disorder. *Hum Mol Genet* 15:2438-2445.
- Maes M (2008) The cytokine hypothesis of depression: inflammation, oxidative & nitrosative stress (IO&NS) and leaky gut as new targets for adjunctive treatments in depression. *Neuro Endocrinol Lett* 29:287-291.
- Maher B (2008) Personal genomes: The case of the missing heritability. *Nature* 456:18-21.

- Mahley RW, Rall SC, Jr. (2000) Apolipoprotein E: far more than a lipid transport protein. *Annu Rev Genomics Hum Genet* 1:507-537.
- Malkesman O, Scattoni ML, Paredes D, Tragon T, Pearson B, Shaltiel G, Chen G, Crawley JN, Manji HK (2010) The female urine sniffing test: a novel approach for assessing reward-seeking behavior in rodents. *Biol Psychiatry* 67:864-871.
- Manolio TA, et al. (2009) Finding the missing heritability of complex diseases. *Nature* 461:747-753.
- Marin-Garcia P, Sanchez-Nogueiro J, Gomez-Villafuertes R, Leon D, Miras-Portugal MT (2008) Synaptic terminals from mice midbrain exhibit functional P2X7 receptor. *Neuroscience* 151:361-373.
- Masin M, Young C, Lim K, Barnes SJ, Xu XJ, Marschall V, Brutkowski W, Mooney ER, Gorecki DC, Murrell-Lagnado R (2011) Expression, assembly and function of novel C-terminal truncated variants of the mouse P2X7 receptor: Re-evaluation of P2X7 knockouts. *Br J Pharmacol*.
- McKinney WT, Jr., Bunney WE, Jr. (1969) Animal model of depression. I. Review of evidence: implications for research. *Arch Gen Psychiatry* 21:240-248.
- McQuillin A, Bass NJ, Choudhury K, Puri V, Kosmin M, Lawrence J, Curtis D, Gurling HM (2009) Case-control studies show that a non-conservative amino-acid change from a glutamine to arginine in the P2RX7 purinergic receptor protein is associated with both bipolar- and unipolar-affective disorders. *Mol Psychiatry* 14:614-620.
- Meyer SE, Carlson GA, Youngstrom E, Ronsaville DS, Martinez PE, Gold PW, Hakak R, Radke-Yarrow M (2009) Long-term outcomes of youth who manifested the CBCL-Pediatric Bipolar Disorder phenotype during childhood and/or adolescence. *J Affect Disord* 113:227-235.
- Mick E, McGough J, Loo S, Doyle AE, Wozniak J, Wilens TE, Smalley S, McCracken J, Biederman J, Faraone SV (2011) Genome-wide association study of the child behavior checklist dysregulation profile. *J Am Acad Child Adolesc Psychiatry* 50:807-817.
- Miller AH, Maletic V, Raison CL (2009) Inflammation and its discontents: the role of cytokines in the pathophysiology of major depression. *Biol Psychiatry* 65:732-741.
- Mineur YS, Prasol DJ, Belzung C, Crusio WE (2003) Agonistic behavior and unpredictable chronic mild stress in mice. *Behav Genet* 33:513-519.
- Modell S, Ising M, Holsboer F, Lauer CJ (2005) The Munich vulnerability study on affective disorders: premorbid polysomnographic profile of affected high-risk probands. *Biol Psychiatry* 58:694-699.
- Monteggia LM, Luikart B, Barrot M, Theobald D, Malkovska I, Nef S, Parada LF, Nestler EJ (2007) Brain-derived neurotrophic factor conditional knockouts show gender differences in depression-related behaviors. *Biol Psychiatry* 61:187-197.
- Morilak DA, Frazer A (2004) Antidepressants and brain monoaminergic systems: a dimensional approach to understanding their behavioural effects in depression and anxiety disorders. *Int J Neuropsychopharmacol* 7:193-218.
- Moy SS, Nadler JJ, Perez A, Barbaro RP, Johns JM, Magnuson TR, Piven J, Crawley JN (2004) Sociability and preference for social novelty in five inbred strains: an approach to assess autistic-like behavior in mice. *Genes Brain Behav* 3:287-302.
- Murase S, Horwitz AF (2002) Deleted in colorectal carcinoma and differentially expressed integrins mediate the directional migration of neural precursors in the rostral migratory stream. *J Neurosci* 22:3568-3579.
- Murray CJ, Lopez AD (1997) Alternative projections of mortality and disability by cause 1990-2020: Global Burden of Disease Study. *Lancet* 349:1498-1504.
- Myers AJ, et al. (2007) A survey of genetic human cortical gene expression. *Nat Genet* 39:1494-1499.

- Nemeroff CB (1988) The role of corticotropin-releasing factor in the pathogenesis of major depression. *Pharmacopsychiatry* 21:76-82.
- Nestler EJ, Gould E, Manji H, Buncan M, Duman RS, Greshenfeld HK, Hen R, Koester S, Lederhendler I, Meaney M, Robbins T, Winsky L, Zalcman S (2002) Preclinical models: status of basic research in depression. *Biol Psychiatry* 52:503-528.
- Nestler EJ, Hyman SE (2010) Animal models of neuropsychiatric disorders. *Nat Neurosci* 13:1161-1169.
- Nicke A, Kuan YH, Masin M, Rettinger J, Marquez-Klaka B, Bender O, Gorecki DC, Murrell-Lagnado RD, Soto F (2009) A functional P2X7 splice variant with an alternative transmembrane domain 1 escapes gene inactivation in P2X7 knock-out mice. *J Biol Chem* 284:25813-25822.
- Nomoto H, Yonezawa T, Itoh K, Ono K, Yamamoto K, Oohashi T, Shiraga F, Ohtsuki H, Ninomiya Y (2003) Molecular cloning of a novel transmembrane protein MOLT expressed by mature oligodendrocytes. *J Biochem* 134:231-238.
- North RA, Surprenant A (2000) Pharmacology of cloned P2X receptors. *Annu Rev Pharmacol Toxicol* 40:563-580.
- O'Tuathaigh CM, Babovic D, O'Sullivan GJ, Clifford JJ, Tighe O, Croke DT, Harvey R, Waddington JL (2007) Phenotypic characterization of spatial cognition and social behavior in mice with 'knockout' of the schizophrenia risk gene neuregulin 1. *Neuroscience* 147:18-27.
- Oh-hashii K, Naruse Y, Amaya F, Shimosato G, Tanaka M (2003) Cloning and characterization of a novel GRP78-binding protein in the rat brain. *J Biol Chem* 278:10531-10537.
- Palanza P (2001) Animal models of anxiety and depression: how are females different? *Neurosci Biobehav Rev* 25:219-233.
- Papp L, Vizi ES, Sperlagh B (2004) Lack of ATP-evoked GABA and glutamate release in the hippocampus of P2X7 receptor^{-/-} mice. *Neuroreport* 15:2387-2391.
- Pelegri P (2008) Targeting interleukin-1 signaling in chronic inflammation: focus on P2X(7) receptor and Pannexin-1. *Drug News Perspect* 21:424-433.
- Popa D, El YM, Vaugeois JM, Hamon M, Adrien J (2006) Homeostatic regulation of sleep in a genetic model of depression in the mouse: effects of muscarinic and 5-HT1A receptor activation. *Neuropsychopharmacology* 31:1637-1646.
- Rao U, Hammen CL, Poland RE (2009) Risk markers for depression in adolescents: sleep and HPA measures. *Neuropsychopharmacology* 34:1936-1945.
- Rasenick MM, Chaney KA, Chen J (1996) G protein-mediated signal transduction as a target of antidepressant and antibipolar drug action: evidence from model systems. *J Clin Psychiatry* 57 Suppl 13:49-55.
- Rodriguez CI, Buchholz F, Galloway J, Sequerra R, Kasper J, Ayala R, Stewart AF, Dymecki SM (2000) High-efficiency deleter mice show that FLPe is an alternative to Cre-loxP. *Nat Genet* 25:139-140.
- Roger S, Mei ZZ, Baldwin JM, Dong L, Bradley H, Baldwin SA, Surprenant A, Jiang LH (2010) Single nucleotide polymorphisms that were identified in affective mood disorders affect ATP-activated P2X7 receptor functions. *J Psychiatr Res* 44:347-355.
- Romanowski CP, Fenzl T, Flachskamm C, Wurst W, Holsboer F, Deussing JM, Kimura M (2010) Central deficiency of corticotropin-releasing hormone receptor type 1 (CRH-R1) abolishes effects of CRH on NREM but not on REM sleep in mice. *Sleep* 33:427-436.

- Routledge C, Middlemiss DN (1996) The 5-HT hypothesis of depression revisited. *Mol Psychiatry* 1:437.
- Ruoslahti E (1996) RGD and other recognition sequences for integrins. *Annu Rev Cell Dev Biol* 12:697-715.
- Sanchez-Nogueiro J, Marin-Garcia P, Miras-Portugal MT (2005) Characterization of a functional P2X(7)-like receptor in cerebellar granule neurons from P2X(7) knockout mice. *FEBS Lett* 579:3783-3788.
- Sankoorikal GM, Kaercher KA, Boon CJ, Lee JK, Brodtkin ES (2006) A mouse model system for genetic analysis of sociability: C57BL/6J versus BALB/cJ inbred mouse strains. *Biol Psychiatry* 59:415-423.
- Schnutgen F, De-Zolt S, Van SP, Hollatz M, Floss T, Hansen J, Altschmied J, Seisenberger C, Ghyselinck NB, Ruiz P, Chambon P, Wurst W, von MH (2005) Genomewide production of multipurpose alleles for the functional analysis of the mouse genome. *Proc Natl Acad Sci U S A* 102:7221-7226.
- Schnutgen F, Hansen J, De-Zolt S, Horn C, Lutz M, Floss T, Wurst W, Noppinger PR, von MH (2008) Enhanced gene trapping in mouse embryonic stem cells. *Nucleic Acids Res* 36:e133.
- Scott LJ, et al. (2009) Genome-wide association and meta-analysis of bipolar disorder in individuals of European ancestry. *Proc Natl Acad Sci U S A* 106:7501-7506.
- Shyn SI, Hamilton SP (2010) The genetics of major depression: moving beyond the monoamine hypothesis. *Psychiatr Clin North Am* 33:125-140.
- Shyn SI, Shi J, Kraft JB, Potash JB, Knowles JA, Weissman MM, Garriock HA, Yokoyama JS, McGrath PJ, Peters EJ, Scheftner WA, Coryell W, Lawson WB, Jancic D, Gejman PV, Sanders AR, Holmans P, Slager SL, Levinson DF, Hamilton SP (2011) Novel loci for major depression identified by genome-wide association study of Sequenced Treatment Alternatives to Relieve Depression and meta-analysis of three studies. *Mol Psychiatry* 16:202-215.
- Sim JA, Young MT, Sung HY, North RA, Surprenant A (2004) Reanalysis of P2X7 receptor expression in rodent brain. *J Neurosci* 24:6307-6314.
- Skaper SD, Debetto P, Giusti P (2010) The P2X7 purinergic receptor: from physiology to neurological disorders. *FASEB J* 24:337-345.
- Sklar P, et al. (2008) Whole-genome association study of bipolar disorder. *Mol Psychiatry* 13:558-569.
- Sluyter R, Stokes L, Fuller SJ, Skarratt KK, Gu BJ, Wiley JS (2010) Functional significance of P2RX7 polymorphisms associated with affective mood disorders. *J Psychiatr Res* 44:1116-1117.
- Smith EN, et al. (2009) Genome-wide association study of bipolar disorder in European American and African American individuals. *Mol Psychiatry* 14:755-763.
- Solle M, Labasi J, Perregaux DG, Stam E, Petrushova N, Koller BH, Griffiths RJ, Gabel CA (2001) Altered cytokine production in mice lacking P2X(7) receptors. *J Biol Chem* 276:125-132.
- Soronen P, Mantere O, Melartin T, Suominen K, Vuoriolehto M, Rytala H, Arvilommi P, Holma I, Holma M, Jylha P, Valtonen HM, Haukka J, Isometsa E, Paunio T (2011) P2RX7 gene is associated consistently with mood disorders and predicts clinical outcome in three clinical cohorts. *Am J Med Genet B Neuropsychiatr Genet* 156B:435-447.
- Sperligh B, Kofalvi A, Deuchars J, Atkinson L, Milligan CJ, Buckley NJ, Vizi ES (2002) Involvement of P2X7 receptors in the regulation of neurotransmitter release in the rat hippocampus. *J Neurochem* 81:1196-1211.

- Sperlagh B, Vizi ES, Wirkner K, Illes P (2006) P2X7 receptors in the nervous system. *Prog Neurobiol* 78:327-346.
- Stagljar I, Korostensky C, Johnsson N, te HS (1998) A genetic system based on split-ubiquitin for the analysis of interactions between membrane proteins in vivo. *Proc Natl Acad Sci U S A* 95:5187-5192.
- Stefano L, Rössler OG, Griesemer D, Hoth M, Thiel G (2007) P2X(7) receptor stimulation upregulates Egr-1 biosynthesis involving a cytosolic Ca(2+) rise, transactivation of the EGF receptor and phosphorylation of ERK and Elk-1. *J Cell Physiol* 213:36-44.
- Steiger A, Kimura M (2010) Wake and sleep EEG provide biomarkers in depression. *J Psychiatr Res* 44:242-252.
- Stokes L, Fuller SJ, Sluyter R, Skarratt KK, Gu BJ, Wiley JS (2010) Two haplotypes of the P2X(7) receptor containing the Ala-348 to Thr polymorphism exhibit a gain-of-function effect and enhanced interleukin-1beta secretion. *FASEB J* 24:2916-2927.
- Surprenant A, Rassendren F, Kawashima E, North RA, Buell G (1996) The cytolytic P2Z receptor for extracellular ATP identified as a P2X receptor (P2X7). *Science* 272:735-738.
- Taylor SR, Gonzalez-Begne M, Sojka DK, Richardson JC, Sheardown SA, Harrison SM, Pusey CD, Tam FW, Elliott JI (2009) Lymphocytes from P2X7-deficient mice exhibit enhanced P2X7 responses. *J Leukoc Biol* 85:978-986.
- Thaminy S, Auerbach D, Arnoldo A, Stagljjar I (2003) Identification of novel ErbB3-interacting factors using the split-ubiquitin membrane yeast two-hybrid system. *Genome Res* 13:1744-1753.
- Torres GE, Egan TM, Voigt MM (1999) Hetero-oligomeric assembly of P2X receptor subunits. Specificities exist with regard to possible partners. *J Biol Chem* 274:6653-6659.
- Tremblay LK, Naranjo CA, Cardenas L, Herrmann N, Busto UE (2002) Probing brain reward system function in major depressive disorder: altered response to dextroamphetamine. *Arch Gen Psychiatry* 59:409-416.
- Vicente-Manzanares M, Choi CK, Horwitz AR (2009) Integrins in cell migration--the actin connection. *J Cell Sci* 122:199-206.
- Viiikki M, Kampman O, Anttila S, Illi A, Setälä-Soikkeli E, Huuhka M, Mononen N, Lehtimäki T, Leinonen E (2011) P2RX7 polymorphisms Gln460Arg and His155Tyr are not associated with major depressive disorder or remission after SSRI or ECT. *Neurosci Lett* 493:127-130.
- Wagner KV, Wang XD, Liebl C, Scharf SH, Müller MB, Schmidt MV (2011) Pituitary glucocorticoid receptor deletion reduces vulnerability to chronic stress. *Psychoneuroendocrinology* 36:579-587.
- Worthington RA, Smart ML, Gu BJ, Williams DA, Petrou S, Wiley JS, Barden JA (2002) Point mutations confer loss of ATP-induced human P2X(7) receptor function. *FEBS Lett* 512:43-46.
- Yilmazer-Hanke DM, Wigger A, Linke R, Landgraf R, Schwegler H (2004) Two Wistar rat lines selectively bred for anxiety-related behavior show opposite reactions in elevated plus maze and fear-sensitized acoustic startle tests. *Behav Genet* 34:309-318.
- Youngstrom E, Youngstrom JK, Starr M (2005) Bipolar diagnoses in community mental health: Achenbach Child Behavior Checklist profiles and patterns of comorbidity. *Biol Psychiatry* 58:569-575.

8 Acknowledgements

I would like to thank Prof. Dr. Wolfgang Wurst as my thesis supervisor for the opportunity to accomplish my dissertation and Dr. Jan Deussing as my direct supervisor for permanent supervision, guidance and support.

Moreover, I wish to express my gratitude for the time and effort of the examination board, Prof. Dr. Wolfgang Wurst, Prof. Dr. Alfons Gierl and Prof. Dr. Kay Schneitz, for evaluation and examination of my thesis.

I am very grateful to Prof. Dr. Dr. Dr. h.c. Florian Holsboer as director of the Max Planck Institute of Psychiatry for the possibility to carry out my projects for this PhD thesis in an excellent working environment.

Furthermore, I would like to thank my colleagues of the Max Planck Institute of Psychiatry for successful collaboration and support: Nina Dedic, Marcel Schieven, Dr. Katherine Webb and Dr. Judit Oldekamp (RG Deussing); Annette Vogl and Dr. Damian Refojo (RG Refojo); Dr. Vladimira Jakubcakova and Dr. Mayumi Kimura (RG Kimura); Dr. Darina Czamara and Prof. Dr. Bertram Müller-Myhsok (RG Müller-Myhsok); Prof. Dr. Gerhard Rammes (guest, RG Eder); Dr. Susanne Lucae (RG Lucae); Priv.-Doz. Dr. Mathias Schmidt (RG Schmidt).

In addition, I wish to thank the collaborators from the University of Buenos Aires, headed by Prof. Dr. Eduardo Arzt, as well as the cooperation partners from Affectis Pharmaceuticals, Dr. Markus Henniger and Dr. Inge Sillaber, and furthermore, the co-workers from the Helmholtz Zentrum München, Dr. Ralf Kühn, Susanne Bourier, Susanne Weidemann, Adriane Tasdemir and the team of the German Gene Trap Consortium (GGTC).

My gratitude also goes to our technical assistants, our animal care takers and to all colleagues who feel concerned for their help and support over the last years.

My special thanks go to Nina Dedic and Marisa Brockmann for their friendship and support in all situations, and in particular to Nina for great scientific input and advice.

My deep gratitude finally goes to my family, to my partner and to my friends for their continuous patience, encouragement and faith in me.

9 Curriculum vitae

Education

- Since 2007 Max Planck Institute of Psychiatry, Molecular Neurogenetics, Munich/Technische Universität München
PhD thesis
- 2006 – 2007 Max Planck Institute of Psychiatry, Molecular Neurogenetics, Munich/Technische Universität München
Diploma thesis (title: Molecular characterization of conditional CRH overexpressing mice)
- 2002 – 2007 Technische Universität München
Studies of biology (main subject: genetics)
Degree: Diploma in biology

Publications

Aprile-Garcia F., **Walser S.M.**, Dedic N., Paez-Pereda M., Jakubcakova V., Stadler H., Acuña M., Webb K., Czamara D., Liberman A.C., Senin S.A., Gerez J., Hoijman E., Refojo D., Mitkovski M., Oldekamp J., Lucae S., Panhuysen M., Schmidt M.V., Sillaber I., Mueller-Myhsok B., Kimura M., Wurst W., Stühmer W., Holsboer F., Arzt E., Deussing J.M. Heterozygosity of P2RX7 with depression-associated risk allele alters stress response. Manuscript submitted to Nature

Nina Dedic, **Sandra M. Walser** and Jan M. Deussing (2011). Mouse Models of Depression, Psychiatric Disorders - Trends and Developments, Toru Uehara (Ed.), ISBN: 978-953-307-745-1, InTech, Available from: <http://www.intechopen.com/articles/show/title/mouse-models-of-depression>

Lu A., Steiner M.A., Whittle N., Vogl A.M., **Walser S.M.**, Ableitner M., Refojo D., Ekker M., Rubenstein J.L., Stalla G.K., Singewald N., Holsboer F., Wotjak C.T., Wurst W. and Deussing J.M. (2008). Conditional mouse mutants highlight mechanisms of corticotropin-releasing hormone effects on stress-coping behavior. *Mol. Psychiatry* 13, 1028-1042.

Attendance of conferences, symposia and workshops

27. Symposium der AGNP, Munich, Germany (2011) (Poster)

Ringberg Meeting der MPG, Ringberg Castle, Tegernsee, Germany (2011)

4th Annual Meeting of NGFN-Plus and NGFN-Transfer in the Program of Medical Genome Research, Berlin, Germany (2011) (Poster)

14th International Neuroscience Winter Conference, Sölden, Austria (2011)

Harlan – Genetic Drift: Importance & Prevention-Strategies, Munich (2010)

2nd Annual Meeting of NGFN-Plus and NGFN-Transfer in the Program of Medical Genome Research, Berlin, Germany (2009) (Poster)

26. Symposium der AGNP, Munich, Germany (2009) (Poster)

Cologne Spring Meeting, Cologne, Germany (2009)

1st Annual Meeting of NGFN-Plus and NGFN-Transfer in the Program of Medical Genome Research, Munich, Germany (2008) (Poster)

XXVI CINP Congress – 50th Anniversary of the CINP, Munich, Germany (2008) (Poster)

25. Symposium der AGNP, Munich, Germany (2007) (Poster)

Interact PhD Symposium, Munich, Germany (2007) (Poster)

2nd Interdisciplinary Max Planck PhDnet Workshop, Frankfurt/Main, Germany (2007)
(Poster)

Language skills

German	native tongue
English	fluent
French	basic

IT skills

Microsoft Office, VectorNTI Advance 11.0 (Invitrogen), Adobe Photoshop CS2,
Adobe Illustrator CS2, Graphpad Prism 5.0, ImageJ, Reference Manager 11